Master's thesis

NTNU
Norwegian University of Science and Technology
Faculty of Engineering
Department of Geoscience and Petroleum

Erlend Torheim

Condensate Blockage

A study from the Norwegian continental shelf

Master's thesis in Petroleum Geoscience and Engineering
Supervisor: Curtis H. Whitson
June 2020

NTNU
Norwegian University of
Science and Technology

Erlend Torheim

Condensate Blockage

A study from the Norwegian continental shelf

Master's thesis in Petroleum Geoscience and Engineering
Supervisor: Curtis H. Whitson
June 2020

Norwegian University of Science and Technology
Faculty of Engineering
Department of Geoscience and Petroleum

NTNU
Norwegian University of
Science and Technology

Preface

The following report is the final part of my master's degree program in petroleum engineering at the Department of Geoscience and Petroleum at the Norwegian University of Science and Technology (NTNU). This report is a continuation of the specialization project TPG4560 (Torheim 2019), but it should be possible to follow work presented without having to read that work.

Related to my work, I would like to thank Wintershall DEA, with special notice to my supervisor in the company Gerardo Seri, for providing me with the necessary data related to completing this master thesis, as well as knowledge and support when needed.

Also deserving a big thanks is the helpful employees at Whitson AS for guidance, motivation, and educational discussions. I would especially accentuate the excellent guidance from Dr. Kameshwar Singh, Bilal Younus and Mathias Carlsen.

Among my co-students, I would like to thank Markus Hays Nielsen, Madelene Skintveit and Sindre Forsetløkken, for good discussions, brainstorming and knowledge sharing.

Last, but most importantly, I would like to thank my advisor at NTNU Dr. Curtis H. Whiston for supporting me throughout this process, providing the knowledge and experience needed, excellent mentorship, motivation and support. It has been a privilege working with such an inspiring and recognized professional.

Abstract

This Master Thesis is a continuation of the work done in the specialization project TPG4560 in the fall of 2019. Some parts are directly taken from the report “PVT Analysis for Condensate Blockage – A study of gas condensate samples from the Norwegian Continental shelf”. Wintershall DEA provided fluid sample data of a new discovery and potential field development (hereafter called Field A) including an ECLIPSE model of the near well region of the exploration well. The main objective of the project is to study the condensate blockage effects present and the potential impact this will have on the production of Field A.

Condensate blockage is a phenomenon important to understand related to field development of a gas condensate field. Well deliverability can be greatly reduced due to blockage in the near-wellbore region and can lead to an increase in number of wells needed. The pressure drop due to condensate blockage must be weighed relatively to the total pressure drop in the production system. Modelling the pressure drop in the near-wellbore region, using a three-region modelling concept developed by Fevang and Whitson (Fevang and Whitson 1995), is an effective method for studying the importance of condensate blockage. However, before the modelling can be done a basic understanding of the mechanisms and fluid behavior related to the blockage is required.

Having an equation of state (EOS) predicting the correct fluid behavior is crucial for modelling the condensate blockage correctly. Reservoir engineers often work with an EOS developed by a third part or co-worker and it can be difficult to understand the process behind developing and how to use the EOS. Sometimes the quality of the EOS used is unknown. Therefore, a quality control (QC) is important. Younus et al. provides a recommended validation process that can be applied to any EOS model (Younus et al. 2019). Such a QC will make sure that the EOS predicts reliable (at least physical) properties. A modification process of the EOS developed by Consultant A is discussed in this master thesis and a detailed QC can be found in the project report for the specialization project TPG4560 in Appendix C.

Consultant A is a third-party company delivering consultancy to the oil and gas industry and is given an anonymous name for confidentiality reasons. A QC of the black oil tables provided by Consultant A was done and the modified EOS mentioned above was used to generate new black oil tables that were used as the base case fluid model in the study cases.

The major pressure drop due to condensate blockage is in the near-wellbore region and is an effect of reduction in the relative permeability of gas, k_{rg}. In this region both oil and gas flows and k_{rg} can be described as a function of the k_{rg}/k_{ro}-ratio. Therefore, k_{rg}/k_{ro}-ratios at different stages of depletion is obtained using the modified EOS to design core flooding experiments completed on a set of cores with different absolute permeabilities.

Core experiments was conducted by STRATUM Reservoirs on two of the cores taken from the exploration well. This was done to provide relevant relative permeability data input to the reservoir model.

The reservoir model provided by Wintershall DEA is a high-resolution model in the z-direction and was modified to be a simpler “box model”. Averaging methods based on the sum of permeability and height (kh) were utilized to comply the higher permeability layers present in the reservoir zones. Both coarse grid models and fine grid radial models were made and used in the sensitivity study cases.

From simulation studies conducted in this master thesis there is two high-level conclusions that can be drawn:

- Condensate blockage reduces the well deliverability in Field A greatly. If this effect is overlooked wrong investment decisions will be made.
- It is shown that a simple coarse grid model with the generalized pseudopressure well treatment method (Whitson and Fevang 1997) provides good approximations of condensate blockage effects compared to a fine grid model for Field A.

Sammendrag

Denne masteroppgaven er en fortsettelse av arbeidet gjennomført i spesialiserings prosjektet TPG4560. Noen deler av teksten i denne master oppgaven er mer eller mindre tatt direkte fra rapporten “PVT Analysis for Condensate Blockage – A study of gas condensate samples from the Norwegian Continental shelf” skrevet for TPG4560. Wintershall DEA utleverte væske prøve data fra en mulig feltutvikling (Videre kaldt Felt A). En ECLIPSE modell fra området nær borehullet av letebrønnen var også utlevert i forbindelse med denne oppgaven. Målet med denne oppgaven er å studere effekten kondensatblokkering og den mulige innvirkningen dette har på produksjonen av Felt A.

Kondensatblokkeringer er viktig å forstå i relasjon til felt utvikling av et gas kondensat felt. Brønn leveransen kan bli kraftig redusert på grunn av blokkering nært brønnhulls regionen og kan lede til at antall brønner som trengt på feltet øker. Trykkfallet på grunn av kondensatblokkering må veies relativt til det totale trykkfallet i produksjonssystemet. Modellering av trykkfallet i nær-borehulls regionen, ved bruk av et tre-regioners modelleringskonsept utviklet av Fevang og Whitson i 1995 er en effektiv metode for å studere viktigheten av kondensblokkering på en full felt skala. Før modelleringen kan gjennomføres, er det imidlertid nødvendig med en grunnleggende forståelse av mekanismene og væskeatferden relatert til blokkeringen og gas kondensater.

Å ha en tilstandsligning (EOS) som forutsier riktig væskeatferd, er avgjørende for å modellere kondensblokkeringen riktig. Reservoaringeniører jobber ofte med en EOS utviklet av en tredjepart eller en medarbeider, og det kan være vanskelig å forstå prosessen bak utvikling og hvordan man bruker en EOS. Noen ganger er kvaliteten av EOS-en også ukjent. Derfor er en kvalitetskontroll (QC) viktig. Younus et al. gir en anbefalt valideringsprosess som kan brukes på enhver EOS-modell (Younus et al. 2019). En slik QC vil sørge for at EOS-en spår pålitelige (i det minste fysiske) egenskaper. En modifikasjonsprosess av EOS utviklet av Consultant A blir diskutert i denne masteroppgaven og en detaljert QC kan bli funnet i prosjektrapporten for fordypningsprosjektet TPG4560 i vedlegg C.

Konsulent A er et tredjepartsfirma som leverer konsulentvirksomhet til olje- og gassindustrien og får et anonymt navn av taushetsgrunner. En QC av tabellene med svart olje levert av konsulent A ble gjort, og den modifiserte EOS nevnt ovenfor ble brukt til å frembringe nye tabeller med svart olje som ble brukt som base-case fluidmodell i studiene.

Det største trykkfallet på grunn av kondensatblokkering er i området nær borehullet og er en effekt av reduksjon i den relative permeabiliteten til gass, k_{rg}. I dette området kan både olje og gass strømmer og k_{rg} beskrives som en funksjon av k_{rg}/k_{ro}-forholdet. Derfor oppnås k_{rg}/k_{ro}-forhold i forskjellige trinn av uttømmingen ved å bruke den modifiserte EOS for å designe strømningsforsøk på kjerneprøver for å bli gjennomført på et sett med kjerner med forskjellige absolutte permeabiliteter.

Kjerneeksperimenter ble utført av STRATUM Reservoirs på to av kjernene hentet fra letebrønnen. Dette ble gjort for å gi relevant relativ permeabilitetsdatainngang til reservoarmodellen.

Reservoarmodellen levert av Wintershall DEA er en høyoppløselig modell i z-retningen og ble modifisert til å være en enklere "boks modell". Gjennomsnittsmetoder basert på summen av permeabilitet og høyde (kh) ble benyttet for å samsvare med de høyere permeabilitetslagene som er til stede i reservoarsonene. Både grove rutenettmodeller og fine radialmodeller ble laget og brukt i sensitivitetsstudietilfellene.

Fra simuleringsstudier utført i denne masteroppgaven er det to konklusjoner på høyt nivå som kan trekkes:

- Kondensatblokkering reduserer brønnleveransen i felt A kraftig. Hvis denne effekten overses, vil det bli tatt feil investeringsbeslutninger.
- Det er vist at en enkel grov rutenettmodell med den generaliserte pseudopressure-brønnbehandlings-metoden utviklet av Fevang og Whitson (Whitson og Fevang 1997) gir gode tilnærminger av kondensblokkeringseffekter sammenlignet med en finnettmodell for felt A.

Table of Contents

List of Figures

List of Tables

1 Introduction

1.1 Reservoir introduction

Field A was a potential field development in Wintershall DEA's portfolio. The development was in an early stage where studying different challenges that might occur was important. One of these challenges was condensate blockage as the fluid in the reservoir is a gas condensate.

The Field A discovery was made in March 2018 in three separate reservoir zones. Table 1.1 indicates that the porosity in the sandstone reservoir zones is good, but that the permeability is variable ranging from an average of 12.5 md in zone 1 to 0.35 md for zone 3. The purpose of including this table is to get an idea of the characteristics and quality of the reservoir studied in this thesis.

Table 1.1 Petrophysical parameters net reservoir (cutoffs: Vcl < 40%, PHIE > 8%)

Reservoir	Gross Thickness, m TVD	Net Thickness, m TVD	NTG, %	Av. PHIE, %	Av. Sw, %	Av. Vcl, %	Av. perm, md
Zone 1	6.36	4.39	69.1	17.6	37.9	14.6	12.5
Zone 2	56.3	50.3	89.2	18.6	53.9	19.8	2.98
Zone 3	129	93.6	72.5	15.0	67.1	22.9	0.35

1.2 Potential Condensate Blockage issues

Condensate blockage is the stabilization of a two phase gas/oil flow region near the wellbore when the bottom hole flowing pressure (BHFP) drops below the dewpoint pressure (Whitson, Fevang, and Yang 1999). Due to this the relative permeability of the gas may drop and the well deliverability is lowered accordingly. This effect is always present in a gas condensate reservoir, when the BHFP drops below the dewpoint. The question to be answered is how important the effects are in context of the field development.

To evaluate the importance of the condensate blockage, the potential pressure-drop over the blockage region must be compared with the pressure drop in the rest of the production system (pipe and tubing). This is often simulated having a minimum BHFP constraint on the well representing the pressure needed to have pressure support throughout production. Understanding the behavior of the fluid in the near-wellbore region is the first step in the process of determining the impact of the condensate blockage.

1.3 Study Objective

This report presents a study of potential condensate blockage issues for the field development of Field A. There are four main objectives in this study:

1. Introduce and explain condensate blockage through a literature study. This literature study goes through gas condensates in general, condensate blockage, condensate blockage modeling and treatment of wells in reservoir simulation.
2. Quality control of the black oil tables used in the original ECLIPSE model provided by Wintershall DEA. This will be done by recreating the black oil tables using PhazeComp instead of PVTsim as used by Consultant A. A modified and QC-ed version of the Peng Robinson EOS model developed by Consultant A will be used for the black oil table generation.
3. Description, designing and discussion of relative permeability experiments. STRATUM Reservoirs in Trondheim was provided with two core samples from Field A with the purpose of performing core experiments designed for measuring actual relative permeability data present in the reservoir. The experiments are designed using the same EOS used to generate the black oil tables, plotting k_{rg}/k_{ro} as a function of pressure at different stages of depletion. The importance of accurate relative permeability data is studied as a study case in the next step.
4. Simulation study cases covering the effects of condensate blockage will be conducted to verify the importance of the phenomenon for Field A. This will be done using the black oil tables generated by the modified EOS model in the base case and verifying that relevant relative permeability data is being used from the core experiments done by STRATUM Reservoirs.

1.4 Scope of Work

This report is divided into five main parts. The first part is a summary of a literature review related to understanding condensate blockage, as well as researching the theory behind the modelling of condensate blockage. This is covered in Chapter 2 and 3. The second part is dedicated to the fluid models used on the study cases with special notice to the black oil tables. This part contains a summary of the EOS developed by Consultant A and the modifications done to it. From there a regeneration process of the black oil tables made by Consultant A with the modified EOS is performed to compare the tables from Consultant A with the tables generated by the modified EOS. The third part is covering a laboratory study, both theory and results of a core experiment designed to obtain relevant relative permeability data representing

the near wellbore region where condensate blockage occurs. Part four is describing the reservoir simulation model from base case to the different sensitivity study cases performed and conclusions drawn from the study. The results of the simulations are presented and discussed. The last part covers the recommendations for further work.

It should be emphasized that the work done and discussed in this thesis has a root in the report form the specialization project TPG4560. Observations/results from the specialization project report will not always be included in detail in this thesis, but where it is suitable a summary will be included. The project report will be included in Appendix C of this thesis and can be read as an introduction to this thesis. In the bigger picture the project report TPG4560 is a study, QC and modification process of the EOS developed by Consultant A, while the master thesis is a study of the condensate blockage effects in Field A, using what was found in TPG4560. Keep in mind that it is important to understand the basics of the fluid present in the reservoir before tackling the condensate blockage modeling and study.

The main goal is to study the effect condensate blockage will have on the field development of Field A and describe a process for how to model condensate blockage in reservoir models. These two documents, i.e. the thesis and the project report can be viewed as a guide on how to deal with condensate blockage from fluid to simulation.

2 Gas Condensates and Condensate Blockage

This section is a summary of the project report delivered in the specialization project TPG4560 covering the principles and concepts around condensate blockage. Therefore, the text in this section will be very similar to what is found in the project report for TPG4560. Again, the project report can be found in Appendix C of this thesis (Torheim 2019).

2.1 Gas Condensates

A reservoir fluid is formally classified as a gas condensate if the reservoir temperature is less than the cricondentherm (where the fluid will never enter a two-phase region) and greater than the critical temperature (Whitson and Brulé 2000). Figure 2.1 shows this graphically.

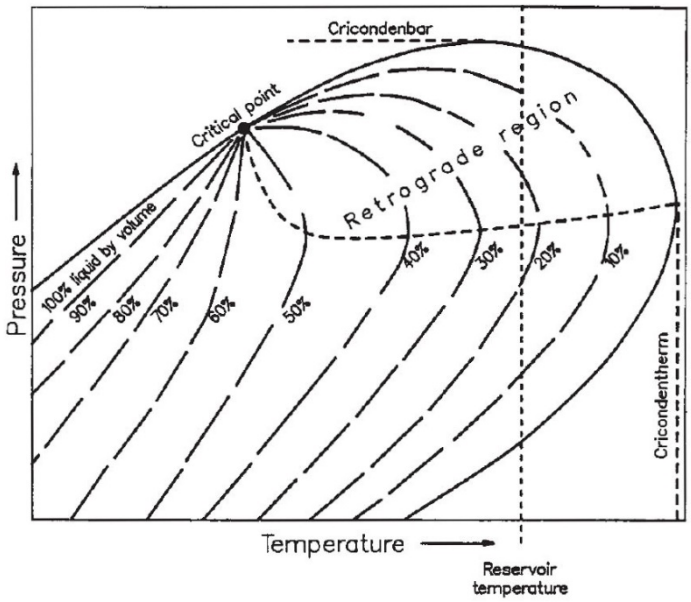

Figure 2.1 Hypothetical p-T diagram for a gas condensate fluid (Whitson and Brulé 2000)

Typical retrograde gas condensate reservoirs present a gas-oil ratio (GOR) ranging from 3000 to 150000 scf/STB (535 to 26720 Sm3/Sm3). This corresponds to a condensate-gas ratio (CGR) of 350 to 5 STB/MMscf (0.002 to 0.00003 Sm3/Sm3). Liquid gravities are typically in the range between 40 to 60° API.

Gas condensate engineering is for the most part regular gas engineering, with some extent of additional engineering due to surface condensate production and retrograde condensate left

in the reservoir. It can be argued that gas condensate engineering is 80% traditional gas engineering and 20% “extra” engineering (Whitson, Fevang, and Yang 1999). The main characteristics of a gas condensate can be summarized as follows (Whitson and Mott 2005):

1. The already mentioned retrograde condensation happening in the reservoir. This liquid phase usually has no or very low mobility, except from in the near wellbore region.
2. Surface condensate production may lead to a significant increase in the income of a gas condensate field. Processing methods and optimization at surface will decide the “extra” income from the surface condensate.
3. Recoveries by depletion will typically range from 60-80% for gas and 20-40% for condensate, with lower condensate recoveries for richer fluids.
4. Gas cycling is a potential method for increasing the condensate recoveries but requires injection gas. The injection gas can either be the produced gas or purchased injection gas. (Gas cycling will not be covered in this report).
5. Condensate blockage can become a significant contributor to pressure drop and thus reduction in well deliverability after the BHFP falls below the dewpoint pressure. This is an important consideration for low and medium permeability gas condensate reservoirs.

For more in-depth theory on gas condensates PVT experiments, initial fluids in place and depletion recovery read section 2.2.2 in the project report in Appendix C.

2.2 Condensate Blockage

Condensate blockage is the stabilization of a two-phase gas/oil flow region near the wellbore when the BHFP drops below the dewpoint pressure (Whitson, Fevang, and Yang 1999). For a field development the well deliverability reduction due to condensate blockage is only important when the BHFP reaches a minimum and the well is forced to go on decline (Fevang and Whitson 1995). Condensate blockage is an important factor to consider for field development strategy of the field (i.e. number of wells, subsea compression etc.). For a gas condensate field experiencing large pressure drops due to condensate blockage, more wells are needed to deliver higher production from the field. Pressure losses due to condensate blockage must be compared and included to the pressure losses in the rest of the production system. To evaluate and model condensate blockage effects correctly there are three main considerations of importance: **The producing GOR, PVT properties (black oil or compositional) and gas-oil relative permeabilities.**

2.2.1 Condensate blockage modeling

To understand the effect condensate blockage has on well deliverability the gas condensate rate equation is introduced. Equation (2.1) and (2.2) describe the general volumetric rate equation for a gas condensate well, with a compositional formulation and in terms of black-oil PVT respectively.

$$q_g = C\left(\frac{RT_{SC}}{p_{SC}}\right)\beta_S \int_{p_{wf}}^{p_R}\left(\frac{\rho_o k_{ro}}{M_o \mu_o} + \frac{\rho_g k_{rg}}{M_g \mu_g}\right) dp \tag{2.1}$$

$$q_g = C\int_{p_{wf}}^{p_R}\left(\frac{k_{ro}}{B_o \mu_o} R_s + \frac{k_{rg}}{B_g \mu_g}\right) dp \tag{2.2}$$

The relative permeability k_{rg} and k_{ro} are defined relative to the absolute permeability i.e. the ability to flow fluid through the porous medium when only one phase is present in the rock (Schlumberger 2019) and not to permeability at irreducible saturations. In the two equations above the gas rate constant C includes the basic reservoir properties as shown by Eq. (2.3).

$$C = \frac{2\pi ckh}{ln(r_e/r_w) - 0.75 + s} \tag{2.3}$$

Where c varies depending on the units and β_s is the surface gas mole fraction in the wellstream. Other parameters are the drainage radius r_e, the wellbore radius r_w, the permeability k and the thickness h of the layer being produced. The skin factor s includes non-ideal flow effects like damage, well stimulation and drainage geometry. One method for dealing with condensate blockage is to include a “condensate blockage” skin factor in the equation above included with the skin factor for non-ideal flow effects. However, this is not ideal as the skin factor may vary with pressure and flow rate and it would be difficult to use this approach in a coarse grid (full field) model (Mott 1999). With the following proposed pseudopressure method from Fevang and Whitson condensate blockage effects are treated based on grid cell pressure and producing GOR i.e. no need for local grid refinement or introducing a “condensate blockage” skin factor that is most certainly wrong.

In 1995 Fevang and Whitson presented a method for calculating gas condensate well deliverability based on observation of three regions a gas condensate well experiences in the depletion process. The so called **three region model** is an accurate model for calculating well deliverability of a gas condensate well undergoing depletion. Figure 2.2 is included to get a

picture of the three different regions that for a given producing condition may exist. An important assumption is that the flow condition in the three regions is pseudo-steady state, i.e. steady-state conditions at a given time, but the steady state condition changes during depletion.

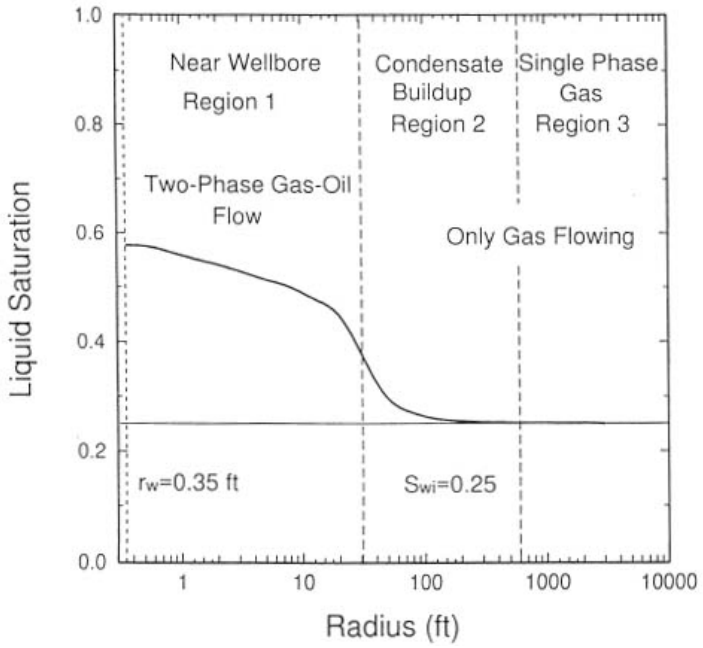

Figure 2.2 The three regions of flow behavior in Fevang and Whitson's three-region model (Fevang and Whitson 1996)

The three-region model is based on decomposing the pseudopressure integral in Eq. (2.1) and (2.2) into three parts representing the pressure drop in the three different regions. This is shown in Eq. (2.4). The different integrals for the different regions will be defined further down under the description of each region.

$$\Delta p_p = \int_{p_{wf}}^{p_R} \left(\frac{k_{rg}}{B_{gd}\mu_g} + \frac{k_{ro}}{B_o\mu_o} R_s \right) dp = \Delta p_{p1} + \Delta p_{p2} + \Delta p_{p3} \qquad (2.4)$$

Region 1 is the region where both gas and condensate flow simultaneously. Because of the reduction in relative permeability of gas, region 1 is the main source of reduction in well deliverability. This region will always exist if the BFHP is less than the dewpoint of the flowing composition entering the region. The flowing GOR is constant, meaning that the single-phase gas entering the region has the same composition as the produced wellstream mixture. The condensate saturation is determined as a function of radius to ensure that all liquid that condenses from the single-phase gas entering Region 1 has enough mobility to flow through

and out of the region without any net accumulation. The *solution* CGR decreases with pressure, and since pressure decreases towards the wellbore the liquid saturation increases (Fevang 1995). Region 1 will increase with time and the outer boundary moves outwards as a result. The liquid saturation closest to the wellbore will also decrease with time, as the gas entering the region gets leaner throughout production.

Equation (2.5) shows the pseudopressure integral of Region 1 in terms of black-oil PVT properties.

$$\Delta p_{p1} = \int_{p_{wf}}^{p^*} \left(\frac{k_{ro}}{B_o \mu_o} R_s + \frac{k_{rg}}{B_g \mu_g} \right) dp \tag{2.5}$$

The integral ranges from the BHFP, p_{wf}, to the dewpoint of the producing wellstream p^*. This dewpoint will be lower than the initial dewpoint p_d. The equation is solved using the modified Evinger-Muskat approach modified for gas condensates. The producing GOR and PVT properties are needed.

$$R_p = R_s + \left(\frac{k_{rg}}{k_{ro}} \right) \left(\frac{\mu_o B_o}{\mu_g B_{gd}} \right) (1 - r_s R_p) \tag{2.6}$$

Equation (2.6) describes the producing GOR (Fetkovich et al. 1986) which is the modified version of the producing GOR defined by Evinger and Muskat for an oil reservoir in Eq. (2.7). A derivation of equation (2.6) can be found in the appendix of the included project report for TPG4560.

$$R_p = R_s + \left(\frac{k_{rg}}{k_{ro}} \right) \left(\frac{\mu_o B_o}{\mu_g B_{gd}} \right) \tag{2.7}$$

Rearranging Eq. (2.6) yields k_{rg}/k_{ro} given in Eq. (2.8) as a function of pressure as the PVT properties and producing GOR are functions of pressure.

$$\frac{k_{rg}}{k_{ro}}(p) = \left(\frac{R_p - R_s}{1 - r_s R_p} \right) \frac{\mu_g B_{gd}}{\mu_o B_o} \tag{2.8}$$

Relative volume from a CCE experiment can be used to express Eq. (2.8) as a function of $V_{ro} = V_o / V_{tot}$ at each pressure in the CCE experiment as shown in Eq.(2.9).

$$\frac{k_{rg}}{k_{ro}}(p) = \left(\frac{1}{V_{roCCE}} - 1\right)\frac{\mu_g}{\mu_o} \tag{2.9}$$

When both oil and gas phases are mobile, as in Region 1, k_{rg} and k_{ro} can be expressed directly as a function of the ratio defined in Eq. (2.9). This is equivalent to saying that k_{rg} and k_{ro} can be evaluated directly as a function of pressure, $k_{rg}(p) = f\left[k_{rg}/k_{ro}(p)\right]$ and $k_{ro}(p) = f\left[k_{rg}/k_{ro}(p)\right]$. Chapter 5 of this thesis evaluates in detail the plots of $k_{rg}/k_{ro}(p)$ used for designing the relative permeability experiments for obtaining relevant data needed to correctly model the reduction in well deliverability due to condensate blockage.

From a reservoir simulation point of view relative permeability data is included in the model through saturation tables. Table 2.1 is a conceptual table showing how the relationship $k_{rg}/k_{ro}(p)$ is used to find the k_{rg} and k_{ro} values from the table. As shown by the table it is not necessary to know saturation to calculate the pseudopressure integral for Region 1. This emphasizes the importance of having realistic relative permeability tables in the model.

Table 2.1 Conceptual saturation table inputted to reservoir simulators.

S_o	k_{rg}	k_{ro}	$\frac{k_{rg}}{k_{ro}}(p)$
0		0	
s_{oc}		0	inf
			High
? ←	x ←	x ←	*known*
			Low
$1 - s_w - s_{gc}$	0		0
$1 - s_w$	0		

Region 2 will always co exists with Region 1 after reservoir pressure drops below the dewpoint pressure (no Region 3). All three regions will exist if the reservoir is slightly undersaturated and the BHFP is less than the dewpoint pressure, while region 2 may be negligible for highly undersaturated reservoirs. Region 2 is the region where only gas is flowing i.e. oil mobility is practically zero, while condensate starts to accumulate. The condensate saturation can be

approximated by the liquid dropout curve of a CVD experiment, corrected for water saturation. According to Fevang and Whitson the size and importance of Region 2 is greater for lean gas condensates (Fevang and Whitson 1995). Equation (2.10) show the pseudopressure integral for region 2.

$$\Delta p_{p2} = \int_{p*}^{p_d} \frac{k_{rg}}{B_g \mu_g} dp \tag{2.10}$$

In this region the relative permeability of gas is a function of oil saturation $k_{rg}(S_o)$, where S_o is estimated as a function of CVD relative oil volumes. $V_{roCVD}(p) = V_o(p)/V_d$ will give $S_o(p) = [V_{roCVD}(p)](1 - S_w)$, where $(1 - S_w)$ is the correction for the present water saturation. The accumulation of condensate due to the gas flowing in Region 2 gets higher, i.e. the oil saturation increases, towards Region 1 shown in Figure 2.2. When CVD relative volume data are missing, it can be calculated from Eq. (2.11) below (Fevang and Whitson 1995)

$$(V_{roCVD})_k = \frac{N_{k-1} - G_{k-1}(r_s)_k}{1 - (r_s R_s)_k} (B_o)_k \tag{2.11}$$

where k is the current pressure step. N_{k-1} and G_{k-1} is defined as follows in Eq. (2.12) and (2.13).

$$N_{k-1} = \left(\frac{V_{roCVD}}{B_o} + \frac{1 - V_{roCVD}}{B_{gd}} r_s \right)_{k-1} \tag{2.12}$$

$$G_{k-1} = \left(\frac{V_{roCVD}}{B_o} R_s + \frac{1 - V_{roCVD}}{B_{gd}} \right)_{k-1} \tag{2.13}$$

Region 3 is existing if the reservoir is undersaturated and will exist while the reservoir pressure is above the dewpoint pressure. As gas is the only phase present only PVT properties are relevant. Equation (2.14) shows the pseudopressure integral of Region 3 which is the traditional single phase pseudopressure function.

$$\Delta p_{p3} = k_{rg}(S_{wi}) \int_{p_d}^{p_R} \frac{1}{B_{gd} \mu_g} dp \tag{2.14}$$

3 Treatment of Wells in Reservoir Simulation

Before going into detail about how the provided single well reservoir model is converted to a simpler synthetic model (Chapter 6 of this thesis) knowledge of how wells are treated in reservoir simulators, with special notice to Schlumberger's industry reference software ECLIPSE, is important.

3.1 Normal Well Treatment

Wells traditionally follow the rate equation found exemplified in Eq. (2.1) and (2.2) in the section above. Every well needs to be connected to grid blocks through connecting grid blocks, where every connection has its own connection transmissibility factor. This value can be directly specified by the engineer (as is the case for the provided original reservoir model), or it can be calculated by the reservoir simulation software using the following equations for cartesian and radial grids respectively (Schlumberger 2017b).

$$T_{wj} = \frac{c\theta kh}{ln(r_o/r_w) + s} \tag{3.1}$$

$$T_{wj} = \frac{c\theta kh}{\frac{{r_2}^2}{{r_2}^2 - {r_w}^2} ln(r_2/r_w) - 0.5 + s} \tag{3.2}$$

In Eq. (3.1) r_o is the pressure equivalent radius of the grid block and is defined as the distance from the well at which the local pressure is equal to the nodal average pressure of the block. For cartesian systems the Peacmans's formula for grid blocks in which the permeability may be anisotropic is used and defined in Eq.(3.3). The well is assumed to penetrate the full thickness of the block, through its center, perpendicularly to two if its faces (Schlumberger 2017b).

$$r_o = 0.28 \frac{\left[D_x^2 \left(\frac{k_y}{k_x}\right)^{\frac{1}{2}} + D_y^2 \left(\frac{k_x}{k_y}\right)^{\frac{1}{2}} \right]^{\frac{1}{2}}}{\left(\frac{k_y}{k_x}\right)^{\frac{1}{4}} + \left(\frac{k_x}{k_y}\right)^{\frac{1}{4}}} \tag{3.3}$$

In Eq. (3.3) D_x and D_y are the x and y dimensions of the grid block and k_x and k_y is the directional permeabilities in the x and y directions. In Eq. (3.2) r_2 is the outer radius of the grid block.

The other parameters in the equations are as follows:

- r_w is the wellbore radius
- c is the unit conversion factor and is dependent on the units used in the model.
- θ is the angel of the segment connection with the well in radians. For cartesian grids this value is 2π because the connection is assumed to be in the center of the grid block.
- kh is the effective permeability times the net thickness of the connection. For vertical wells, the permeability used is the geometrical mean of the x– and y-direction permeabilities, $k = \left(k_x k_y\right)^{\frac{1}{2}}$. If the well is for example penetrating in the x-direction (horizontal well), the quantities k_y and k_z will be used instead.
- s is the skin factor

Horizontal wells may be penetrating the well in either the x- or y-direction in a cartesian grid, making it necessary to substitute the appropriate components of permeability and block dimensions in the equations above in this section. An example can be for a well penetrating in the x-direction leading to a substitution of D_x and k_x with D_z and k_z.

3.2 Generalized Pseudopressure Well Treatment

The generalized pseudopressure (GPP) well treatment method accounts for localized near-wellbore multiphase flow behavior and is an important application to gas condensate wells due to potential condensate blockage as discussed in Chapter 2. When the method was developed the general idea was that at a given well-grid cell at a given time step, the flowing composition produced (or injected into) from a cell is assumed known and relates rate to BHFP and average grid-cell pressure using the following (Whitson and Fevang 1997):

- Produced (or injected) composition.
- Appropriate relative permeabilities.
- PVT calculations at a few pressures from the grid-cell average pressure to the limiting (minimum or maximum) BHFP. The PVT calculation will vary depending the type of simulator being used: a compositional or black-oil model.

In a compositional simulator the PVT calculations constitute exactly a CCE of the produced composition, starting at the average grid-cell pressure and extending to the limiting BHFP. In a black-oil model, the pseudopressure well treatment is precalculated before the simulation starts, with pseudopressure tables generated as function of rate, BHFP, grid-cell pressure, and producing GOR.

The pseudopressure function is given in Eq. (3.4) under.

$$m(p) = m_t(p) = \int_{p_{min}}^{p} \lambda_t(p)dp \tag{3.4}$$

Gas and oil rates are than calculate respectively with Eq (3.5) and (3.6)

$$q_g = \beta_s C\left[m_t(p_G) - m_t(p_{wf})\right] \tag{3.5}$$

$$q_o = (1 - \beta_s) C\left[m_t(p_G) - m_t(p_{wf})\right] \tag{3.6}$$

where C is the steady state well constant given as follows in Eq. (3.7).

$$C = \frac{2\pi ckh}{ln(r_o/r_w) + s} \tag{3.7}$$

The surface phase separation β_s differs depending on the type of simulator used. For a black oil simulator, the parameter is the volume fraction of separator gas $= 1/(1 + Rp)$ and for a compositional simulator it is the mole fraction of separator gas.

In the equations above c is the units constant, r_o is the Peaceman radius given in Eq. (3.3) and the skin factor s accounts for non-ideal flow effects and well geometry. The r_o parameter can also be some properly chosen equivalent drainage radius instead of the Peaceman radius.

The total mobility is given in Eq. (3.8) under. The gas mobility is dependent on the type of simulator being used. Equation (3.9) is for a black-oil simulator and Eq. (3.10) for a compositional simulator. Similarly, oil mobility is given in Eq. (3.11) and (3.12).

$$\lambda_t = \lambda_g + \lambda_o \tag{3.8}$$

$$\lambda_g = \frac{k_{rg}}{\mu_g B_g} + \frac{k_{ro}}{\mu_o B_o} R_s \tag{3.9}$$

$$\lambda_g = \frac{k_{rg}\rho_g}{\mu_g M_g} \tag{3.10}$$

$$\lambda_o = \frac{k_{ro}}{\mu_o B_o} + \frac{k_{rg}}{\mu_g B_g} r_s \tag{3.11}$$

$$\lambda_o = \frac{k_{ro}\rho_o}{\mu_o M_o} \tag{3.12}$$

The procedure of making the precalculated table mentioned above for the pseudopressure function can be divided into steps as done by Fevang and Whitson in their paper on the generalized pseudopressure method (Whitson and Fevang 1997). For a single-phase grid cell, the steps are as follows:

1. The upper saturation pressure is calculated which defines the pressure boundary p between Region 1 and upper Region 3 (The three-region model is discussed in Chapter 2 of this thesis). If a saturation pressure is not found the mixture is assumed single-phase at all pressures from p_G to p_{min}. p_G is the well grid cell average pressure.

2. A stability test at p_{min}, which is the minimum BHFP constraint, is made and can have the following outcomes:

    a. If p_{min} is unstable it means that there are two phases. A lower single-phase Region 3 does not exist.
    b. If p_{min} is stable it means that there is only one phase. The lower dewpoint pressure is then calculated which defines a lower limit of Region 1, $p > p_{min}$. This situation, which is a single-phase lower Region 3, is very seldom.

3. The boundaries and existence of Region 1 and Region 3 are defined by p_{min}, p, p and p_G. Single-phase λ_t values at any of the pressures mentioned are used in constructing the piecewise-linear $m(p)$ function in upper and lower Regions 3.

4. In the case of the existence of a two-phase Region 1 at least two Region 1 "interior" λ_t values should be calculated at equidistant pressures between the upper and lower bounds of Region 1. It is possible to user-define several interior λ_t values to be

calculated in the reservoir simulator, but according to Fevang and Whitson (Whitson and Fevang 1997) two values should usually be sufficient. Linear extrapolation of the two rightmost interior λ_t values should be used for determining λ_t at the upper bound Region 1. The same principle is used if a lower Region 3 exists where linear extrapolation of the two left-most interior λ_t values should be used to determine λ_t at the lower bound of Region 1.

For a two-phase gas/oil grid cell there does not exist a single-phase upper Region 3, meaning that $p = p_G$. The process is as follows:

1. A stability test as in step 2 above is performed and there could be two options as described above (a. and b.).

2. The boundaries and existence of Region 1 and Region 3 are now defined by $p_{min}, p, p = p_G$. Single-phase λ_t values at any of the pressures mentioned are used in constructing the piecewise-linear $m(p)$ function in lower Regions 3 (if it exists). Extra single-phase Region 3 λ_t values can also be calculated by user specifications.

3. Minimum two Region 1 "interior" λ_t values should be calculated at equidistant pressures between upper and lower bounds of Region 1. The same user-defined additional λ_t values applies here as well as in step 4 above. Linear extrapolation of the two rightmost interior λ_t values should be used for determining λ_t at the upper bound Region 1. Again, the same principle is used if a lower Region 3 exists where linear extrapolation of the two left-most interior λ_t values should be used to determine λ_t at the lower bound of Region 1.

In the descriptions above an upper and lower dewpoint refers to dewpoints found in a phase diagram where it is possible for given composition to have a lower dewpoint as illustrated below in Figure 3.1.

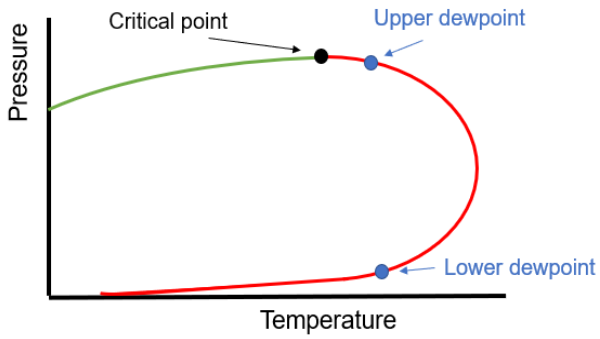

Figure 3.1 Upper and Lower dewpoint concept schematic

A fundamental assumption in the aspect of the application of the pseudopressure proposed by Fevang and Whitson is that Region 2 does not exist within the well grid cell and that the numerical grids surrounding the well grid cell treats Region 2 sufficiently accurate (Whitson and Fevang 1997).

3.2.1 Application of GPP in ECLIPCE

The GPP option is activated for individual wells by entering GPP in item 8 of the WELSPECS keyword (ECLIPSE 100) or item 9 of WELSPECL ECLIPSE 300) (Schlumberger 2017a). Figure 3.2 below shows an example of an ECLIPSE file with and without the pseudopressure method applied to the well.

```
--
WELSPECS
    PROD 1*  6  6    1*  GAS    6*    /
/

--                              RELPERM   CF    DIA     KH    S
COMPDAT
    PROD     6  6  1 22   OPEN      1*    1*   0.1905    1*   0 /
/

--                        OIL  WAT  GAS     LIQ  RESV BHP    THP  VLP Table
WCONPROD
    PROD   OPEN   GRAT   1*   1*    1.0E6    2*        100    1*     1 /
/
```

```
--
WELSPECS
    PROD 1*  6  6    1*  GAS 1* GPP 4*  /
/

--                              RELPERM   CF    DIA     KH    S
COMPDAT
    PROD     6  6  1 22   OPEN      1*    1*   0.1905    1*   0 /
/

--                        OIL  WAT  GAS     LIQ  RESV BHP    THP  VLP Table
WCONPROD
    PROD   OPEN   GRAT   1*   1*    1.0E6    2*        100    1*     1 /
/
```

Figure 3.2 Example ECLIPSE WELSPECS with applied GPP

4 Fluid Modeling

Black Oil Table Comparison of Consultant A and Modified EOS.

In a reservoir simulator one or more fluid models are needed to describe the phase behavior of the fluids present in the reservoir as it is produced or injected fluid into. There are two types of fluid models commonly used in a simulator. The first is a compositional fluid model i.e. using an EOS and fluid compositions directly in the simulator. An EOS is a fluid model that takes molar composition and predicts phase behavior of the fluid over a wide range of pressures and temperatures. Using the compositional model directly in the simulator will result in a reservoir simulation model that is more computationally costly compared to the alternative. The second method is using the EOS and fluid compositions to generate pre calculated black oil tables providing the simulator with PVT properties used in predicting the phase behavior of the fluid.

4.1 EOS Used for Generating Black Oil Tables

Consultant A provided Wintershall DEA with black oil tables generated for Field A. The tables can be found in the report of the development of the EOS provided to Wintershall DEA by Consultant A. These are the same black oil tables found in the original single well reservoir model provided by Wintershall DEA for this study. The reservoir model itself is discussed in more detail in Chapter 6. To verify the quality of the black oil tables and understand how they were generated in PVTsim by Consultant A, a comparison study was conducted and is described in this chapter.

The original black oil tables from Consultant A was compared to PhazeComp generated black oil tables with the original EOS developed by Consultant A. The EOS was imported manually to PhazeComp. The modified EOS discussed in the specialization project assignment (TPG4560 report), and in this section, is also used for generating black oil tables to compare with the already existing tables in the ECLIPSE model. This will provide a basis for deciding if the black oil tables generated using the modified EOS should be used over the Consultant A generated tables. Table 4.1 includes the modified EOS discussed in section 4.3. As mentioned earlier the detailed study and QC of the fluid samples and EOS is found in Appendix C including the project report of TPG4560.

Table 4.1 Component properties in Peng Robinson modified EOS for Field A

Component Properties								
Component Name	MW	T_{ci} (°C)	p_{ci} (bar)	ω_i	s_i	SG	Vc (cm3/mol)	$Crit\ Z$
N2	28.014	-146.95	33.944	0.04	0.16687	0.28314	90.196	0.29178
CO2	44.01	31.05	73.765	0.225	0.00061	0.76242	94.063	0.27433
C1	16.043	-82.55	46.002	0.008	0.14947	0.14612	98.594	0.2862
C2	30.07	32.25	48.839	0.098	0.06522	0.3304	145.183	0.27924
C3	44.097	96.65	42.455	0.152	0.06308	0.50971	200.103	0.2763
I-C4	58.124	134.95	36.477	0.176	0.06202	0.57045	262.311	0.28199
N-C4	58.124	152.05	37.997	0.193	0.05342	0.59058	254.795	0.27385
I-C5	72.151	187.25	33.843	0.227	0.05732	0.62952	308.01	0.27231
N-C5	72.151	196.45	33.741	0.251	0.03078	0.63585	310.555	0.26837
C6	86.178	234.25	29.688	0.296	0.0245	0.67086	376.034	0.26462
C7	96	288.95	29.452	0.337	0.09058	0.73676	388.411	0.24477
C8	107	308.442	25.819	0.374	0.16051	0.75546	433.276	0.23134
C9	121	333.701	22.266	0.42	0.23073	0.77375	490.538	0.21647
C10	134	355.667	19.82	0.463	0.27723	0.78741	543.509	0.20604
C11-C12	154.797	388.787	17.008	0.525	0.32827	0.80512	627.672	0.19397
C13	175	415.738	15.687	0.584	0.32959	0.81916	705.424	0.1932
C14	190	435.295	14.967	0.626	0.32586	0.82818	762.829	0.19383
C15	206	456.02	14.286	0.67	0.32341	0.83681	824.482	0.19428
C16	222	475.579	13.729	0.712	0.31875	0.84462	886.25	0.19545
C17-C18	243.761	503.119	13.015	0.768	0.31782	0.85419	971.19	0.19584
C19-C23	285.117	548.481	12.254	0.864	0.29288	0.86987	1131.863	0.20303
C24-C80	401.363	672.732	10.964	1.048	0.2373	0.90311	1595.856	0.22248

Table 4.2 Binary interaction parameters in Peng Robinson modified EOS

Binary Interaction Parameters		
	N2	CO2
N2		
CO2	-0.017	
C1	0.0311	0.12
C2	0.0515	0.12
C3	0.0852	0.12
I-C4	0.1033	0.12
N-C4	0.08	0.12
I-C5	0.0922	0.12
N-C5	0.1	0.12
C6	0.08	0.12
C7	0.08	0.1
C8	0.08	0.1
C9	0.08	0.1
C10	0.08	0.1
C11-C12	0.08	0.1
C13	0.08	0.1
C14	0.08	0.1
C15	0.08	0.1
C16	0.08	0.1
C17-C18	0.08	0.1
C19-C23	0.08	0.1
C24-C80	0.08	0.1

4.2 Check of Samples Used in EOS by Consultant A

This section is written about in the report of the specialization project TPG4560, but it is important to include here as well as some inconsistencies in the compositions used by Consultant A was found doing a lumping of lab reported composition with PhazeComp. Again, the text will be quite similar to what is found in the project report included in Appendix C (Torheim 2019).

It has been noticed that the lumped composition of the samples used both as in-situ and contaminated fluids in the EOS does not match in the heavier components with a lumping done in PhazeComp. Table 4.3 includes a comparison of the Consultant A defined in-situ fluid for the 22-compoent system and the corresponding lumping of the composition done in PhazeComp. The project report includes the full versions of the tables, as well as the same tables for the existing 10-component system designed by Consultant A for compositional reservoir simulation.

Table 4.3 Composition used by Consultant A vs lumped in PhazeComp form C36+ composition reported by CoreLab. *Decontaminated* samples

Component	**21364-IB, res zone 1**		**34428-IB, res zone 2**	
	Consultant A mole %	PhazeComp mole %	Consultant A mole %	PhazeComp mole %
N2	0.5540	0.5535	0.483	0.483
CO2	1.8340	1.8344	2.291	2.291
C1	85.2050	85.2028	86.248	86.247
C2	4.5660	4.5665	5.008	5.008
:	:	:	:	:
:	:	:	:	:
C15	0.0480	0.0481	0.026	0.026
C16	0.0370	0.0372	0.021	0.021
C17-C18	0.0560	0.0566	0.027	0.026
C19-C23	0.0950	0.0864	0.036	0.034
C24-C80	0.0510	0.0586	0.019	0.021

What can be seen from the table is that something is going on in the C19-C23 and C24-C80 composition of the Consultant A defined fluid for the 22-component EOS. This does not follow a normal lumping as is done in PhazeComp where the components are simply just added together. Why this compositional “tweak” has been done is unknown, but a likely reason could be that the composition has been changed to fit the EOS calculated CCE data to the

experimental data. Table 4.4 includes the same trend for the oil-based mud (OBM) contaminated sample.

Table 4.4 Composition used by Consultant A vs lumped in PhazeComp form C36+ composition reported by CoreLab. C*ontaminated* samples.

Component	**21364-IB, contaminated**		**34428-IB, contaminated**	
	Consultant A	PhazeComp	Consultant A	PhazeComp
	mole %	mole %	mole %	mole %
N2	0.5510	0.5514	0.4800	0.4800
CO2	1.8270	1.8268	2.2770	2.2770
C1	84.8540	84.8473	85.7250	85.7177
C2	4.5470	4.5474	4.9770	4.9772
:	:	:	:	:
:	:	:	:	:
C15	0.0730	0.0727	0.0620	0.0620
C16	0.0450	0.0449	0.0320	0.0320
C17-C18	0.0650	0.0653	0.0390	0.0393
C19-C23	0.0920	0.0908	0.0300	0.0409
C24-C80	0.0530	0.0601	0.0280	0.0267

To quantify the effect of the compositional difference in the heavier components, a comparison of the liquid dropout curve was made from a CCE experiment in PhazeComp. Figure 4.1 shows this graphically and Table 4.5 includes the PhazeComp reported root-mean-square error (RMS) from the experimental data for the two samples.

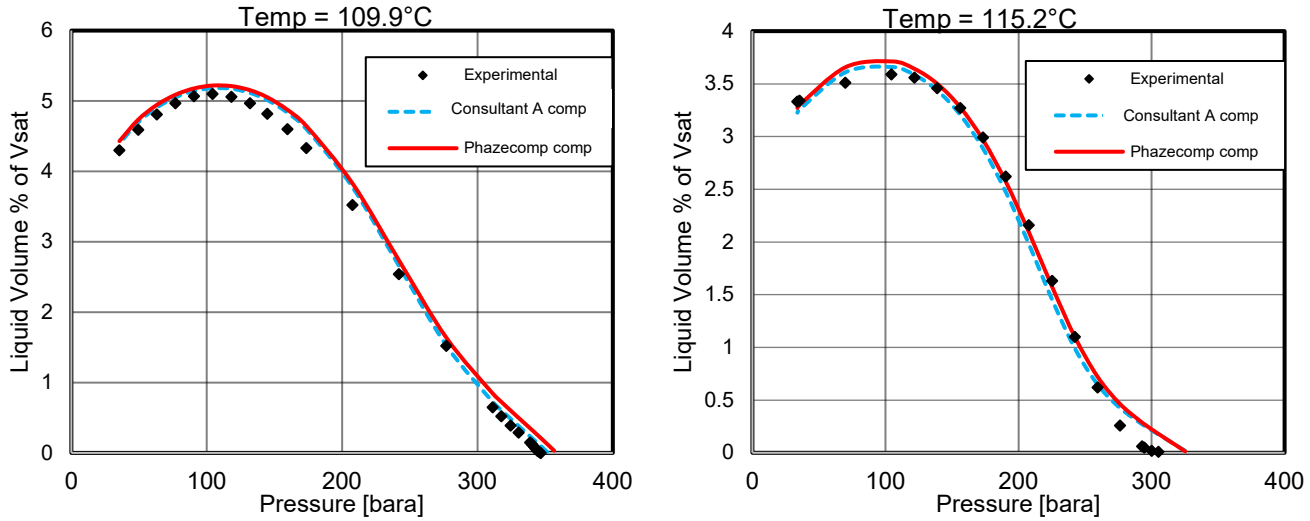

Figure 4.1 Sample 21364-IB and 34428-IB liquid dropout curve comparing Consultant A reported and PhazeComp calculated composition

Table 4.5 RMS % error from experimental data comparing calculations dne with compositions in table 4.3

	Sample 21364-IB - contaminated		Sample 34428-IB – contaminated	
	Consultant A comp	PhazeComp comp	Consultant A comp	PhazeComp comp
RMS % Err	**2.56**	**3.95**	**3.76**	**3.48**

The results presented in the table above indicate that the difference in composition makes a difference in the liquid dropout curve. For sample 21364-IB the Consultant A defined composition matches the experimental data better than the composition lumped in PhazeComp. For sample 34428-IB the situation is opposite.

The dewpoint is another other measured property that can be checked to quantify what difference the composition make. Table 4.6 summarizes the dewpoint calculated by the EOS for the different sample compositions and the measured dewpoint form the lab CCE experiments. In this case both the dewpoints calculated with the Consultant A reported compositions are closer to the measured dewpoint. The two checks done her can be an indication that Consultant A has allowed the composition to change to better match the liquid drop out curve and dewpoint for the contaminated sample. The effect is minimal, and one should keep in mind that the samples in the experiments are OBM-contaminated.

Table 4.6 Dewpoint from CCE experiment compared with calculated dewpoint from EOS

	Sample 21364-IB - contaminated			Sample 34428-IB – contaminated		
	Experimental	Consultant A comp	PhazeComp comp	Experimental	Consultant A comp	PhazeComp comp
p_d [bara]	**346.6**	**352.2**	**358.3**	**335.6**	**327.5**	**326.9**

4.3 Summary of Modifications to Original EOS

To be concise and without ambiguity, an EOS naming convention is used and defined together with an explanation of differences between each EOS used. In this section there will be four different names given in the figures:

- **DP-EOS-REPORT:** Black oil table generated in PVTsim by Consultant A. Found in the original ECLIPSE model discussed in Chapter 6.
- **DP-EOS-Phz:** The original Consultant A EOS imported into PhazeComp. Volume

shifts are calculated from the temperature dependent volume shifts used by PVTsim. No viscosity modifications are made (i.e. that nothing is done to get more realistic viscosities for the oil). The composition used is the exact composition that Consultant A uses.

- **DP-EOSmod-Phz:** The Consultant A EOS modified with new volume shifts (Soreide correlation) and LBC viscosity correlation discussed in this section (and in TPG4560 report). The composition used is the exact composition that Consultant A uses.
- **DP-EOSmod-Phz-x:** Same as "DP-EOSmod-Phz" only that the composition used is the one lumped in PhazeComp as discussed in TPG4560 final report and section 4.2. This is included this to verify what difference the small difference in composition does on the black oil table generation.

From the name giving above there are two major differences between the Consultant A original EOS and the modified version. The differences are described and corrected for as follows.

Volume shifts are in the Consultant A original EOS temperature dependent and is expressed in the EOS parameter table as two constants C_{pen} and C_{penT} with units [cm3/mol] and [cm3/mol °C] respectively. These parameters are used for calculating the temperature dependent volume shift parameter c_i for each component using Eq. (4.1). T_{ref} in the equation is 288.15 K according to the PVTsim user manual (CALSEP).

$$c_i = C_{peni} + C_{penTi}\left(T_R - T_{ref}\right) \tag{4.1}$$

PhazeComp only accepts volume shift factors in a dimensionless form which implies that c_i must be converted to a dimensionless form. Equation (4.2) is used for this conversion.

$$s_i = \frac{c_i}{b_i} \tag{4.2}$$

In the equation, b_i is the "repulsion" parameter in the Peng-Robinson equation defined in Eq. (4.3). The constant Ω_{bPR} = 0.007780 for Peng-Robinson.

$$b_i = \frac{RT_{ci}}{P_{ci}}\Omega_{bPR} \tag{4.3}$$

A significant inconsistency was found in the QC of the EOS imported into PhazeComp as a part of the research for the specialization project. The volume shifts found by using the procedure above, which is a consistent conversion of the volume shifts from PVTsim to PhazeComp, yielded non-monotonic increasing component densities when plotted against component molecular weight. This is non-physical behavior and corrections had to be made. Figure 4.2 shows the non-monotonic trend in the black dots and the correction in the blue dots. The correction is described under.

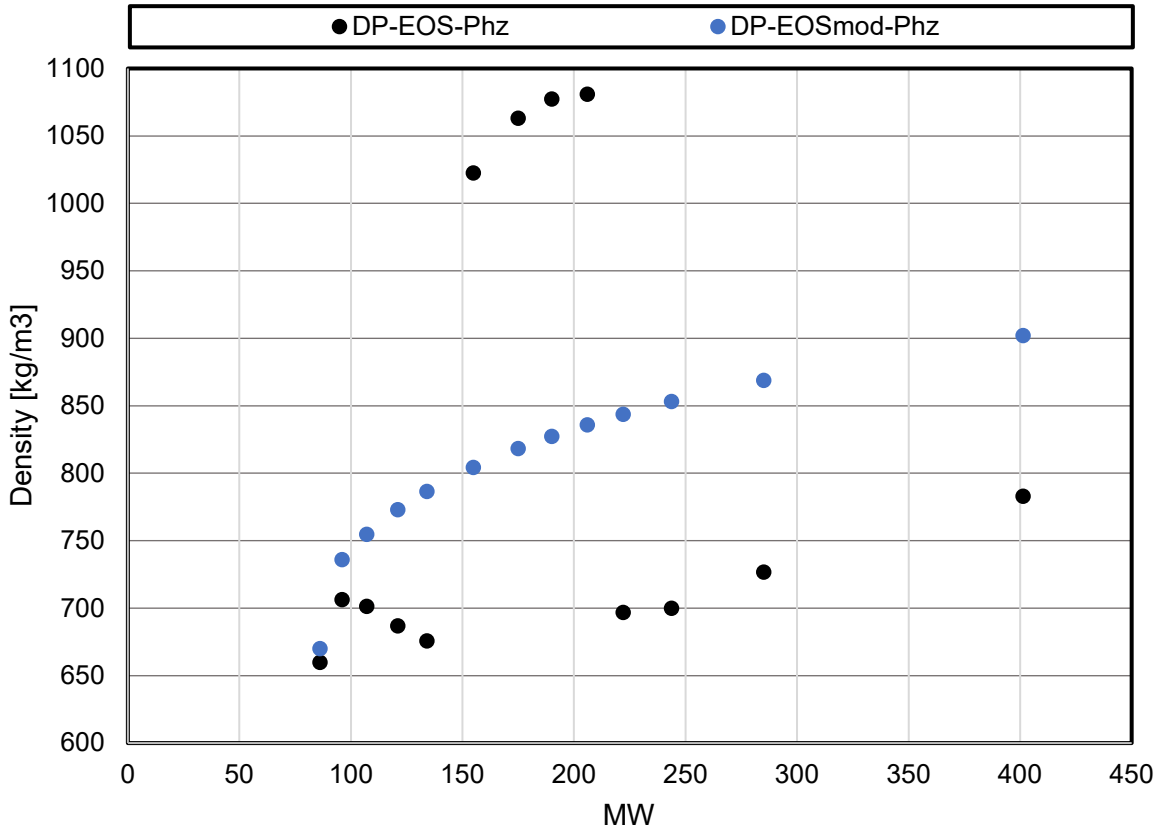

Figure 4.2 Monotonicity check for component densities at surface conditions

Oil density measurements do not exist in the CoreLab report of the laboratory tests done on the samples, which makes it impossible to match the densities to measured values. For this reason, the Soreide correlation in Eq. (4.4) was used with PhazeComp default constants (C_f = 29 and n = 13) to estimate specific gravities for C6+ components based on the molecular weights given in the EOS. Volume shift factors were then calculated in PhazeComp based on the new specific gravities.

$$\gamma_i = 0.2855 + C_f(M_i - 66)^n \tag{4.4}$$

The reservoir consists of three different zones where the new volume shift parameters obtained from the Soreide estimated specific gravities are assumed equal for each reservoir zone. Figure 4.2 shows the new component densities calculated at surface conditions plotted against molecular weight. The trend is monotonically increasing which means that the modified EOS predicts physically realistic component densities compared to the original Consultant A EOS imported to PhazeComp.

Viscosity modeling is the other major difference between the two EOS models considered in this study. Consultant A used the corresponding state principle viscosity model (CSP), which is the Pedersen model in this case. In PhazeComp and the modified EOS the LBC viscosity model is utilized. There is no reported tuning of the viscosity model to known viscosity correlations or condensate samples in the Consultant A EOS report. The reason for this could be that Consultant A assumes that the CSP method predicts the oil viscosity well enough. It is in fact known that the CSP method shows better prediction capability for oil viscosity compared to the LBC correlation by default, but the LBC correlation is the most widely used model due to the simplicity and flexibility (Yang et al. 2007) . The CSP method is not implemented in PhazeComp meaning that the LBC model is used.

Because the default LBC correlation predicts unrealistic oil viscosities the EOS model must be tuned to reliable viscosity data. As mentioned, there are no available separator oil viscosity data. This leads to tuning of the LBC model based on calculated viscosity data from viscosity correlations (Yang et al. 2007). The process used is as follows:

1. The method of Orrick and Erbar (Poling et al. 1987) is used to estimate reliable component liquid viscosities at atmospheric pressure and reservoir temperature in an excel sheet. In this case 109.9 °C is chosen (temperature of reservoir zone 1).
2. The estimated component viscosities are then inputted to PhazeComp in separate CCE experiments at surface pressure and reservoir temperature for each component starting from C_7.
3. The “Crit-Z” parameter in PhazeComp (i.e. the critical Z-factor) can change under regression to match exactly the inputted component viscosities.
4. The new set of “Crit-Z” values obtained from this process is used for the rest of the mixture calculations. The “Crit-Z” values are found in Table 4.1

A result of the process described above should be that the component viscosities increase monotonically when plotted against the molecular weight. Figure 4.3 includes this plot for the

untuned and tuned LBC model and as expected the trend is monotonic increasing for the calculated component viscosities using the tuned LBC viscosity model.

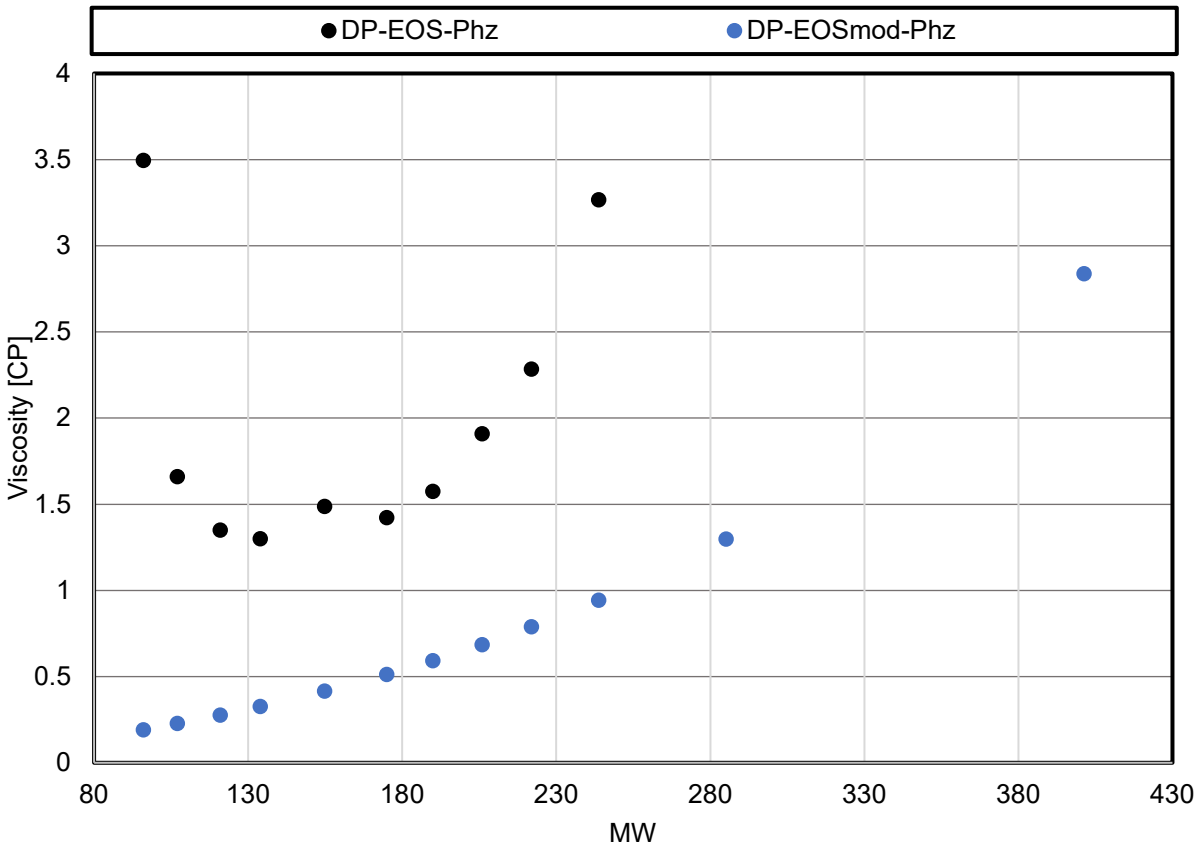

Figure 4.3 Monotonicity QC of component viscosity plotted against molecular weight.

Doing the modifications to the EOS in PhazeComp as described above ensured an EOS that in this case predicts physically realistic single carbon number component properties. More in depth QC of the EOS and the matching of the PVT experiments done by the CoreLab can be found in the project report for the specialization project included in Appendix C. It is shown that the other component properties summarized in Table 4.1 does follow a monotonic trend when plotted against molecular weight as they should (Younus et al. 2019).

4.4 Black Oil Tables

The first question that was raised under this topic was if the black oil tables reported by Consultant A could be remade using PhazeComp and the original EOS. Figure 4.4 includes plots of **DP-EOS-REPORT** and **DP-EOS-Phz** following the naming section 4.2. This is the comparison of the black oil tables **Before** the modifications was done to the EOS as discussed in the section above. The figure is for reservoir zone 1 with a reservoir pressure of 362.7 bara

and temperature of 109.9 °C.

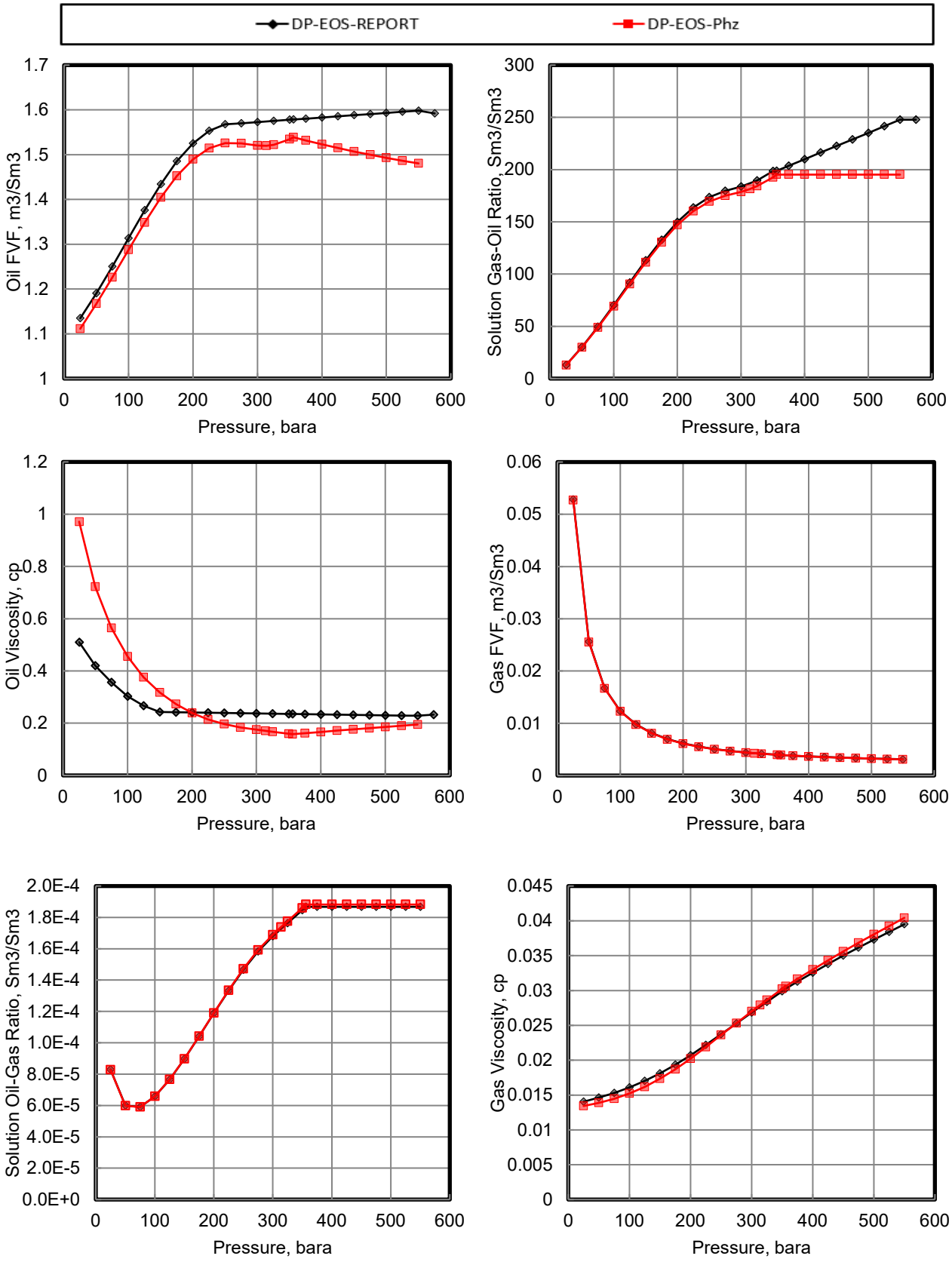

Figure 4.4 Black oil table comparison of "**DP-EOS-REPORT"** and "**DP-EOS-Phz"** for reservoir zone 1

From the figure the biggest differences are for the properties related to the condensate. That makes sense because of the lack of modifications to the LBC viscosity correlation at this stage (as discussed in the section above) and the lack of separator oil samples to match. The saturation pressure calculated for the composition used is 355.9 bara (Torheim 2019). It is also noticeable that the “DP-EOS-REPORT” data is extrapolated data with a linear trend after the saturation pressure (dewpoint).

The EOS with the modifications discussed in section 4.3 was used for making the same plots as above. The composition was still the same as used by Consultant A for the original black oil table (‘DP-EOS-REPORT’). This was given the name “**DP-EOSmod-Phz**” and the data plotted in Figure 4.5 under. Also included in that figure is the “**DP-EOSmod-Phz-x**” which is the same modified EOS used as DP-EOSmod-Phz, the only difference is that the composition lumped in PhazeComp as discussed in section 4.2 is used . Similar comparisons for reservoir zone 2 and 3 can be found in Appendix A where “**DP-EOSmod-Phz-x**” is compared with the original black oil tables generated by Consultant A “**DP-EOS-REPORT**”.

What can be seen from Figure 4.5 is that the modifications did some changes to the black oil tables, as expected. The main difference is in the viscosity of the oil, which is important for condensate blockage. The LBC viscosity model is used and tuned to relevant viscosities using the method of Orrick and Erbar as described in section 4.3 above. A varying condensate viscosity and slight differences in the other PVT properties seen in the modified EOS generated black oil tables compared to the original black oil table could potentially give differences in productivity forecast due to condensate blockage when doing a sensitivity study on the black oil table used in the reservoir simulation models.

For the base case models made for the study cases described in Chapter 6 and 7 the black oil tables made with the modified EOS and the PhazeComp lumped compositions will be used. In other words, the “DP-EOSmod-Phz-x” black oil table plotted in pink below.

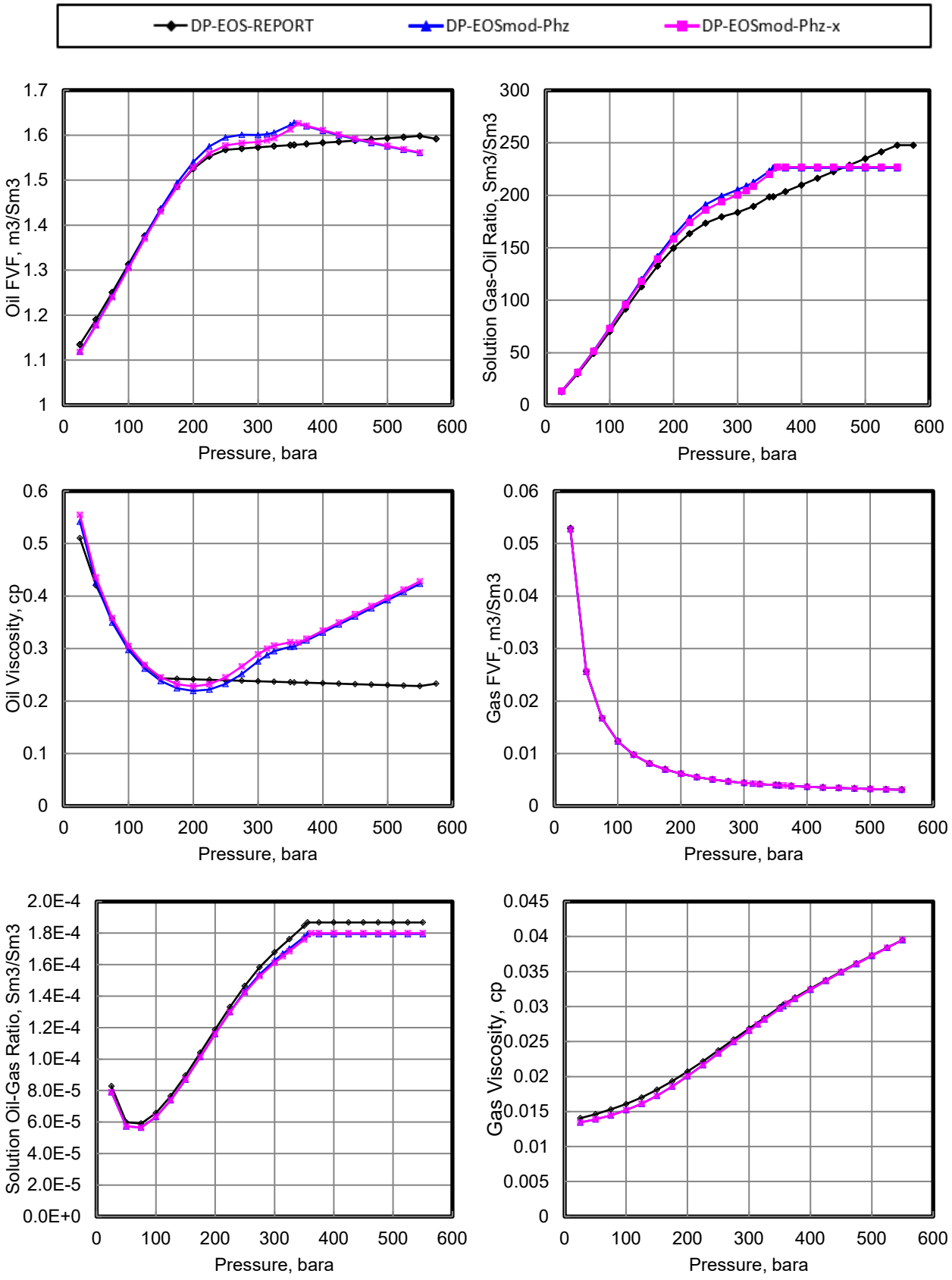

Figure 4.5 Black oil table comparison of "**DP-EOS-REPORT"**, "**DP-EOSmod-Phz"** and "**DP-EOSmod-Phz-x"** for reservoir zone 1.

5 Relative Permeability Considerations

As discussed in section 2.2 relative permeability is one the important properties when modeling condensate blockage, if not the most important. Having a model with relative permeability curves that yields a to high gas relative permeability will result in production forecasts that are too optimistic compared with reality. The same applies to having a too pessimistic set of relative permeability curves, giving an unrealistically large pressure loss in the near wellbore region (Region 1). It is therefore considered important to do a sensitivity study on the rel-perm of gas and oil to study the effects it has on condensate blockage.

This chapter is divided into two main parts. The first part is dedicated to the relative permeability data already existing in the model provided by Wintershall DEA and modifications made to the data. The second part focuses on the laboratory experiments done by Stratum reservoirs. In section 5.2 an introduction to the experiments for measuring relative permeability for condensate blockage (Region 1) is given, followed by the explanation of the lab setup and interpretation of the measured lab data in section 5.3.

5.1 Original Model Rel Perm Data.

The gas-oil relative permeability data from the original model was taken plotted in Figure 5.1 and included in Table 5.1.

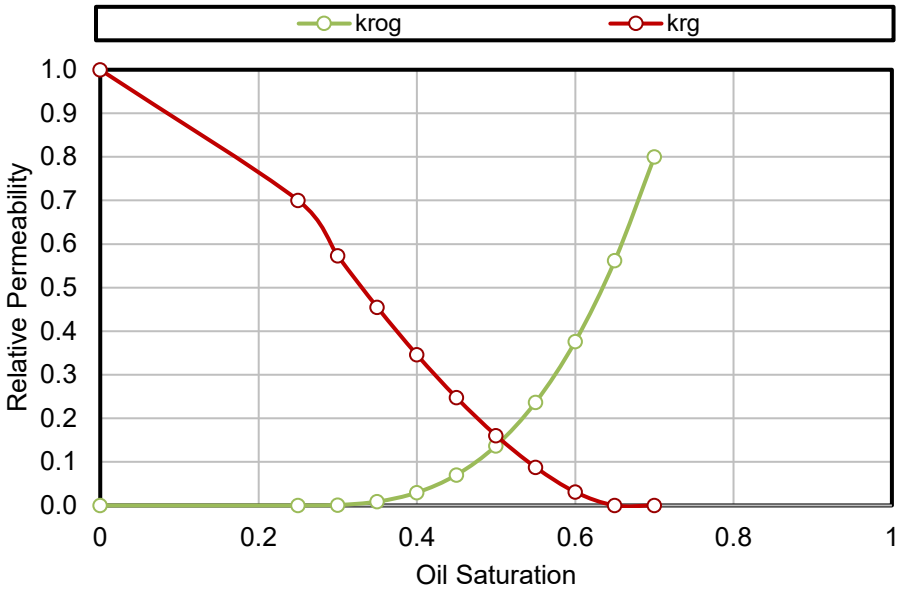

Figure 5.1 Gas-Oil rel-perm data from original model

Table 5.1 Gas-oil rel-perm data from original model. Blue = calculated values.

S_g	k_{rg}	k_{ro}	S_o	$\frac{k_{rg}}{k_{ro}}$
0	0	0.8	0.7	0
0.05	0	0.5619	0.65	0
0.1	0.0309	0.3764	0.6	0.08
0.15	0.0875	0.237	0.55	0.37
0.2	0.1607	0.1372	0.5	1.17
0.25	0.2475	0.0702	0.45	3.53
0.3	0.3459	0.0296	0.4	11.69
0.35	0.4547	0.0088	0.35	51.67
0.4	0.5729	0.0011	0.3	520.82
0.45	0.7	0	0.25	--
0.7	1	0	0	--

As discussed, the relative permeability in Region 1 is only a function of $k_{rg}/k_{ro}(p)$. Figure 5.2 includes a plot of k_{rg} vs k_{rg}/k_{ro} for the data in Table 5.1 This is a fundamental plot in concept of condensate blockage for Region 1.

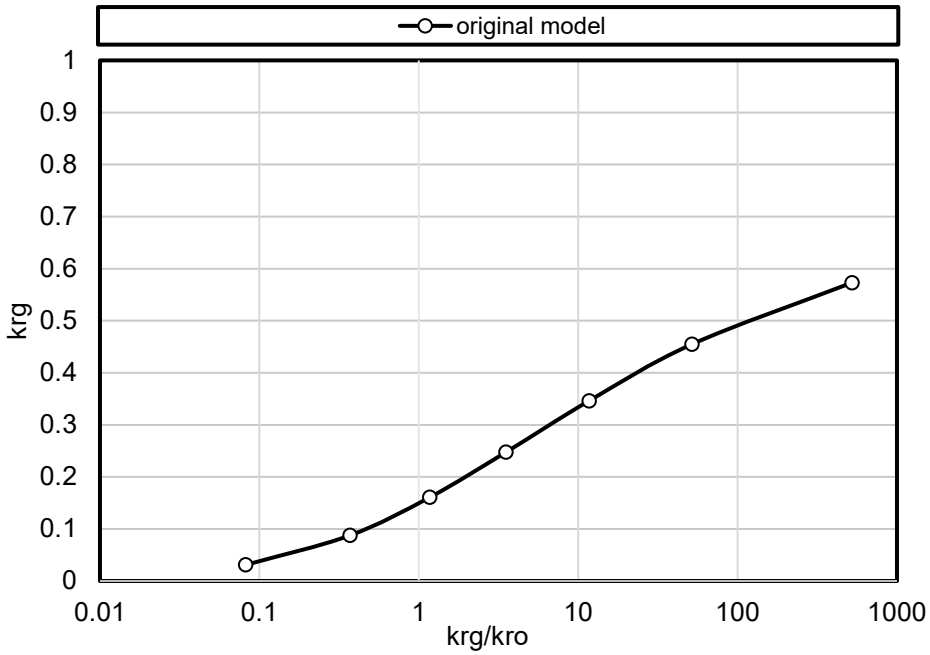

Figure 5.2 k_{rg} vs k_{rg}/k_{ro} original rel-perm data

From the figure it is found that at the crossing point of the relative permeability curves, i.e. k_{rg}/k_{ro} = 1, the value of k_{rg} is approximately equal to 0.16. This relative permeability curve is very optimistic, and certainly for a low-permeability rock as found in Field A. The usual upper limit of the crossing-point (k_{rg}/k_{ro} = 1) is k_{rg} = 0.1, applicable to higher-permeability rock. According to Fevang and Whitson in their paper on modelling gas condensate well deliverability condensate blockage is only dependent on the relative permeabilities within the range of

1<k_{rg}/k_{ro}<50. This usually represents gas and oil relative permeabilities ranging from 0.05 to 0.3 and gas relative permeability at low oil saturations, i.e. k_{rg} > 0.3, only affects deliverability for richer gas condensates (Fevang and Whitson 1995). As can be seen from the solution oil-gas ratio in the black oil tables included in section 4.4 and Table 7.2 the condensate considered in this thesis is lean. As a k_{rg} of 0.05 is the approximate lowest value in the relevant range of krg/kro the gas relative permeability data from Table 5.1 had to be modified to give k_{rg} = 0.05 at k_{rg}/k_{ro} = 1. This was done with a Corey function defined in Eq. (5.1) under.

$$k_{rg} = k_{rgro} * \left(\frac{S_g - S_{gc}}{1 - S_{org} - S_{wc} - S_{gc}} \right)^{n_g} \tag{5.1}$$

In the equation k_{rgro} is the relative permeability of gas at $S_o = S_{org}$ i.e. the residual oil saturation to gas. The gas saturation S_g is found in Table 5.1 , while the critical gas saturation S_{gc}, residual oil saturation S_{org} to gas and connate water saturation S_{wc} are all found in Table 5.2 below.

Table 5.2 Saturation table end-point values and exponent

S_{wc}	CONNATE WATER SATURATION	0.3
S_{gc}	CRITICAL GAS SATURATION	0.05
S_{org}	CRITICAL OIL SATURATION IN GAS AT CONNATE WATER	0.25
n_g	EXPONENT FOR ANALYTICAL k_{rg}	4.1

The exponent n_g was changed with a try and error approach until the k_{rg} value at k_{rg}/k_{ro} = 1 was approximately 0.05. As can be seen from the table n_g ended up being 4.1. With the modification done to the relative permeability of gas following Eq. (5.1) the data in Table 5.1 was modified to the data found in Table 5.3

Table 5.3 Modified Gas-oil rel-perm data from original model. Blue = calculated values

S_g	k_{rg}	k_{rg} modified	k_{ro}	S_o	$\frac{k_{rg}}{k_{ro}}$	$\frac{k_{rg}}{k_{ro}}$ modified
0	0	**0**	0.8	0.7	0	**0**
0.05	0	**0**	0.5619	0.65	0	**0**
0.1	0.0309	**0.0001**	0.3764	0.6	0.08	**0.0004**
0.15	0.0875	**0.0024**	0.237	0.55	0.37	**0.01**
0.2	0.1607	**0.0125**	0.1372	0.5	1.17	**0.09**
0.25	0.2475	**0.0408**	0.0702	0.45	3.53	**0.58**
0.3	0.3459	**0.1019**	0.0296	0.4	11.69	**3.44**
0.35	0.4547	**0.2152**	0.0088	0.35	51.67	**24.45**
0.4	0.5729	**0.4049**	0.0011	0.3	520.82	**368.08**
0.45	0.7	**0.7**	0	0.25	--	--
0.7	1	**1**	0	0	--	--

Figure 5.3 and Figure 5.4 show the changes in the curve for the relative permeability of gas and the change when plotted against k_{rg}/k_{ro}. This will later be used to quantify the importance of relative permeability in the condensate blockage study cases.

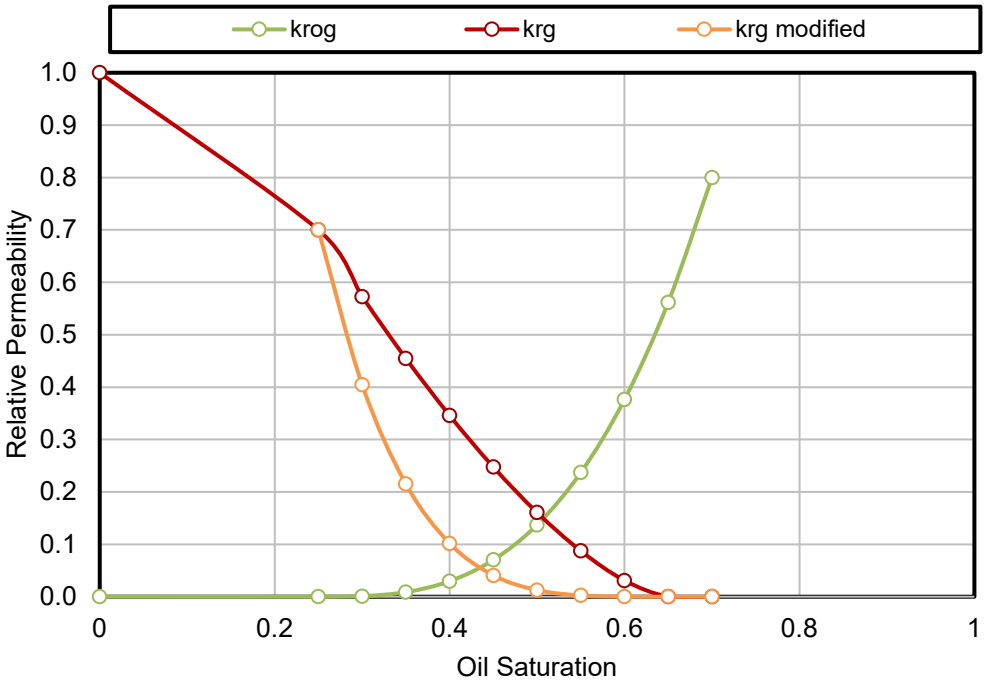

Figure 5.3 Gas-Oil rel-perm data modified

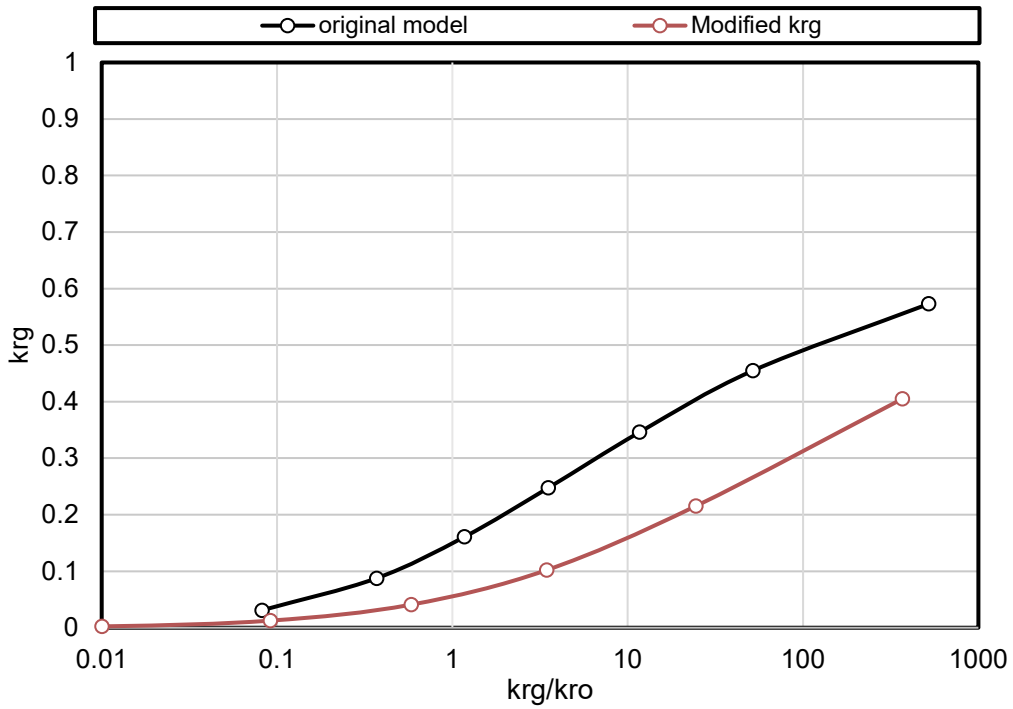

Figure 5.4 k_{rg} vs k_{rg}/k_{ro} modified rel-perm data

5.2 LAB Experiments for Measuring Relative Permeability

5.2.1 Steady State Laboratory Experiment.

The experiments order from STRATUM Reservoirs are in this case steady-state (SS) experiments. This is for replicating the flow near the wellbore, which is, for the purpose of condensate blockage studies, a pseudo steady-state process. Pseudo steady state means that there are SS conditions at a given time, but the steady state condition changes throughout depletion. The change in SS condition is reflected through different k_{rg}/k_{ro} ratios. Steady state simply implies that the mixture entering Region 1 (discussed in section 2.2) is the same mixture leaving. A core plug can be considered a volume element of the Region 1.

5.2.2 Fluid system

Fevang discusses three different fluid systems for performing relative permeability experiments in his PhD. These are reservoir fluid-, synthetic fluid- and simple fluid-systems. Experiments should be conducted at as near reservoir conditions as possible with actual reservoir fluids for best possible results (Fevang 1995). If this is not possible, for whatever reason, usable results can be obtained using synthetic or even simple fluid systems at ambient temperatures.

Reservoir fluid systems has the main advantage in avoiding large uncertainties in oil viscosities. In sample studies at the laboratories oil viscosity is almost never measured and viscosity correlations does not usually predict oil viscosity accurate (Fevang 1995). Consequences of not having correct oil viscosity is that oil saturation will be wrong as the oil mobility is a function of, amongst others, oil viscosity. Other benefits of having a reservoir fluid system is that the relevant k_{rg}/k_{ro}-ratio range is covered and having measurements at conditions like the actual conditions existing near the wellbore.

Synthetic fluid systems have the advantage that phase behavior and physical properties as a function of pressure and temperature may already be known or can be easily measured, and the conditions for retrograde condensation is closer to ambient conditions. This can save time and cost for the experiments and if the synthetic fluid system is selected properly, desired phase behavior can be obtained. To make sure that this phase behavior is obtained a design plot for both the reservoir gas and the synthetic gas condensate must be made and synthetic CVD gases will be chosen so that they cover the relevant krg/kro ratio (Fevang 1995).

Simple fluid systems are typically consisting of nitrogen gas (N_2) and a synthetic oil

representing the condensate. These systems are often used when the experiment is conducted at ambient pressure and temperature. In such experiments the phase behavior does not replicate the behavior in the reservoir and interfacial tension (IFT), and viscosity ratio is far from the actual gas condensate system in the reservoir. The advantages for a simple fluid system are that the equipment needed is much simpler leading to time and cost-efficient experiments.

The relative permeability from low-pressure experiments, as completed by STRATUM Reservoirs in this study, will provide the most pessimistic condensate blockage effect because they do not measure the potential improvement of k_{rg} due to high-flow capillary numbers. If reservoir/well modeling of the condensate blockage using these "immiscible" rock curves result in significant well deliverability loss, a high-pressure set of relative permeability lab tests should be run to quantify the capillary number improvement.

5.3 STRATUM LAB Results

STRATUM Reservoirs in Trondheim was provided with two core samples from Field A. Table 5.4 includes an overview of the two samples. The objective was implementation of steady state core flooding experiments designed for obtaining relative permeability data in the near wellbore region. Gas relative permeability, $k_{rg} = f(k_{rg}/k_{ro})$, is considered the most important relative permeability data when studying condensate blockage. As discussed in this section the experiments conducted for this study is using a *simple fluid system* and held at ambient pressures and temperatures.

Table 5.4 General core sample information used in calculations

Sample no.	Length (cm)	Diameter (cm)	Area (cm^2)	ϕ	k (md)
4	5.7	3.8	11.34	0.259	56.4
50	4.58	3.8	11.34	0.217	6.20

5.3.1 Designing the laboratory experiments

Having correct relative permeability data is one of the most important factors for getting the near wellbore modelling right. For Region 1 this is done by measuring k_{rg} at relevant k_{rg}/k_{ro} ratios for representative core samples. Plots of $k_{rg}/k_{ro}(p)$ for different stages of depletion are made using the EOS discussed in the project report for the specialization project TPG4560 and in section 4 of this report. These plots are used for designing relative permeability

experiments to secure relevance of the measurements done in the lab. All ten decontaminated samples discussed the TPG4560 report have a plot made. The included plots are three samples representing the three reservoir zones. The rest of the plots is found in Appendix C.

For the cores available from the Field A exploration well it is preferred to do experiments on three standard core plugs: a 1-md core, 10-md core and 50-md core approximately. The flow near the wellbore is as discussed, a steady-state process where, at any radius, the mixture entering a volume element is the same mixture leaving (Fevang and Whitson 1995). This means that steady state flow experiments through a core with different mixtures representing different k_{rg}/k_{ro} ratios would represent the volume element at different times of depletion. According to Fevang five of these mixtures should be run through each core with two different flow tests representing a lower and higher rate. The ratio for the tests should range approximately from a maximum of 50 to the minimum value calculated from Eq. (2.9) in section 2.2.1 (Fevang and Whitson 1995). From the figures following the lowest value is found in zone 1 (Figure 5.5), where k_{rg}/k_{ro} is approximately 5. From the figures below it was decided that a relevant range for the core experiments was from k_{rg}/k_{ro} = 5 to k_{rg}/k_{ro} = 100 (gray zones).

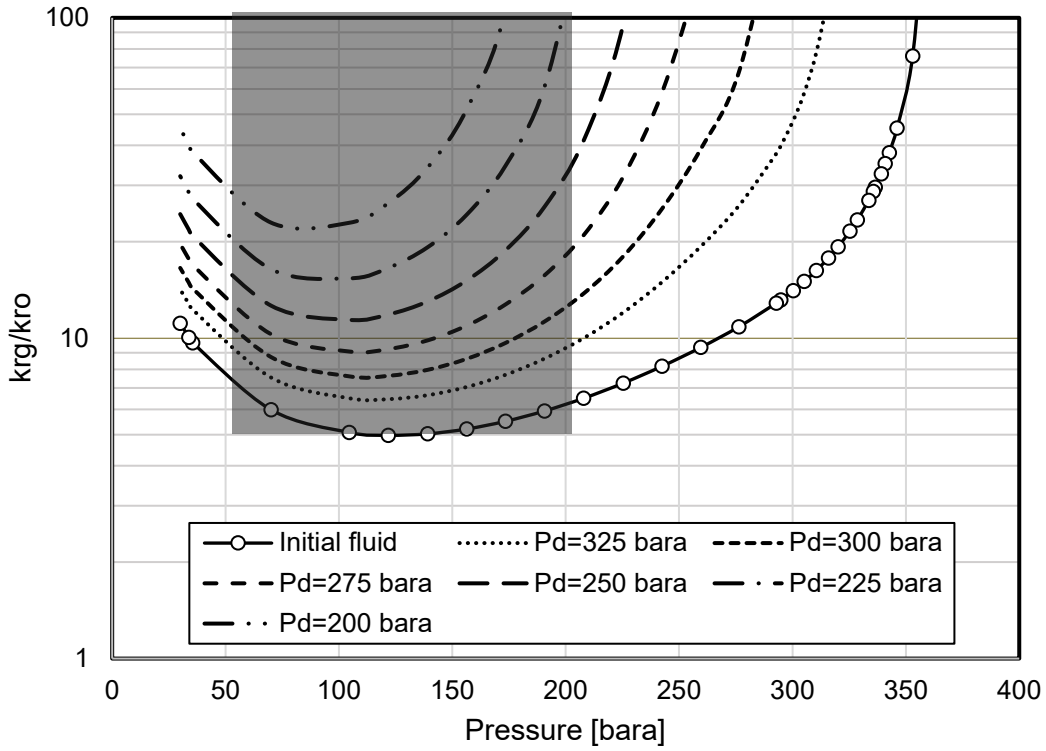

Figure 5.5 k_{rg}/k_{ro} for sample 21364-IB from reservoir zone 1. T_R = 109.9 °C and p_{Ri} = 362.7 bara, based on "**DP-EOSmod-Phz-x**" calculations

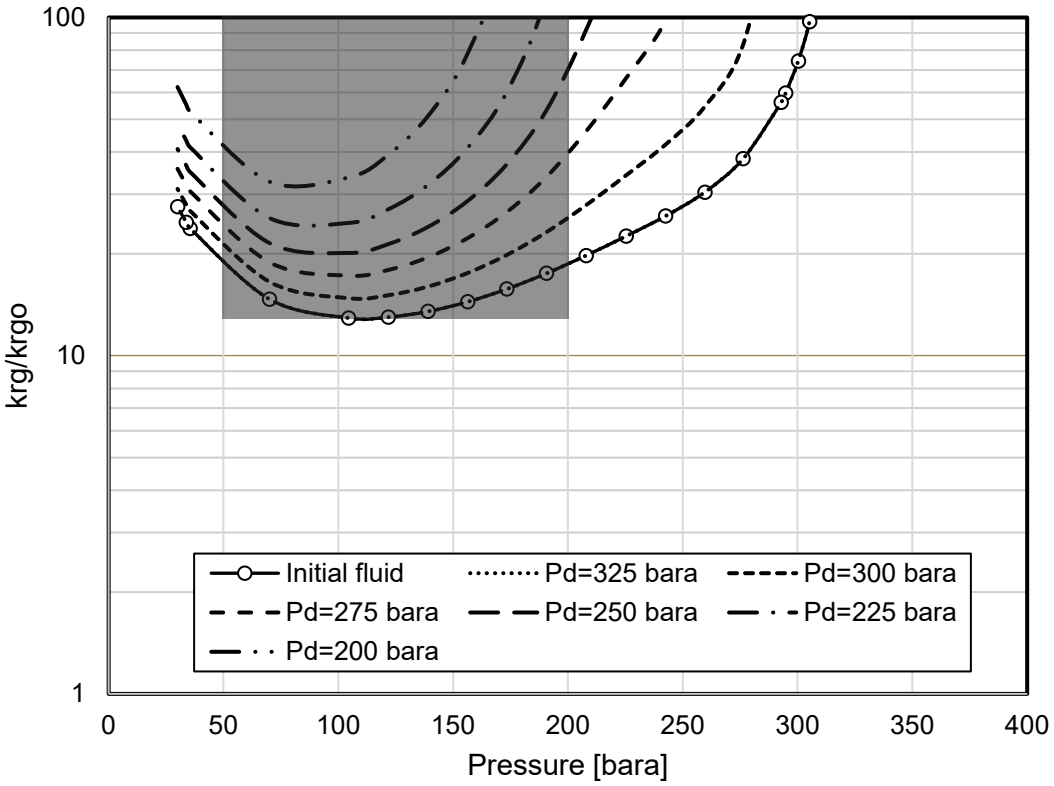

Figure 5.6 k_{rg}/k_{ro} for sample 34428-IB from reservoir zone 2. T_R = 115.2 °C and p_{Ri} = 374.3 bara, based on "**DP-EOSmod-Phz-x**" calculations

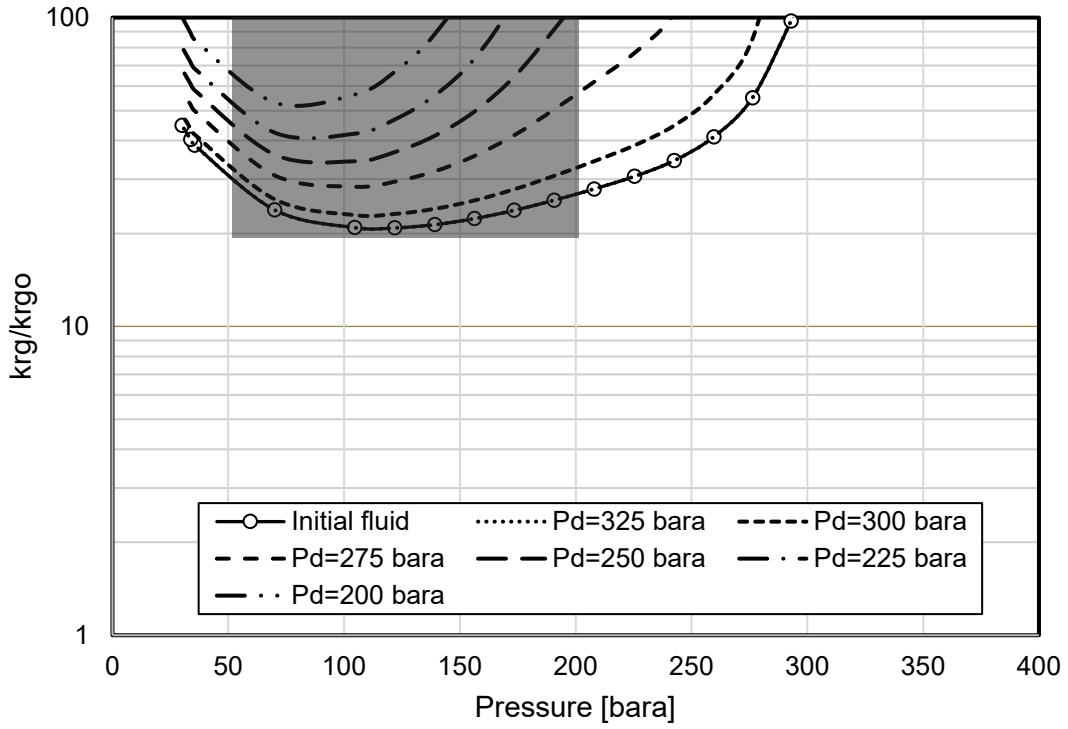

Figure 5.7 k_{rg}/k_{ro} for sample 28346-IB from reservoir zone 3. T_R = 121.2 °C and p_{Ri} = 385.7 bara, based on "**DP-EOSmod-Phz-x**" calculations.

Form STRATUM Reservoir information about the pumps that were used, and fluid properties was given. The Quizix type pumps used had a range from 0.001 cc/min to 50 cc/min both for the gas and oil phase. As it was decided to use a *simple fluid system* nitrogen (N_2) was the gas phase used and the oil phase was the synthetic oil "Isopar-L". The viscosity and density data of the Isopar L fluid was provided by the lab and is found in Table 5.5.

Table 5.5 Viscosity and density for the Isopar-L batch

Temperature (°C)	Viscosity (cp)	Density (g/cc)	Curve fitted data	
			Viscosity (cp)	Density (g/cc)
20	1.3084	0.7591	1.3085	0.7591
25	1.1941	0.7555	1.1934	0.7555
30	1.0914	0.7519	1.0921	0.7518
40	0.9226	0.7446	0.9233	0.7446
50	0.7904	0.7373	0.7896	0.7372
60	0.6837	0.7299	0.6823	0.7298
70	0.5949	0.7224	0.5951	0.7224

For both cores there should be two set of rates giving in the design, giving one lower and one higher rate run of the 5 k_{rg}/k_{ro} ratios. The design calculations assume k_{rg} values at the relevant k_{rg}/k_{ro} and uses Darcy's equation to calculate the rates for a rate relationship with the given viscosity. Eq (5.2) show the relationship used to calculate the relevant rates.

$$\frac{q_g}{q_o} = \frac{k_{rg}}{k_{ro}} * \frac{\mu_o}{\mu_g} \tag{5.2}$$

The equation is nothing more than the ratio of Darcy's equation for gas and oil solved for rate. From that relationship the design was calculated.

The first core designed for was the core sample with ID 4 in Table 5.4. The design was based on using a constant gas rate and changing the oil rate for generating the different krg/kro ratios required. Table 5.6 and 5.7 includes the design and the expected pressure drop calculated Darcy's equation for the higher permeability core. The Second core was based on having constant oil rates as the permeability if the core is much lower than the first core. Table 5.8 and 5.9 includes the design for the second core.

Table 5.6 Experiment design core sample 4, High rate

$\frac{k_{rg}}{k_{ro}}$	k_{rg} estimate	k_{ro}	$\frac{q_g}{q_o}$	q_o [cc/min]	q_g [cc/min]	Δp [atm]
5	0.12	0.024	332	0.1207	40	0.904
10	0.18	0.018	663	0.0603	40	0.603
20	0.22	0.011	1326	0.0302	40	0.493
50	0.35	0.007	3315	0.0121	40	0.310
100	0.5	0.005	6630	0.0060	40	0.217

Table 5.7 Experiment design core sample 4, Low rate

$\frac{k_{rg}}{k_{ro}}$	k_{rg} estimate	k_{ro}	$\frac{q_g}{q_o}$	q_o [cc/min]	q_g [cc/min]	Δp [atm]
5	0.12	0.024	332	0.0603	20	0.452
10	0.18	0.018	663	0.0302	20	0.301
20	0.22	0.011	1326	0.0151	20	0.247
50	0.35	0.007	3315	0.0060	20	0.155
100	0.5	0.005	6630	0.0030	20	0.108

Table 5.8 Experiment design core sample 50, High rate

$\frac{k_{rg}}{k_{ro}}$	k_{rg} estimate	k_{ro}	$\frac{q_g}{q_o}$	q_o [cc/min]	q_g [cc/min]	Δp [atm]
5	0.12	0.024	332	0.0070	2.321	1.638
10	0.18	0.018	663	0.0070	4.641	2.184
20	0.22	0.011	1326	0.0070	9.282	3.575
50	0.35	0.007	3315	0.0070	23.205	5.617
100	0.5	0.005	6630	0.0070	46.411	7.864

Table 5.9 Experiment design core sample 50, Low rate

$\frac{k_{rg}}{k_{ro}}$	k_{rg} estimate	k_{ro}	$\frac{q_g}{q_o}$	q_o [cc/min]	q_g [cc/min]	Δp [atm]
5	0.12	0.024	332	0.0035	1.160	0.819
10	0.18	0.018	663	0.0035	2.321	1.092
20	0.22	0.011	1326	0.0035	4.641	1.787
50	0.35	0.007	3315	0.0035	11.603	2.809
100	0.5	0.005	6630	0.0035	23.205	3.932

5.3.2 Lab setup

STRATUM Reservoirs in Trondheim was provided with the design presented in the section above. Figure 5.5 illustrates the set-up of the experiments. The experiments were conducted at ambient conditions. The pore pressure in the cores were hold constant at 5 bara and a sleeve pressure of 35 bara. As can be seen from the schematic drawing the two Quizix pumps flow gas and oil separately to a mixing point. From there the mixture is brought to the inlet of the core and pushed through. The differential pressure is measured over the core and is later used to calculate the relative permeabilities as discussed in subsection 5.3.3. The pump schedule follows the rates given in the design tables in section 5.3.1. As shown, a separator separates the nitrogen gas from the Isopar-L liquid and the fluids are directed back to the pumps. The experiments were first conducted on the higher perm core followed by the lower perm core.

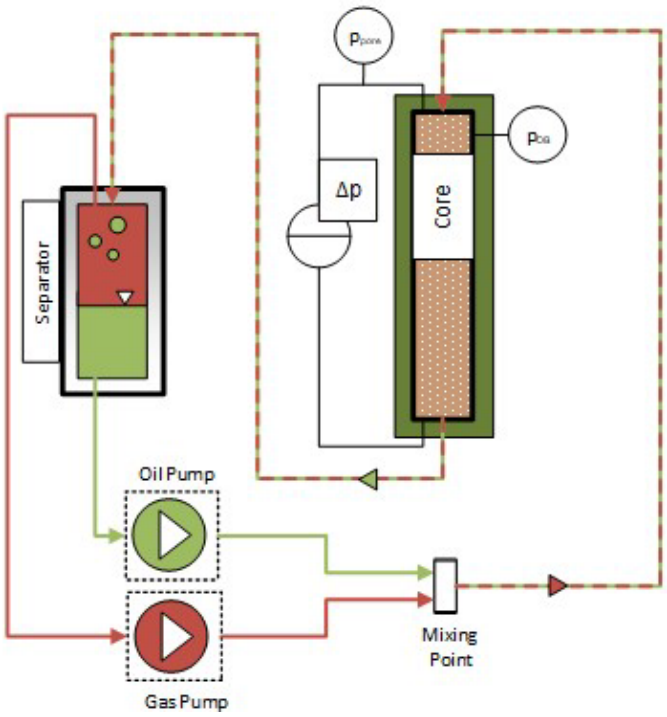

Figure 5.8 Schematic drawing of the laboratory experiment

5.3.3 Interpretation of the results

The measured data must be expressed in a form that can be read by the reservoir simulator. This means expressing the relative permeability data as functions of saturation. Conversion between the lab measured data to $k_{rg}(S)$ and $k_{ro}(S)$ is done by fitting the parameters in a relative permeability model e.g. Corey equation to the steady state k_{rg} vs k_{rg}/k_{ro} data. This is already done in section 5.1 when the original relative permeability data existing in the

reservoir model was modified. The laboratory data should be fitted with the same type of process.

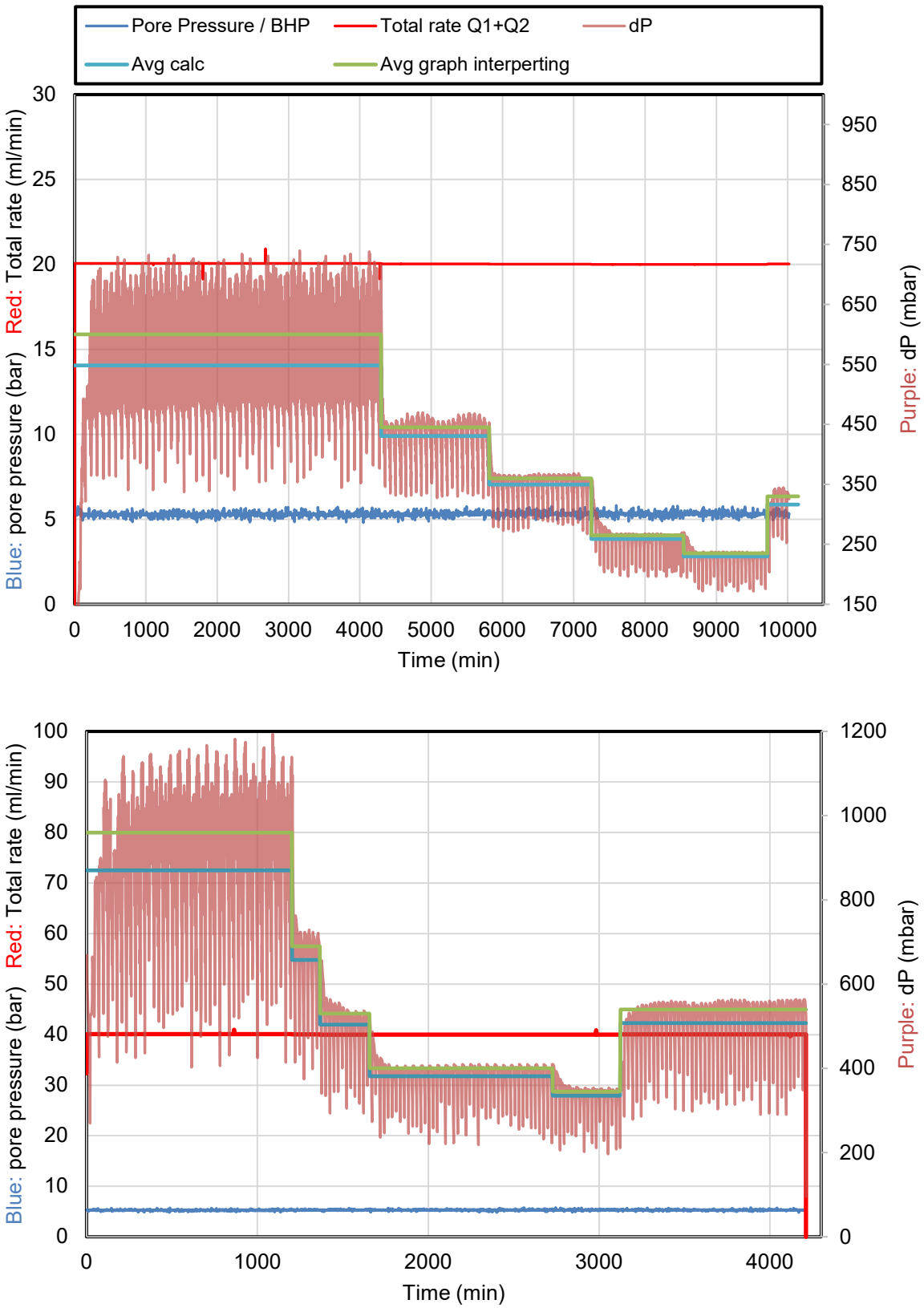

Figure 5.9 Results from lab experiments for core sample no.4

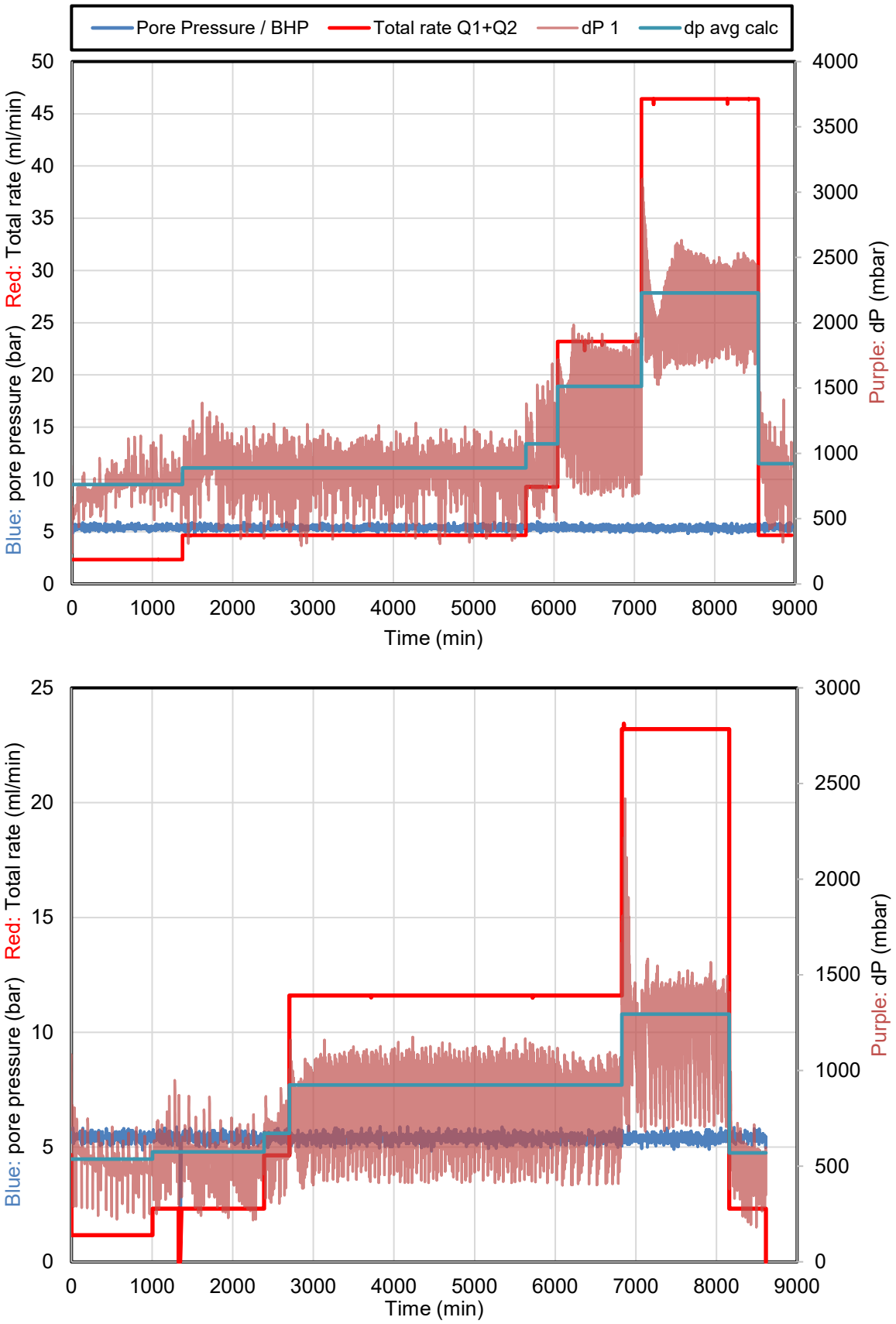

Figure 5.10 Results from lab experiments for core sample no.50

For calculating the relative permeability from the data, the differential pressure over the cores is needed. As can be seen from Figure 5.9 and Figure 5.10 above is that differential pressure varies with high tops and deep valleys. An average over the data was calculated in excel for all four experiments and is represented with the “Avg calc” in the figures. The lab was asked how such data should be interpreted, and the respond was to use an average in the top section. In other words, what is the correct differential pressure to use is up for discussion and no matter what average value is chosen, possible error must be considered. The “Avg graph interpreting” found in the plots in Figure 5.9 is an attempt to follow the average in the top section. For Figure 5.10 the “Avg calc” followed an average of the top section more acceptable and therefore no “Avg graph interpreting” was included.

From the differential pressure data, the relative permeability was calculated using Darcy’s equation presented in Eq. (5.3) under. The second rate for every case was repeated to verify the results and as can be seen from the plots of core sample no.4 the pressure drops over the core did not reach the same pressure drop.

$$k_{rg} = \frac{q_g \mu_g L}{kA\Delta p} \tag{5.3}$$

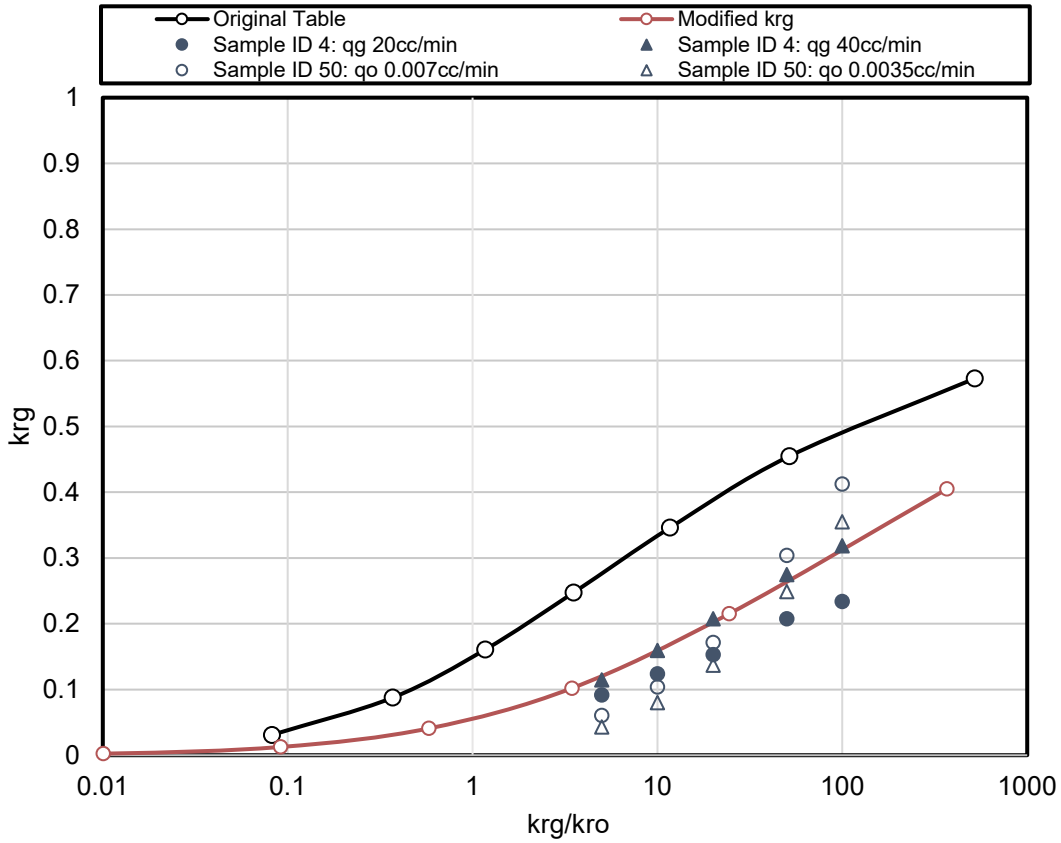

Figure 5.11 k_{rg} vs k_{rg}/k_{ro} modified rel-perm data included lab measured data

Figure 5.11 includes the lab measured relative permeability data obtained from the differential pressure over the cores. Uncertainty must be considered when interpreting the lab results due to uncertainty in the permeability used and assumptions made when designing the lab experiments. However, there is a clear trend that the original relative permeability data is way too optimistic, and the modified data is more in the ballpark of the lab reported data. Section 5.3.4 discussed effects not considered in the calculations.

One important uncertainty in this relative permeability study is the absolute permeability chosen to be the most representable for the cores, see Table 5.4. During the discussion with the laboratory different values have been given for different stages of the experimental process. When the experiments were done on sample ID 50, additional permeability measurements with the purpose of getting more reliable data was conducted. The range of permeabilities reported for the two cores is large, especially for sample ID 50, where the lowest measured permeability is 0.34 and the highest is 11.7 md. The available data is found in Table 5.10. fore core sample ID 4 the Klinkenberg corrected gas permeability is chosen representable for the core. As for core sample ID 50 the nitrogen flooded 4-point measurement is chosen representable for the core (even though it is not an absolute permeability).

Table 5.10 Permeability data reported for the cores from the lab

		Temp	Confining Pressure, bara		
Sample ID				**4**	**50**
Petrophysical measurements from Stavanger (full length)					
Klinkenberg corrected gas permeability, k_L	(md)	Ambient	20	56.4	1.14
Water permeability, k_w	(md)	Ambient	20	42.6	0.34
Petrophysical measurements					
Water permeability, k_w	(md)	Ambient	20	48.0	7.68
Primary drainage to S_{wi} other direction					
$k_g(S_{wi})$ -one-point measurement	(md)	Ambient	20	147.8	11.7
Ambient gas condensate - 5 bar pore pressure, amb. Temp.					
$k_g(S_{wi})$ -4-point measurement	(md)	Ambient	20	83.1	7.93
Propane flood @ 100 bar pore pressure					
$k_g(S_{wi})$ with Propane - 4-point measurement	(md)	Ambient	20		4.89
Nitrogen flood @ 5 bar pore pressure					
$k_g(S_{wi})$ with Nitrogen gas - 4-point measurement	(md)	Ambient	20		6.20

5.3.4 Effects Not Considered in the Lab Calculations.

Fevang discusses in his PHD that **capillary end effects** usually are neglected in the steady state experiments (Fevang 1995). If the steady state experiments are influenced by capillary end effects, it is more complicated to calculate the relative permeability. In the calculations in the section above three important assumptions are made, making it possible to use Eq. (5.3):

- The saturation is constant along the core
- The pressure gradient along the core is constant
- Gas and oil pressure are either equal along the entire core, or uniformly different by a constant capillary pressure.

The capillary end effect is due to that capillary forces existing in a porous medium tend to retain the wetting fluid, resulting in a higher wetting fluid saturation near the outflow end. The end effect creates a capillary transition zone near the outlet end which includes a saturation gradient in the core. The size of the region influenced by capillary end effects depends on the capillary pressure and fluid velocity. If fluid velocity is increased, the extent of the core effected by the capillary end effect decreases leading to that the fraction of the total pressure drop influenced by end effect decreases (Fevang 1995).

From Figure 5.11 the trend is that for the higher flow rates the relative permeability increases. The observation can be explained by that the capillary end effect less prominent for higher flow rates. One other possible explanation is the capillary number effect briefly touched upon in Chapter 9 over the recommendations for further work.

6 The Reservoir Model

The reservoir simulation software used in this study is Schlumberger's industry reference software ECLIPSE. Wintershall DEA provided a section of the full field model of Field A. Figure 6.1 shows the model of the full field. For doing condensate blockage studies the original model provided was converted from a high-resolution model in the z-direction to a model having hundred times less grid blocks in the respective direction in a synthetic model. This section is dedicated to describing the model and the process of converting to a model suited for condensate blockage studies.

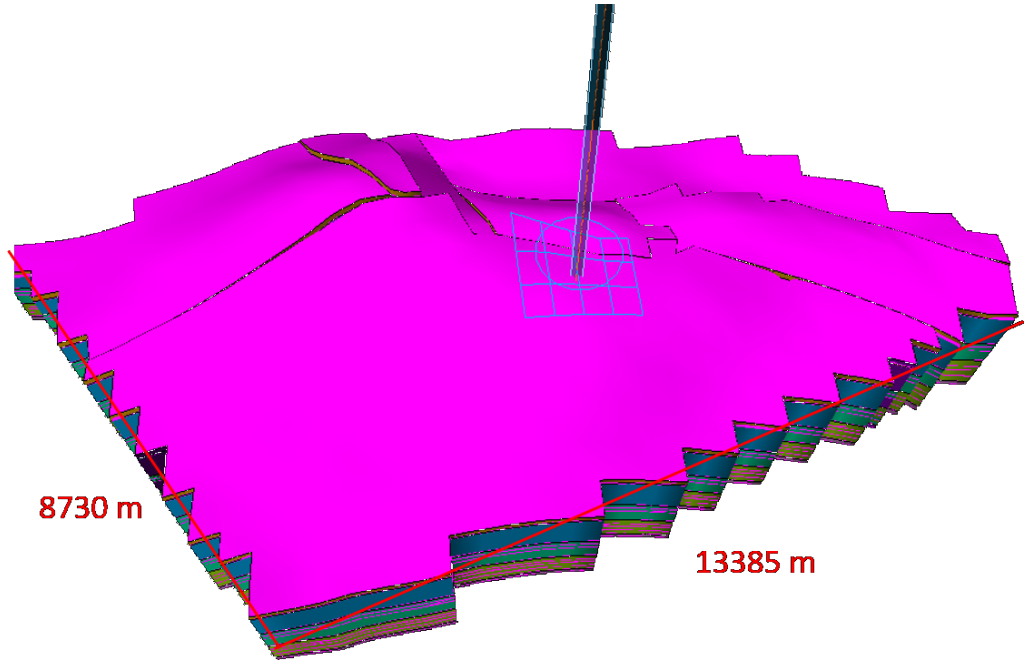

Figure 6.1 Full field reservoir model

6.1 The original model

The original model provided by Wintershall DEA was a snippet of a near well section of the full field model. Figure 6.2 shows the model from different angles and gives an estimate of the lengths of the sides and the height if the reservoir. In the model there are 4 grid blocks in the x-direction, 3 grid blocks in the y-direction and a total of 1995 grid blocks in the z-direction. All together this sums up to a model of 23940 grid blocks. The tops of the different grid blocks are varying.

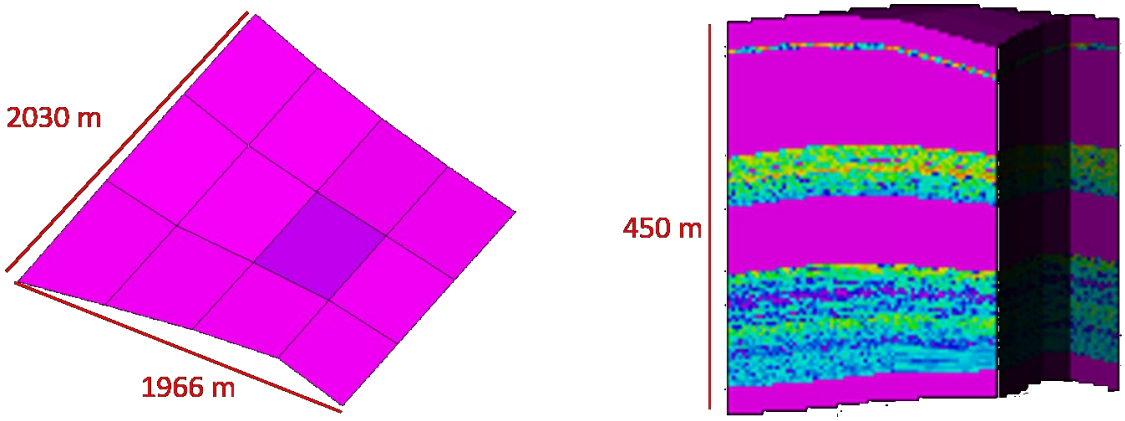

Figure 6.2 Overview of the reservoir model provided by Wintershall DEA. The values in red are approximate values

Table 4.1 includes some basic properties of the provided ECLIPSE model. The gas initially in place (GIIP) is used later as an approximate matching value for generating the synthetic model.

Table 6.1 Original ECLIPSE model basic properties.

Nx	Ny	Nz	Pore volume [Rm^3]	GIIP [Sm^3]
4	3	1995	8.612E+07	7.936E+09

6.2 Conversion of the Original Model to Synthetic Models

For the studies being performed in this master thesis the original single well model was converted from a high-resolution model in the z-direction to a synthetic model with lower resolution in the z-direction. The objective is to make a model that has grid blocks with approximately the same size in the x and y direction as would be found in a full field model and at the same time takes reduction in performance do to condensate blockage into account. The methodology for making the study models is to first make a base case model and from there make modifications to that model for studying different concepts and situations. Making a simpler model from the more complex original model is based on approximately replicating the GIIP in the provided original model to secure a similarity between to the synthetic model.

6.2.1 The Base Case Synthetic Model.

Generating the base case synthetic model is the first step in making the models needed for the study. The aim is to make a simple “box model” based on the original model provided from

Wintershall DEA. Figure 6.3 is a graphical representation of the model. This base case is later modified for doing sensitivity analyses discussed in Chapter 7.

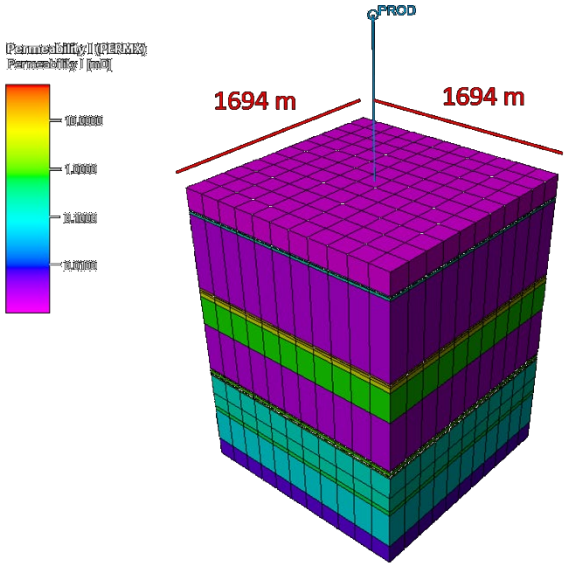

Figure 6.3 The base case model

The main goal for the base case model is to be a simpler synthetic model of the original single well model provided by Wintershall DEA. Approximately matching the GIIP of the original model is securing some similarity between the models. The following step by step process explains how the base case was made:

Step 1: *Exporting the data needed from the original single well ECLIPSE model*
The grid blocks the well is penetrating in the original model was chosen for getting the data the whole new synthetic model was based upon. This corresponds to grid block I = 3, J = 2 in every layer in the model. As can be seen from Figure 6.2 and Table 6.1 the original model is built up of three different reservoirs zones. In all these zones the resolution is high with very many layers. The “sealing zones” between the three reservoir zones represented using a single numerical layer. The data is gathered in an excel sheet manually from the .PRT file outputted from an ECLIPSE run of the model.

Step 2: *Converting from high resolution to low resolution in z-direction.*
This process is based on averaging methods for different parameters gathered in the excel sheet. The first parameter considered is the permeability (PERMX, PERMY and PERMZ) of the grid blocks. It was decided that the base case synthetic single well model should contain around 20 layers in the z direction. This resulted in dividing the first reservoirs zone in 3 layers, the second in 5 layers and the last in 10 layers. It is important to maintain the high permeability zones as they are contributing with the best completion intervals for the well. As the thickness

of reservoir zone 1 is small it is easy to maintain the high perm zones from plotting the permeability versus depth and manually decide the layer outline. For the other two zones an averaging method as follows is used:

- kh is calculated for every layer in the 1995 layered original model.
- The sum of kh is then calculated for every layer and cumulatively reported in every layer. The sum of kh of the present layer (e.g. layer 52) is the sum of kh of the layer above (layer 51) plus the kh of the present layer (layer 52). The sum is then normalized for each reservoir zone to go from 0 to 100
- Based on how many layers the reservoir zone is decided to have a ceiling function is used in excel to generate the layers, with the normalized sum of kh divided by 100 as an input. The ceiling function rounds a given number up to the nearest specified multiple (in our case 1).

Step 3: *Defining parameters for the new layers*

The parameters in the new layers are calculated by dividing the sum of the parameter from the old layers times the height of the old layers with the height of the new layer. This is shown under in Eq. (6.1) for the permeability as an example. The subscripts old and new refers to the original model and the simpler new synthetic model, respectively.

$$k_{new} = \frac{\Sigma k_{old} h_{old}}{h_{new}} \tag{6.1}$$

This process is repeated for every parameter relevant for building the new model. These values are used as a base for matching the synthetic model to the original models in place volumes and in step 5.

The following figure shows the properties plotted against the depth for permeability for the 22 layered synthetic model, with the original model's data plotted in the same plot. The other property plots can be found in Appendix B. Keep in mind the logarithmic scale on the x-axis in this particular plot.

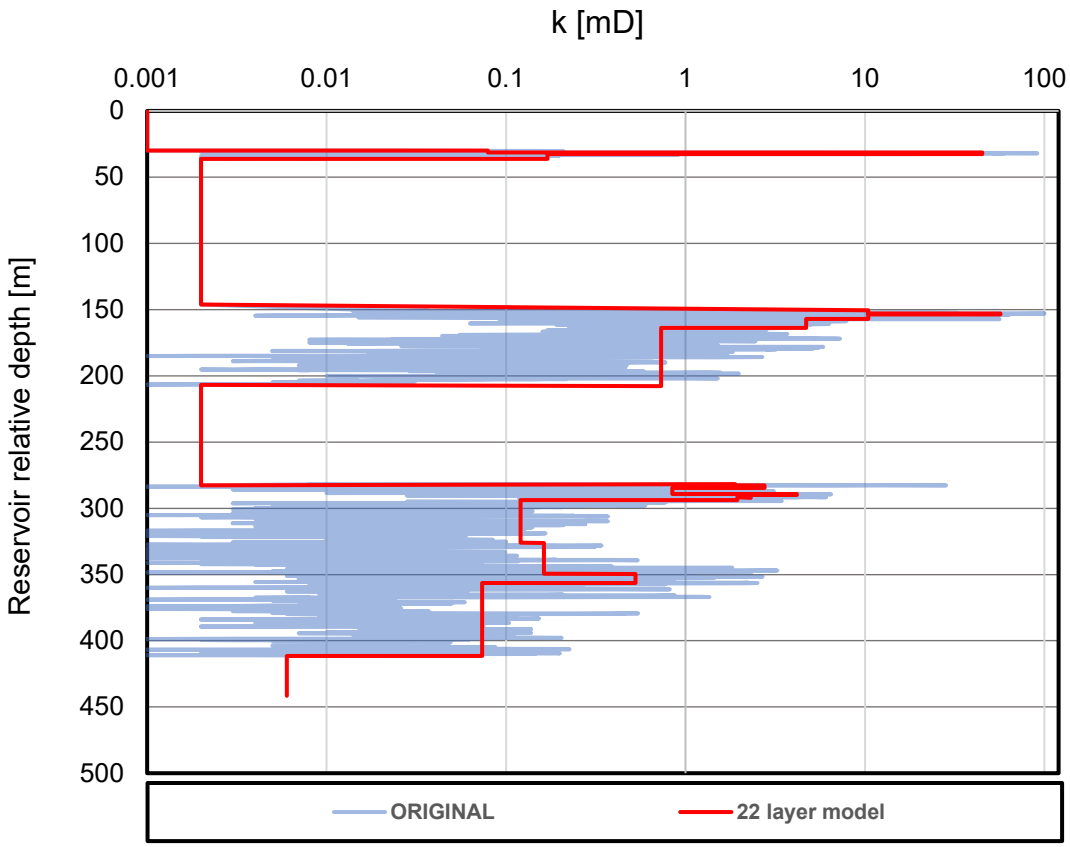

Figure 6.4 Permeability vs relative reservoir depth for the original and 22 layer model

Step 4: *The extension of the x and y sides of the model and the dimensions of the grid blocks.* The main goal for the base case is to get a GIIP that is close to the original model. Choosing an odd number of grid cells in the x and y direction is also important for placing the well in the middle of the model. For the base case it is decided that the grid block dimension should be around 150 meters. By using a try and fail approach for matching the GIIP volumes it is found that 11 grid cells in the x and y direction with a D_x and D_y of 154 meters gave a close match. With these parameters the length of x and y sums to 1694 meters. Table 6.2 summarizes this where the GIIP is approximately matching the original model (see Table 6.1), while the pore volume is larger for the synthetic model.

Keep in mind that the properties used in the synthetic model is only taken from the grid blocks where the original well is penetrating the original model. This could potentially lead to that the porosity data used give a higher pore volume than the original model, as the porosity data in the other grid blocks in the original model will vary compared to the grid blocks where the well is penetrating. The most important property to capture correctly is the permeability as the study objective is condensate blockage effects of the near wellbore region.

Step 5: *Modifications of the Base Case*

To get a broader understanding of how the number of grid cells and their size affects the production of a reservoir model two models with modifications to the grid of the base case was built. Two other models were made from the synthetic base case model with changes in the number of and dimension of grid cells in the x and y direction. The pore volume and GIIP is kept equal for all three cases. This is shown in Table 6.2.

Table 6.2 Base case and modified base case properties

Model note	Nx	Ny	Nz	Dx [m]	Dy [m]	Pore volume [rm^3]	GIIP [sm^3]
Base	11	11	22	154	154	1.122E+08	8.14E+09
Base mod 1	17	17	22	99.647	99.647	1.122E+08	8.14E+09
Base mod 2	7	7	22	242	242	1.122E+08	8.14E+09

The fluid models that are used in all base case models, and other sensitivity models in this study if nothing else is specified, are the black oil tables discussed in section 4.4 of this thesis: "**DP-EOSmod-Phz-x**"

6.2.2 Fine Grid Radial Model

A radial model will generate a denser grid near the wellbore and will therefore take near wellbore flow behavior into account in the simulation. A single well radial model will represent one of the wells simulated in a full field model using local grid refinement. The base case radial model was decided to have 20 grid cells in the radial direction, covering an area equivalent to the synthetic course grid model. Figure 6.5 shows the radial model with 20 grid blocks in the radial direction. In the θ-direction there is only one grid block resulting in that the model is only built up of 20 full circles (or rings) that gets dense in the near wellbore region.

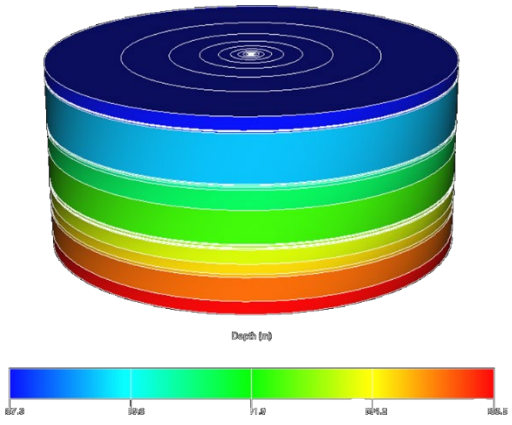

Figure 6.5 The radial base case model

Other radial models were also made with different resolution in the radial direction. The different cases are summarized in Table 6.3 where the only parameter changing is the number of grid cells in the radial direction.

Table 6.3 Radial model and modifications

Model note	Nr	Nθ	Nz	INRAD [m]	OUTRAD [m]	Pore volume [Rm^3]	GIIP [Sm^3]
Base rad	20	1	22	0.09525	955.7	1.122E+08	8.14E+09
Base rad mod 1	10	1	22	0.09525	955.7	1.122E+08	8.14E+09
Base rad mod 2	40	1	22	0.09525	955.7	1.122E+08	8.14E+09

6.2.3 Models with Generalized Pseudopressure Well Treatment

The same models made in section 6.2.1 were also made with the GPP option discussed in Chapter 3. These models are aiming to take condensate blockage into account without having to have a fine grid close to the wellbore. The difference in the models is in the WELSPEC section of the ECLIPSE file where the only thing that is changing is that the GPP option is added to the well as described in section 3.2.1.

7 Simulation Results and Discussion

Now that the fluid models for the three different zones is verified and the original single well model is converted into a simpler synthetic model research and studies can be completed. A set of study cases will be performed as described in table 7.1 where the objective is divided into two main parts. The first is to investigate the effect condensate blockage has on the deliverability of the well in this Field A, the second is a verification that the GPP method in a coarse grid model predicts the condensate blockage effects acceptable compared to the fine grid models.

7.1 The Study Cases

Table 7.1 Overview of study cases

Case model name	Comment
Base case study cases	
BB-E100-COURSE-DX150	Base case cartesian model
BB-E100-COURSE-DX150-GPP	Base case cartesian model with GPP option
BB-E100-RADIAL-NR20	Base case fine grid radial model
Size and number of grid cells study cases	
BB-E100-COURSE-DX250	Sensitivity on lower number of grid cells
BB-E100-COURSE-DX100	Sensitivity on higher number of grid cells
BB-E100-COURSE-DX250-GPP	Sensitivity on lower number of grid cells
BB-E100-COURSE-DX100-GPP	Sensitivity on higher number of grid cells
BB-E100-RADIAL-NR10	Sensitivity on lower number of grid cells
BB-E100-RADIAL-NR40	Sensitivity on higher number of grid cells
Study cases with new relative permeability data as discussed in section 5.3	
BB-E100-COURSE-DX150-RelPermMod	Modified relative permeabilities based on the findings in section 5.3. A "worst case" with k_{rg} = 0.05 at k_{rg}/k_{ro} = 1 is used here
BB-E100-COURSE-DX150-GPP-RelPermMod	
BB-E100-RADIAL-NR20-RelPermMod	
*Study cases with fluid model found in original model "**DP-EOS-REPORT**"*	
BB-E100-COURSE-DX150-OrgBOT	Sensitivity study on using the original black oil tables instead of the modified found in the base case model
BB-E100-COURSE-DX150-GPP-OrgBOT	
BB-E100-RADIAL-NR20-OrgBOT	
Reservoir Quality sensitivity	
BB-E100-COURSE-DX150-k*10-kv/kh=0.5	Permeability multiplied by 10 in all directions
BB-E100-COURSE-DX150-GPP-k*10-kv/kh=0.5	
BB-E100-RADIAL-NR20-k*10-kv/kh=0.5	
BB-E100-COURSE-DX150-k*10-kv/kh=0.05	Same as above, with original k_v/k_h = 0.05
BB-E100-COURSE-DX150-GPP-k*10-kv/kh=0.05	
BB-E100-RADIAL-NR20-k*10-kv/kh=0.05	

Following is a table of the basic reservoir fluid. Well completion and production constraints are also included. In all cases except the "*Study cases with fluid model found in original model "**DP-EOS-REPORT**"* from Table 7.1 the fluid under the name "Base Case" from Table 7.2 is used. The well completion and production constraints found in Table 7.3 applies to all sensitivity cases if nothing else is specified for a specific case.

Table 7.2 Key reservoir fluid properties

Key reservoir fluid properties			
		Base case	***DP-EOS-REPORT****
Zone 1	Initial Reservoir Pressure, bara	362.7	362.7
	Initial Reservoir Temperature, °C	109.9	109.9
	Dewpoint pressure, bara	362.6	356
	Maximum CVD Liquid Dropout V_{roCVD}, %	3.86	--
	Initial Solution OGR r_{si}, sm3/sm3	1.811e-04	1.867e-04
	STO API Gravity, °API	53.65	52.6[1]
Zone 2	Initial Reservoir Pressure, bara	374.3	374.3
	Initial Reservoir Temperature, °C	115.2	115.2
	Dewpoint pressure, bara	319.5	316.3
	Maximum CVD Liquid Dropout V_{roCVD}, %	2.38	--
	Initial Solution OGR r_{si}, sm3/sm3	9.993e-05	1.029e-04
	STO API Gravity, °API	53.59	51.03[1]
Zone 3	Initial Reservoir Pressure, bara	385.7	385.7
	Initial Reservoir Temperature, °C	121.2	121.2
	Dewpoint pressure, bara	310.0	314.0
	Maximum CVD Liquid Dropout V_{roCVD}, %	3.19	--
	Initial Solution OGR r_{si}, sm3/sm3	8.217e-05	8.562e-05
	STO API Gravity, °API	54.21	52.99[1]
Separator conditions: 1st stg 86 bar/40°C, 2nd stg 10 bar/50°C, 3rd stg 3 bar/60 °C * : Sensitivity model in section 7.2.3 [1]: Single stage flash -- : not reported in Consultant A report for decontaminated composition			

Table 7.3 Well completion and production constraints

Well completion, production constraints	
<u>Well completion:</u>	
Well type	Single vertical well in the center for the reservoir
Completed interval of well	Perforated in all reservoir zones
Wellbore radius, m	0.09525
Skin factor, s	0
original k_v/k_h	0.05
<u>Production constrains:</u>	
Max production rate, Sm^3/D	1E6
Minimum BHP, bara	100

7.2 Simulation results

This section is dedicated to presentation and discussion of the simulation results from the study cases presented in table 7.1. Every sensitivity study is presented and discussed in a new subsection. The first subsection “Base Case Study” is proving the importance of taking condensate blockage into account for this gas condensate field even with an optimistic relative permeability data set. Following subsections discussed different situations and sensitivities of parameters impact on the well performance.

7.2.1 Base Case Study

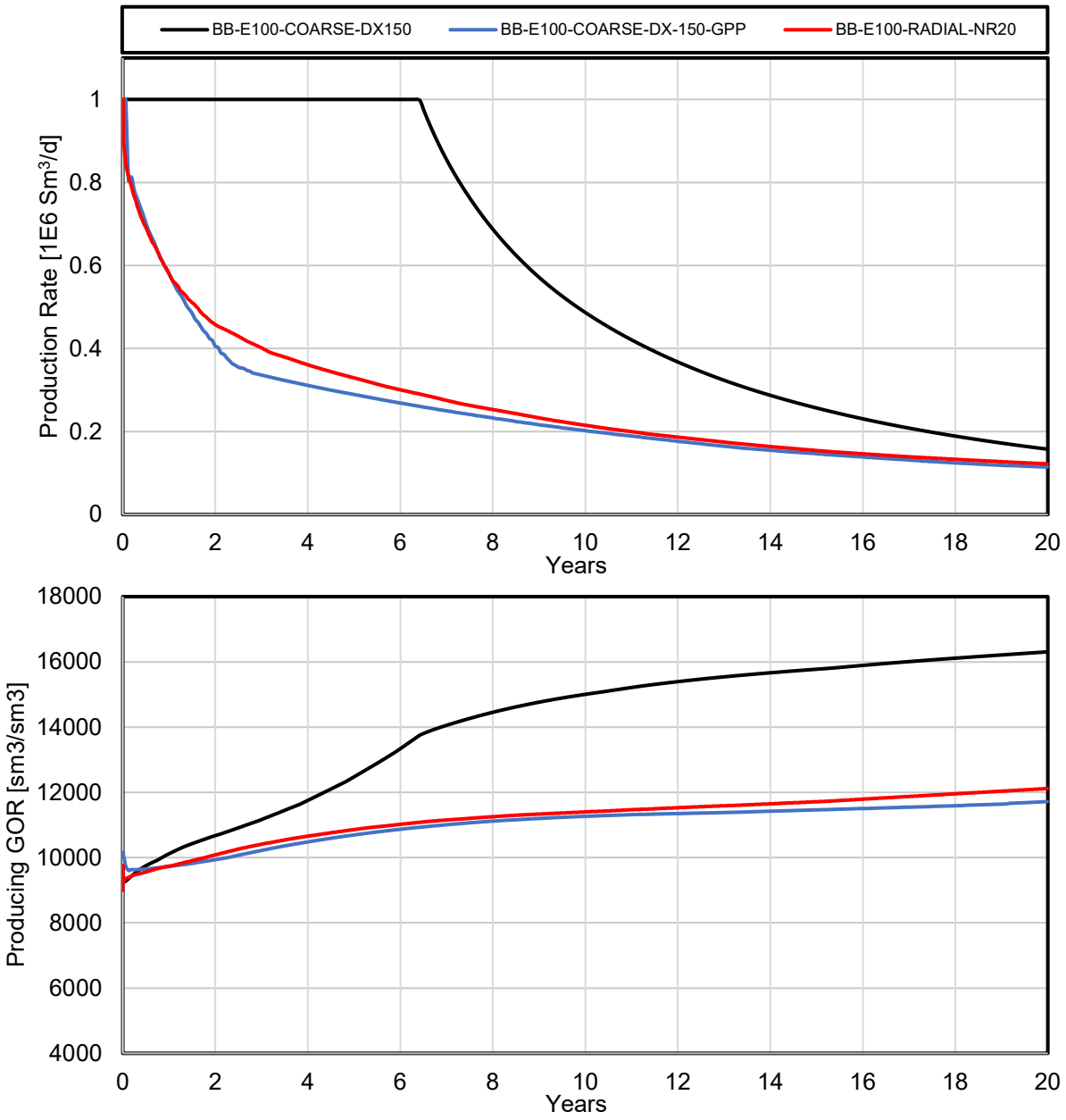

Figure 7.1 Base case coarse, GPP and fine grid radial model: Gas prod rate and GOR

The fine grid radial model and course grid models all had the same production constraints, with a maximum production rate of 1E6 Sm^3/d and a minimum bottom hole flowing pressure of 100 bara. Comparative reservoir performance predictions for the fine-grid radial model and the coarse grid models with and without the GPP, is shown in Figure 7.1. The gas-production plateau for the coarse grid model is approximately six and a half years before the well goes on decline, while the fine grid radial model does not show a plateau period. This is a representation of the big impact ignoring near wellbore effects, i.e. condensate blockage, will have on the gas condensate well. The coarse grid model with the GPP option applied to the well is giving similar results as the fine grid radial model, proving that the GPP option is replicating the condensate blockage effects.

Figure 7.2 shows the well BHFP and average reservoir pressure for the three different base cases. The gas production declines when the BHPF goes on the constraints set to the well. Due to condensate blockage the BHFP drops rapidly for the fine grid radial model and coarse grid model with GPP option. The GOR plot in figure also show what is reflected in the production and pressure plots, where the GOR increases rapidly as the well is on its plateau period for the course grid model without near wellbore effect treatment. As the well goes on decline, the GOR increases less rapidly as expected as the pressure in the reservoir increase at a lower rate. If the coarse grid model without the GPP option is used in a full-field simulation model gas-rate performance will be very optimistic.

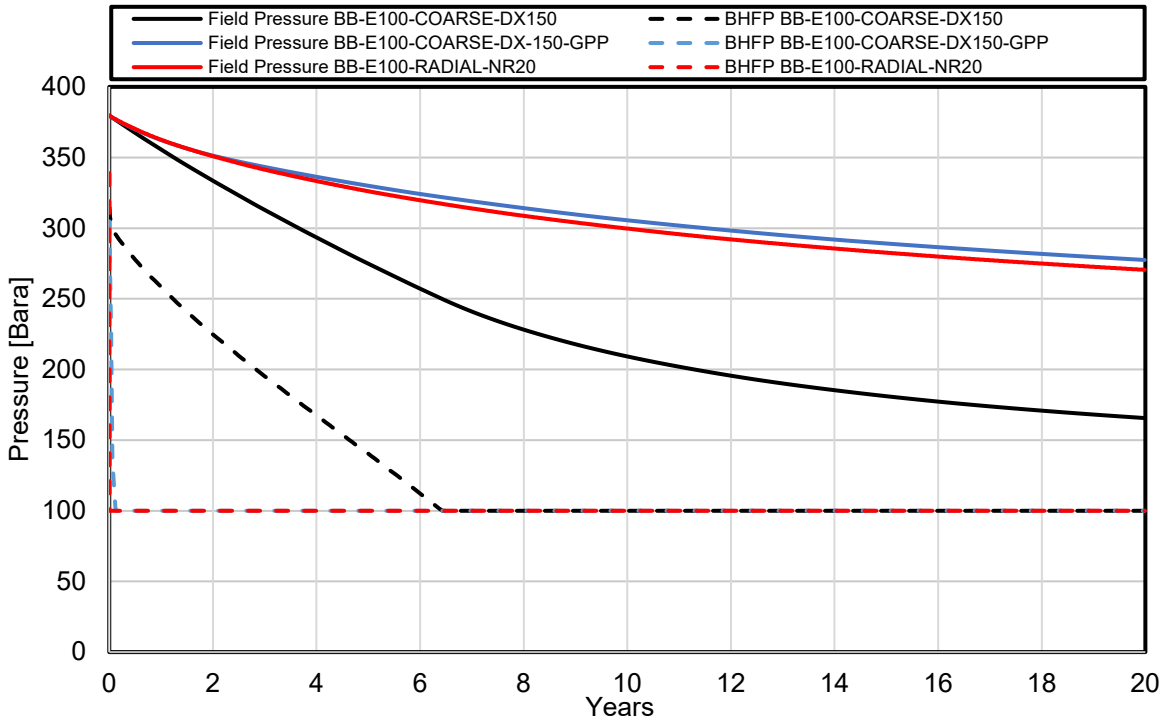

Figure 7.2 Base case coarse, GPP and fine grid radial model: BHFP and avg reservoir pressure

7.2.2 Grid Cell Dimension Sensitivity

Simulation models are sensitive to grid cell size. The general trend in models with “traditional” cores grid cells is that with a denser grid (i.e. larger amount of grid cells with a smaller dimension) give a less optimistic performance. This is explained by that more gird cells gives the model more room to calculate realistic rates as there are more points of calculation. The reason fine grid models are used in the near well region is to capture the pressure drop accurately, which is not captured with a coarse grid model. Figure 7.3 shows that a “traditional” coarse grid model gives a longer plateau for a model with less grid cells and larger dimension than the base case of DX = 150 meters. A model with more grid cells and a smaller dimension gives a shorter plateau period. What can be seen is that the difference is smaller in amount from the model with DX = 250 to the base case, compared to the DX = 100 case. Eventually one will reach a point where the effect of getting a more optimistic production with larger grid cells is neglectable.

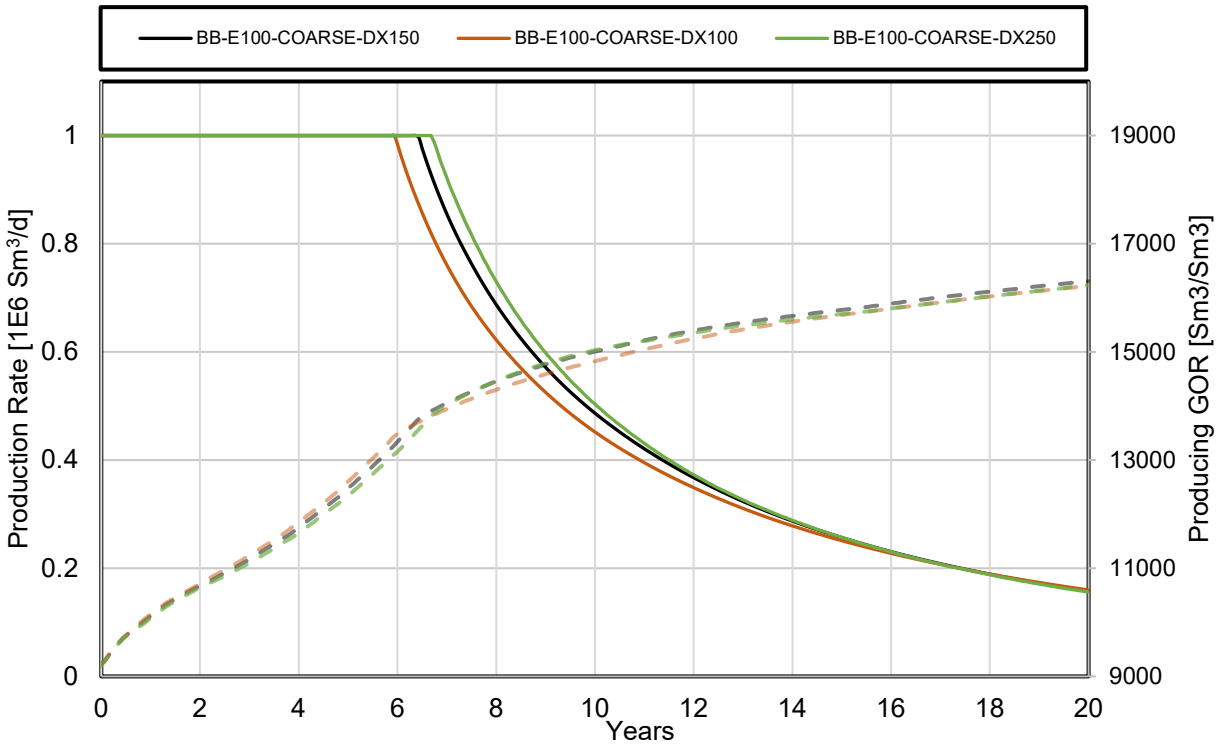

Figure 7.3 Coarse grid: grid sensitivity

The radial model has the same trend as the coarse grid model. A denser grid cell model with 40 grid cells and one with 10 grid cells in the r-direction was made. Figure 7.4 show the trend that a denser grid model gives a lower production due to that condensate blockage effects are more respected with a larger amount of grid cells near the well.

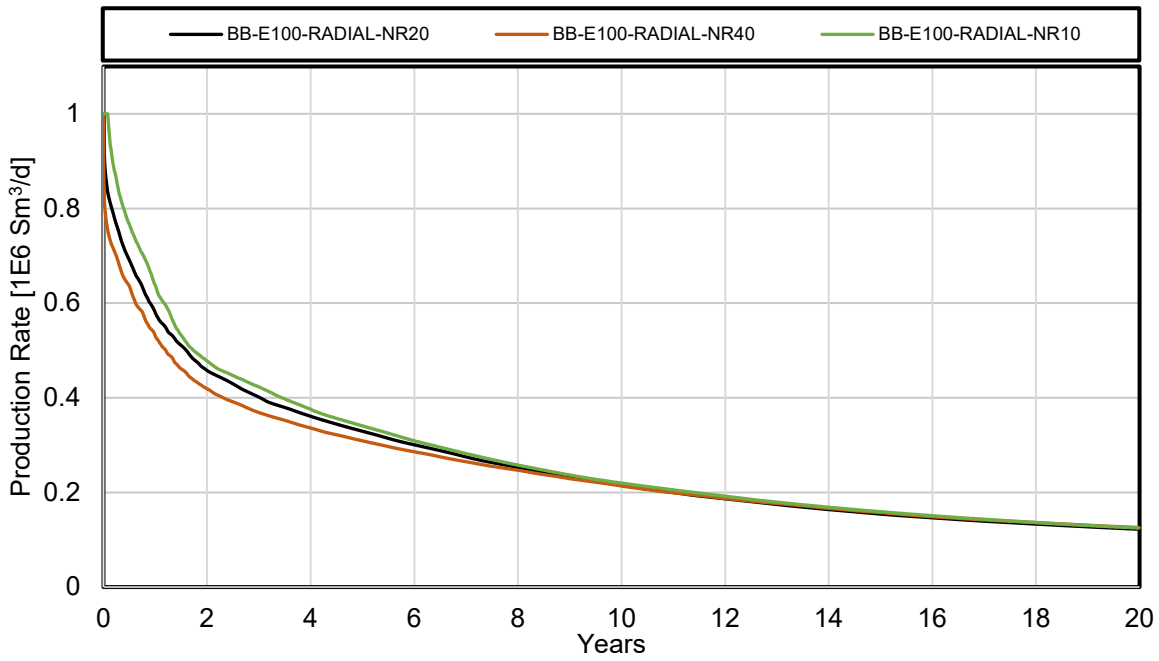

Figure 7.4 Fine grid radial: grid size sensitivity

Figure 7.5 show the coarse grid GPP model grid size sensitivity. In this case it is found that the denser grid size gives slightly better performance than the less dense. This goes against the findings in the other cases where a denser grid gives a slightly worse performance. However, the differences are neglectable, and the model can still be trusted with the GPP.

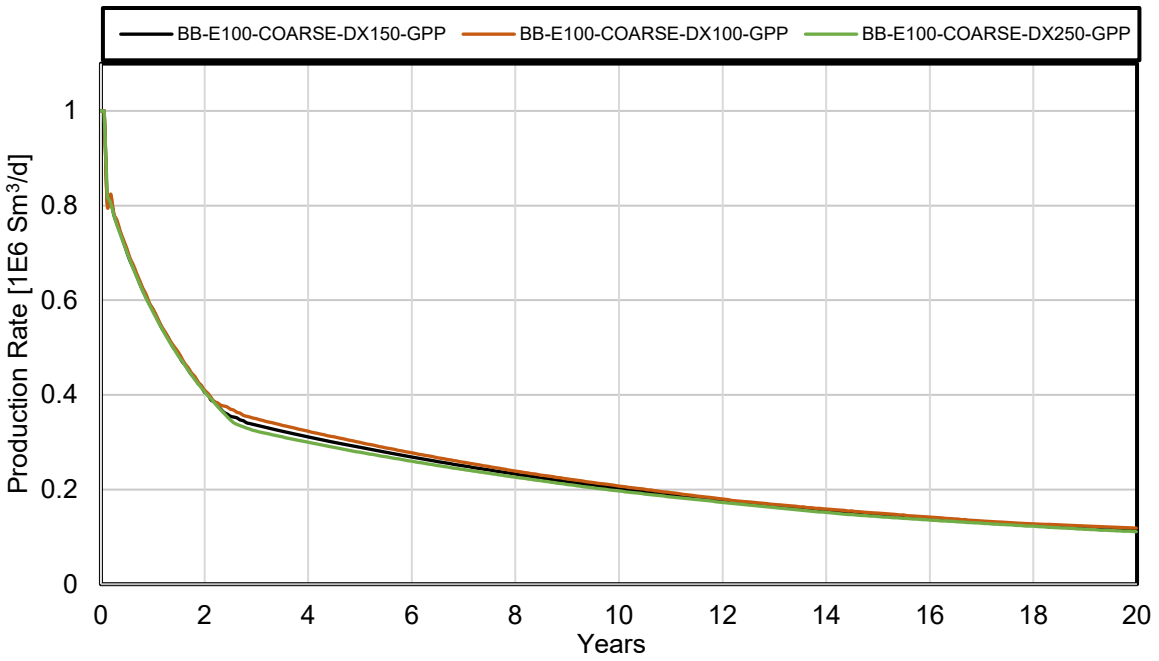

Figure 7.5 Coarse grid with GPP: grid sensitivity

7.2.3 Fluid Model Sensitivity

Chapter 4 of this master's thesis is dedicated to the fluid model used in the reservoir simulation model in this study. As discussed in the model the original fluid model existing in the model provided by Wintershall DEA was replaced by a model generated with a modification of the EOS developed by Consultant A. Therefor a sensitivity on the fluid model is conducted to see the effects modifying and changing the black oil tables has on the well deliverability modeling. The differences in the fluids is represented in Table 7.2.

Figure 7.6 shows a plot of the coarse grid model base case compared with the same model with the original fluid model "-OrgBOT". Again, this model is not including the near wellbore effects. Comparing the plateau period, the model with the modified fluid model, i.e. the base case, has a plateau period approximately 3-4 months longer than the model with the original fluid model. This effect can be explained by the small difference in gas viscosity found in the black oil table of the original model compared with the modified black oil table found in the base case models. The small differences are present from pressures approximately from 300 bara and downwards. Figure 4.5 from chapter 4 and the figures from Appendix A show the gas viscosity graphically. As the average reservoir pressure drops to pressure below 300 bara after approximately 4 years (see Figure 7.2) the viscosity effects will be seen through the whole reservoir depletion.

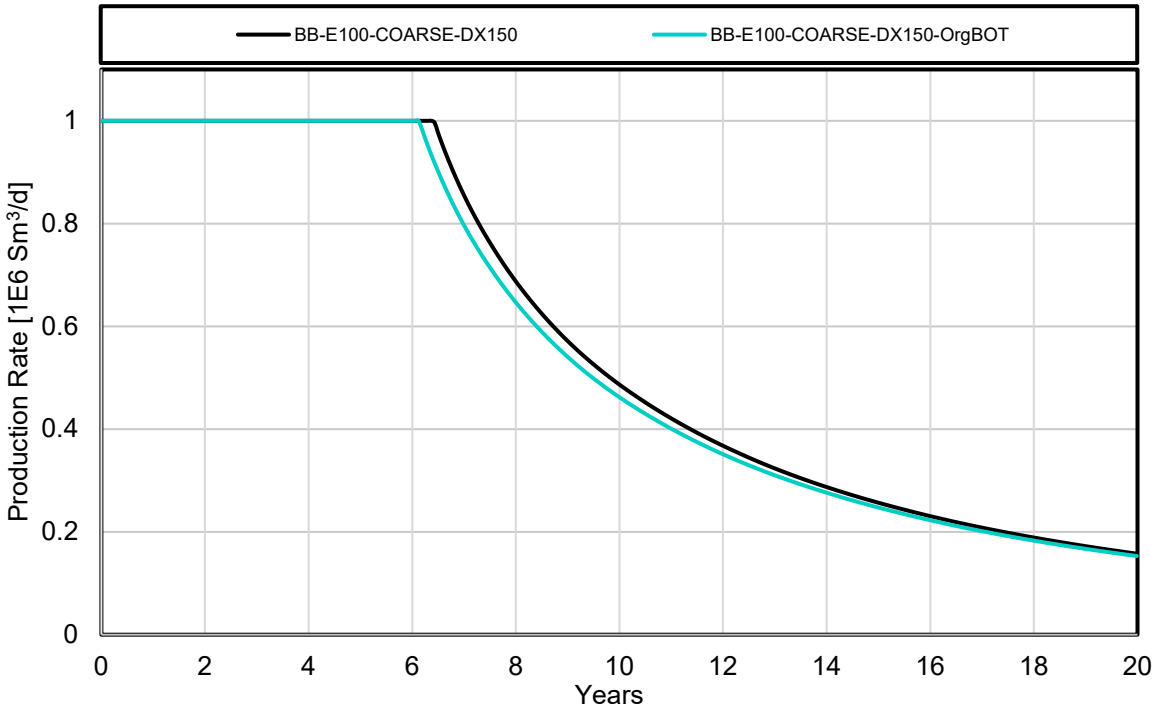

Figure 7.6 Coarse grid: fluid model sensitivity

The fine grid radial model and the GPP model does not show the same differences in deliverability due to the fluid models shown in Figure 7.7 and Figure 7.8. In these two well deliverability calculations other parameters like relative permeability plays a bigger part. Also, the average reservoir pressure does not drop to a pressure where differences in gas viscosities have any significance in the gas flow away from the near wellbore region.

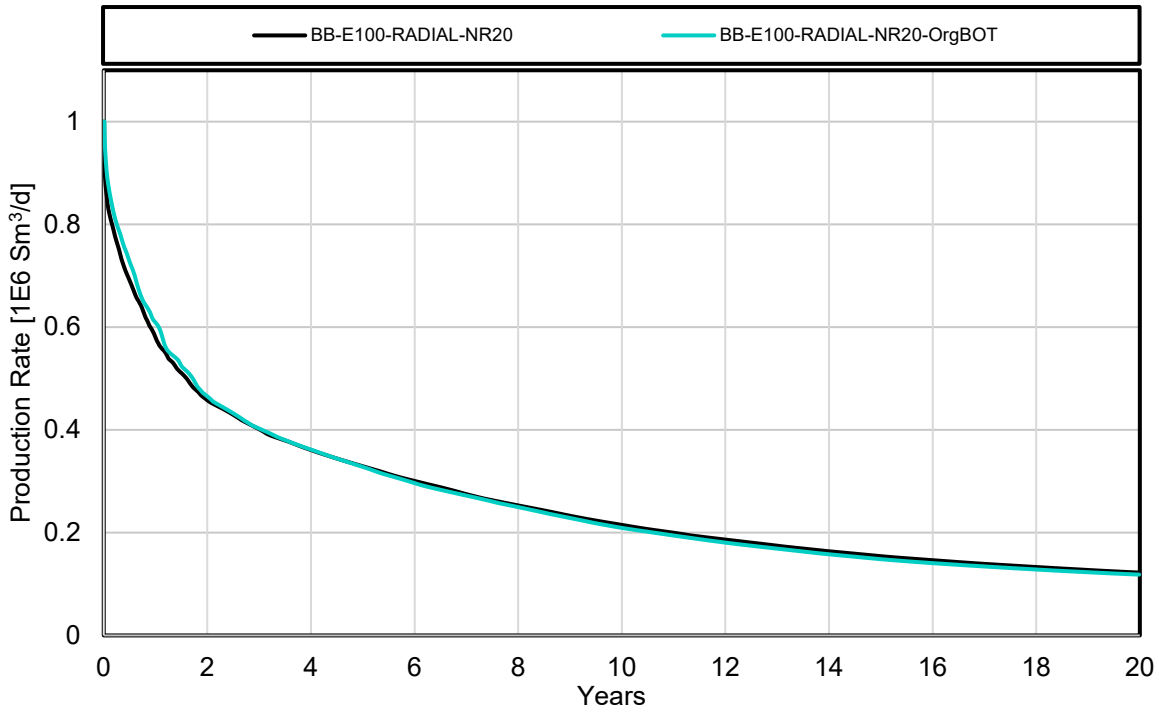

Figure 7.7 Fine grid radial: fluid model sensitivity

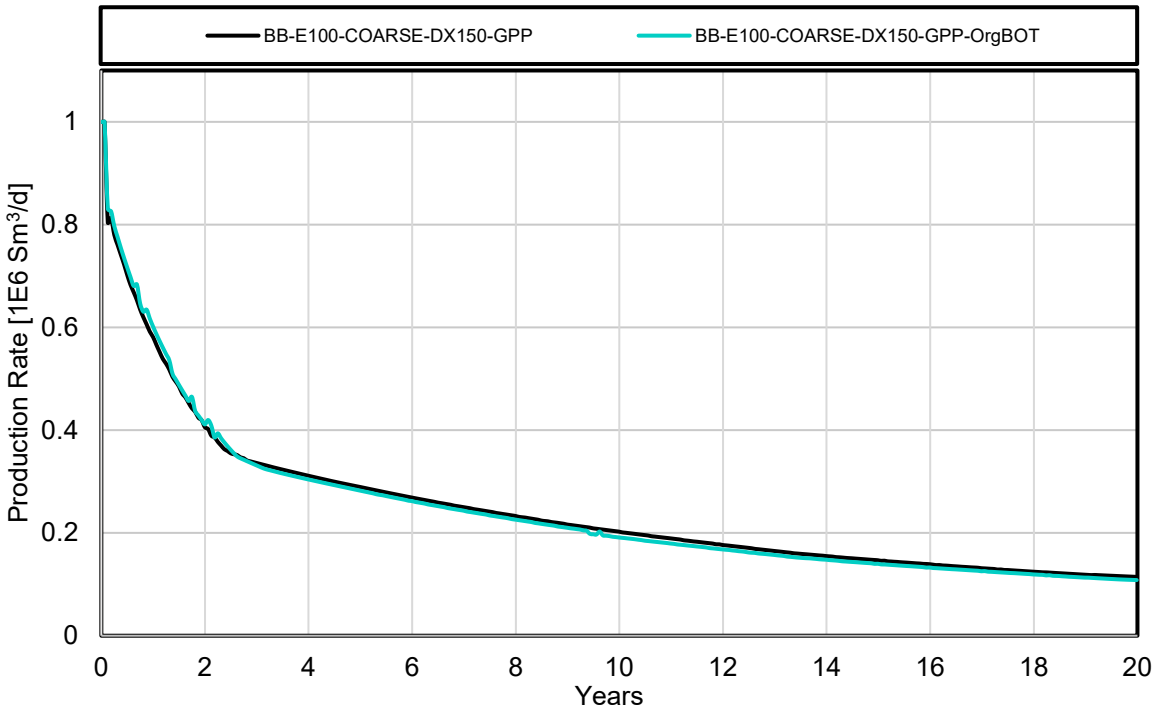

Figure 7.8 Coarse grid with GPP: fluid model sensitivity

7.2.4 Relative Permeability Sensitivity

As discussed in Chapter 5 “Relative Permeability Considerations” the gas relative permeability data found in the original model was very optimistic compared to what would be expected to find in a low permeability reservoir like Field A. As discussed in the Chapter 3 about condensate blockage, accurate relative permeability is important for capturing the well deliverability correctly. This subsection is focusing on the base case study cases with an updated, less optimistic, relative permeability presented in Table 5.3 as “k_{rg}-modified”. In the figures following the naming ending with “-RelPermMod” is using the modified gas relative permeability. As discussed, and confirmed, by the laboratory experiments done by STRATUM Reservoirs the relative permeability used in the “-RelPermMod” is more realistic and comparable to what would in reality be found in the near wellbore section of the reservoir.

Figure 7.9 shows that the modified relative permeability does not impact the coarse grid model well treatment in any significance. This is expected as this model does not “see” the condensate blockage in the near wellbore region where condensate and gas flow simultaneously (Region 1) leading to the reduction in relative permeability.

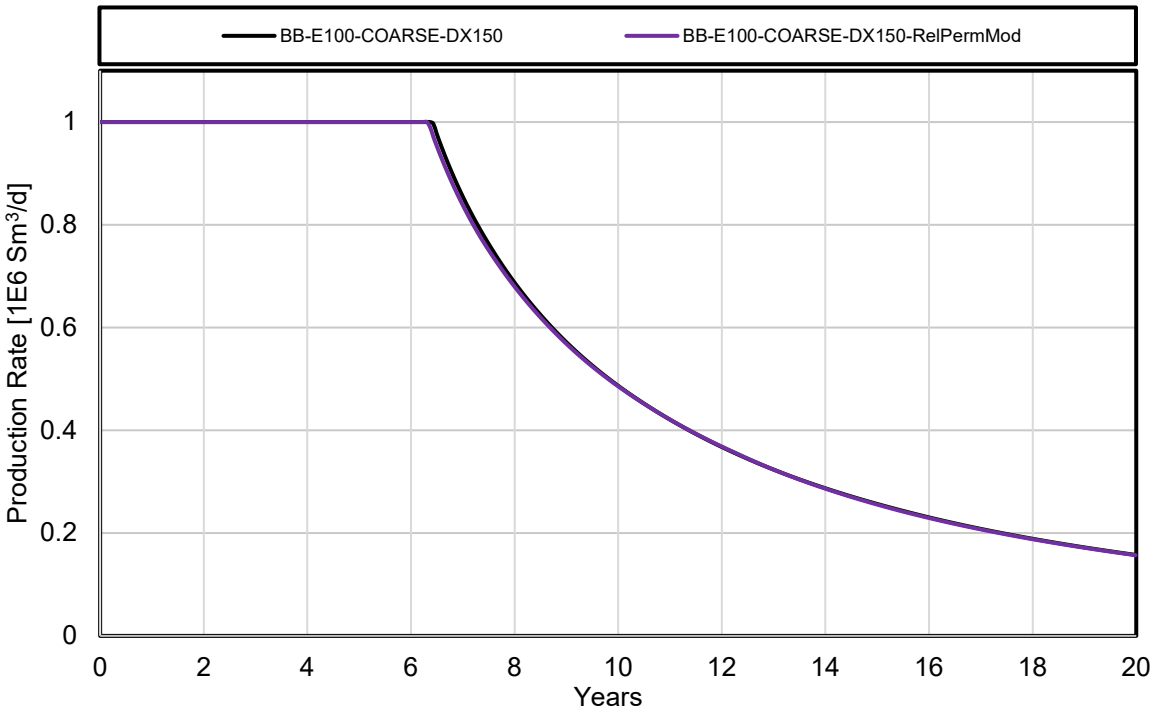

Figure 7.9 Coarse grid: rel-perm sensitivity

Figure 7.10 represent the fine grid model where the modified relative permeability contributes to a large reduction in the well deliverability as expected. The trend from the fine grid radial model is also closely approximated with the GPP option in the coarse grid model as show in Figure 7.11.

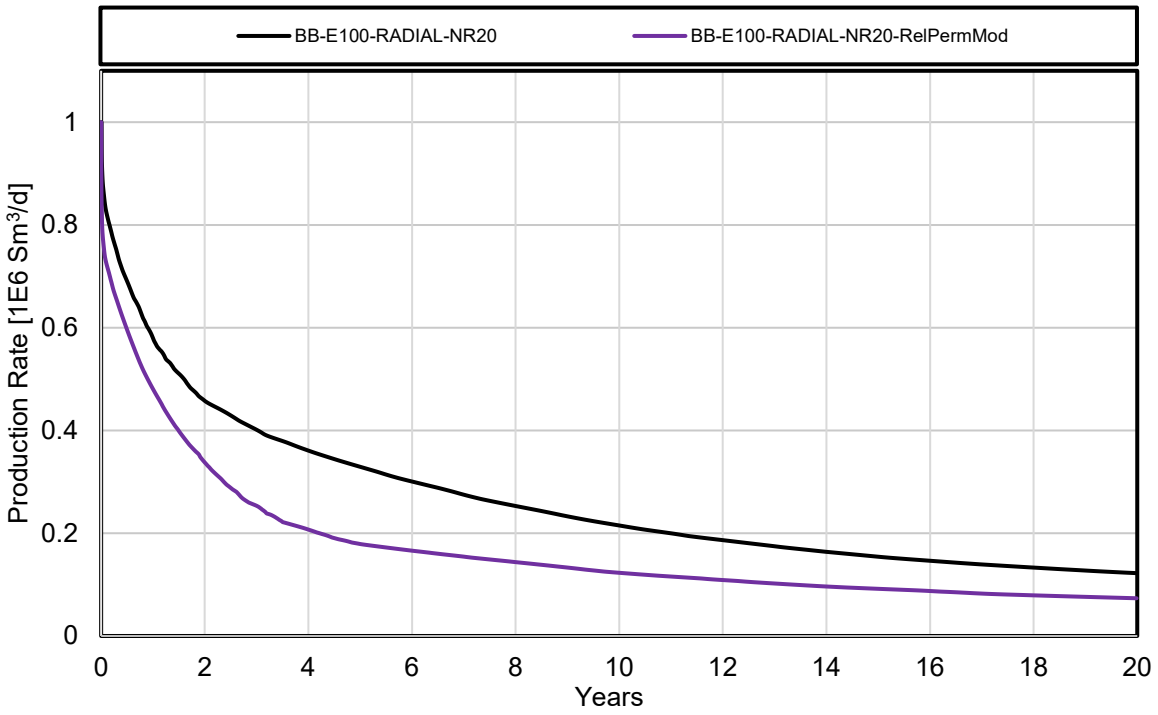

Figure 7.10 Fine grid radial: rel-perm sensitivity

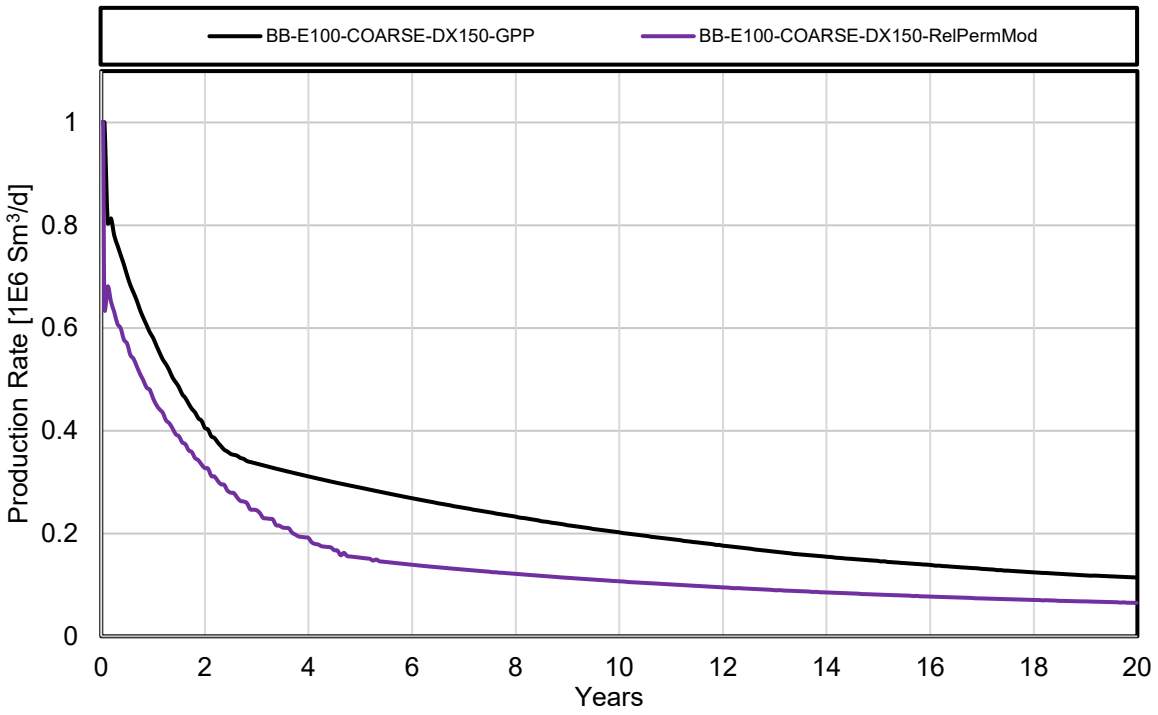

Figure 7.11 Coarse grid with GPP: rel-perm sensitivity

Figure 7.12 indicates that the fine grid and coarse grid model with GPP option are representative of each other in the case of having a modified relative permeability. Compared to Figure 7.1, the fit of the two approaches including condensate blockage effects is even better for this sensitivity case on relative permeability.

Comparing figure 7.1 and 7.12 the area between the black line and red/blue line gets larger for the more realistic relative permeabilities. The area between the two curves represent the loss inn recovery due to condensate blockage. The model with more realistic relative permeability data, expected to be found in Field A, shows a larger area. This is an expected result and ensures that the models capture condensate blockage effects in a correct manner. Compared to the base case study the *results from this sensitivity is the most representative for field A*. This is due to that the relative permeability data used here is confirmed by core experiments to represent Region 1, where the largest loss in well deliverability is present. This emphasizes the importance of having proper relative permeability data in the reservoir simulator.

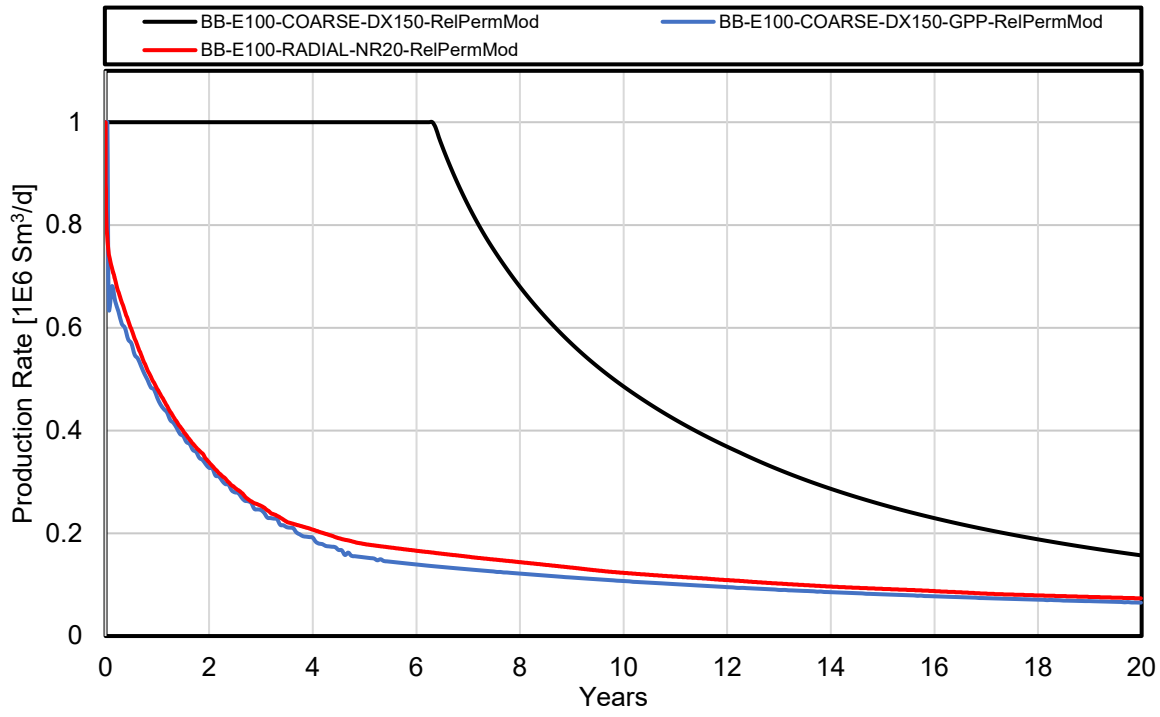

Figure 7.12 Rel-perm sensitivity: coarse, radial and coarse with GPP model

7.2.5 Reservoir Quality Sensitivity

Condensate blockage has a greater impact in reservoirs of poor quality. Field A is as discussed, a low permeability reservoir. An interesting sensitivity case is therefore to multiply the permeability in the reservoir by ten and examine the relative difference in well deliverability reduction due to condensate blockage. There are two study cases presented in this subsection, one being that the permeability in the horizontal and vertical direction is multiplied by 10 (k_v/k_h=0.5) and the case of only multiplying the horizontal permeability (k_v/k_h is kept to the original k_v/k_h = 0.05).

Figure 7.13 show that the plateau period with producing 1E6 Sm^3/d is doubling before the well goes on decline at approximately 13 year of production. There is also a small difference between the cases when it comes to vertical permeability, with a slightly better performance in the k_v/k_h = 0.5 case. From a field development point of view having a reservoir with better quality would lead to the possibility of production the reservoir at a higher rate with a shorter plateau period.

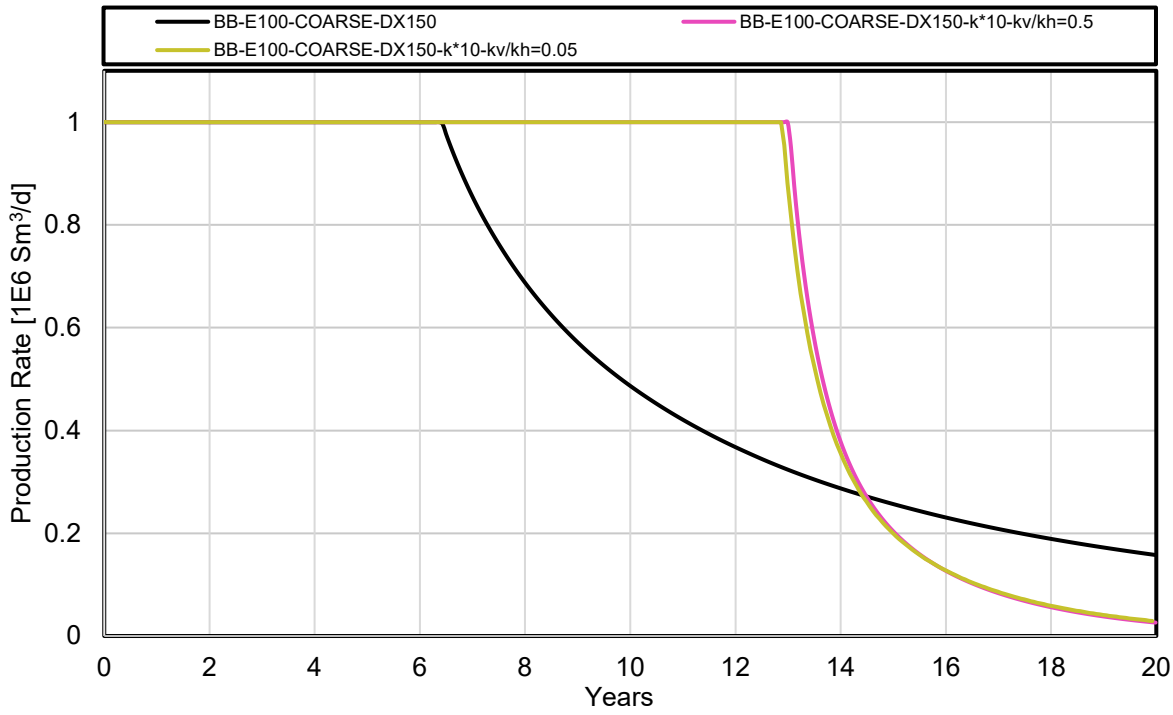

Figure 7.13 Coarse grid: reservoir quality sensitivity

For the models including near wellbore effects in the well deliverability calculations the trend is the same. A longer plateau period is achieved and there is very small difference between the high and low vertical permeability cases. Figure 7.14 and 7.15 shows these trends. Figure 7.15 show a weird “wobbly” trend from 14 to 16 years of production before it goes back to a normal

looking depletion.

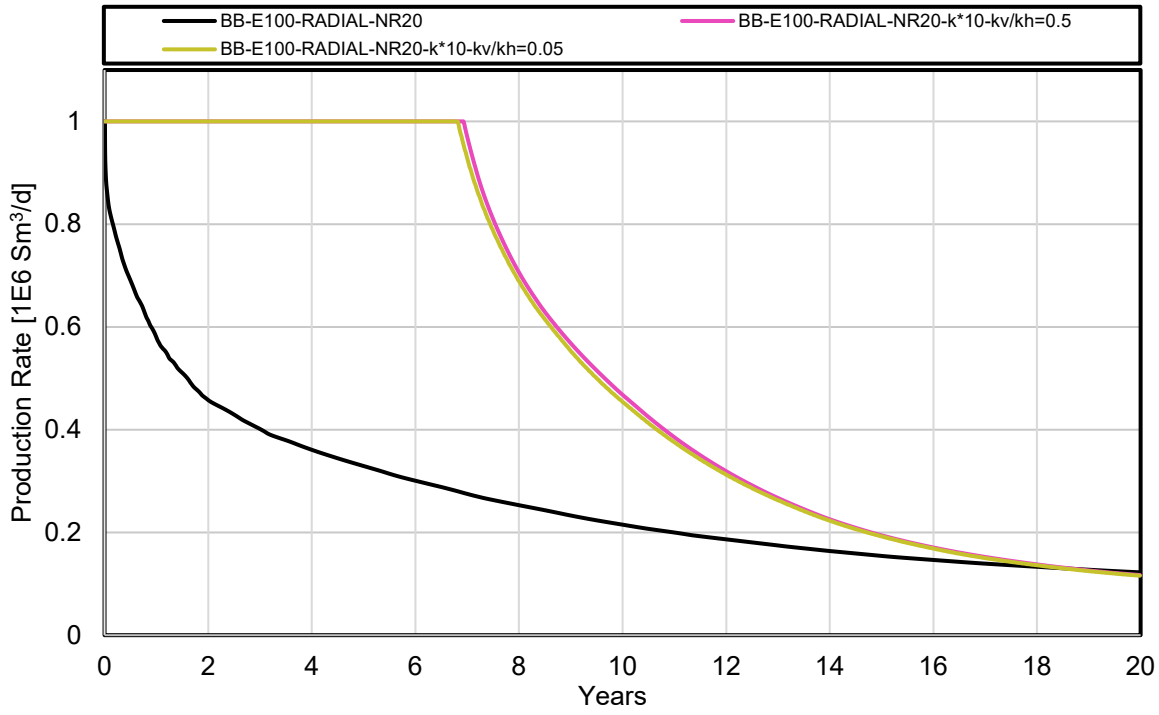

Figure 7.14 Fine grid radial: reservoir quality sensitivity

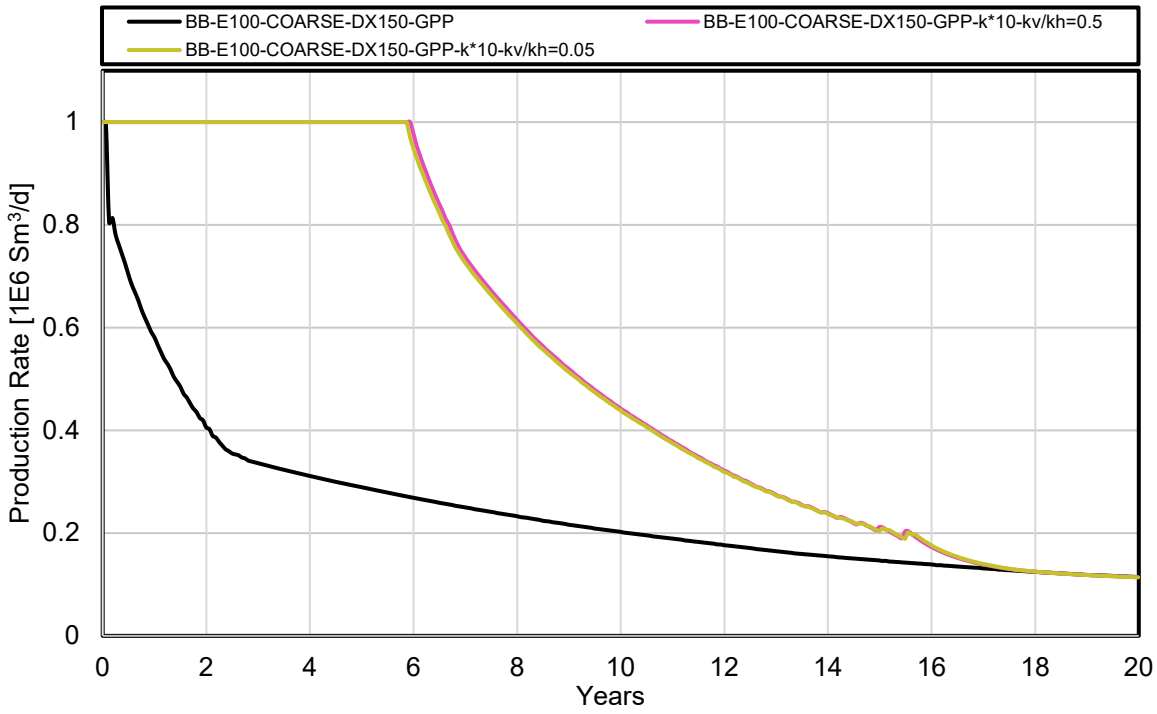

Figure 7.15 Coarse grid with GPP: reservoir quality sensitivity

Figure 7.16 compare the course, fine grid and GPP models for the simulation on better reservoir quality. In this case there are bigger differences between the fine grid and GPP model in deliverability. This can be explained by that a reservoir with a better reservoir quality would need a denser grid than 20 grid cells in the radial direction to capture the effects. Figure 7.5 indicates that the GPP option is more or less constant depending on grid size for the given lean fluid present in the reservoir while Figure 7.4 shows a trend dependent on grid size for the radial model.

The key takeaway from figure 7.16 is that the area between the black line and the red/blue line is significantly smaller than what is found in the cases with lower reservoir quality. This is an expected finding, as the near wellbore effects have a bigger impact on reservoirs of lower quality. It should be emphasized that condensate blockage effects are not unimportant in the case studied in this subsection as the plateau period is significantly reduced. Relatively speaking the condensate blockage effects are greater for the lower permeability cases in figure 7.1 and 7.12. This subsection was added out of curiosity for relative importance of condensate blockage in a thought scenario and is not realistic for Field A as the reservoir quality is too high.

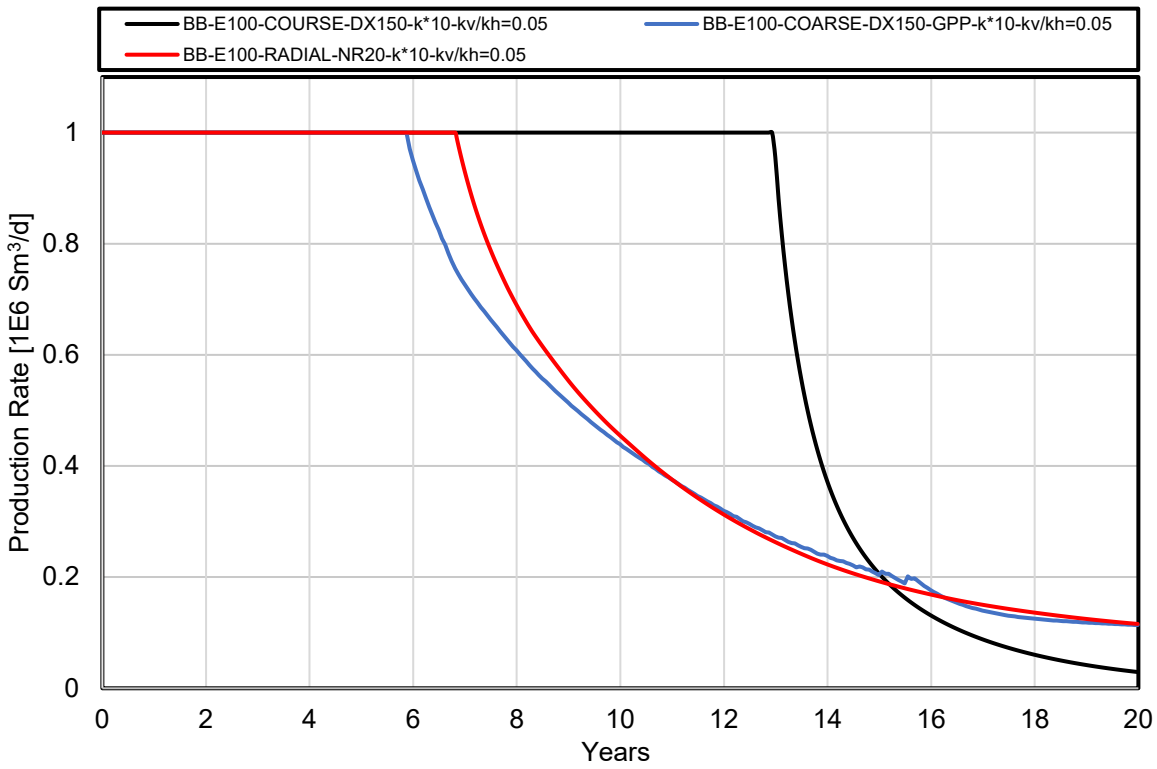

Figure 7.16 Reservoir quality sensitivity: Coarse, radial and coarse with GPP model

8 Conclusions

This study has investigated the effects of condensate blockage for Field A using single-well models with black-oil PVT formulation based on a modified EOS developed in my Specialization Project (Autumn 2019) found in Appendix C. The work also included design and interpretation of special steady-state gas-oil relative permeability measurements conducted at a commercial laboratory (STRATUM Reservoirs).

The following conclusions can be drawn from this study:

1. Condensate blockage effects are found to be very important for the development of Field A. The well deliverability shows a significant reduction due to condensate blockage, with a resulting impact on the plateau period for all simulation cases. The blockage effect will impact decisions such as number of wells, and well completion strategy to minimize the impact of blockage.

2. Coarse grid models based on expected x-y dimensions of the full-field simulation model predict too optimistic well performance compared to models that properly treat the condensate blockage effect.

3. The generalized pseudopressure (GPP) method for calculating well deliverability is found to accurately capture the effect of condensate blockage in coarse grid models, when compared with models that use a high-resolution, local near-well gridding. Consequently, Field A field development reservoir modeling can use coarse x-y gridding with the GPP option, and local grid refinement is not needed to capture condensate blockage effects.

4. For Field A it was found that the full-field model x-y coarse grid size was sufficient to describe the producing GOR performance of a fine-gridded model, and therefore allowed the GPP option to correctly predict the condensate blockage near the well. Only a slight improvement was found by reducing the original x-y coarse grid to a smaller size.

5. Using the modified EOS fluid model (versus the original EOS fluid model) to generate black-oil PVT tables did *not* impact the description of condensate blockage.

6. Condensate blockage is strongly impacted by the gas-oil relative permeability curves used. The relative permeability curves found in the original full-field model were very optimistic (with k_{rg} = 0.16 at the crossing point where k_{rg}/k_{ro} = 1). A more-realistic (for lower-permeability rock) relative permeability curve was used (k_{rg} = 0.05 at k_{rg}/k_{ro} = 1) and shown to have a much larger blockage effect than the original curves.

7. Simple steady state core flooding experiments with a simple fluid system (N_2 and synthetic oil) can be used to capture “immiscible” relative permeability data. Laboratory data that became available only after the simulation study had been completed verified pessimistic “immiscible” relative permeability curves with k_{rg} = 0.05 at k_{rg} = 1.

9 Recommendations for further work

- Given the importance of relative permeability on the magnitude of condensate blockage, it is highly recommended that new relative permeability measurements be made to quantify the impact of capillary number and high velocity flow effects. This is particularly the case if wells are not to be stimulated with hydraulic fracturing. Capillary number is a dimensionless number describing the ratio of viscous to capillary forces (Fevang 1995). $N_c = v_{pg}u_g/\sigma_{go}$ is describing the capillary number. Observations has been made by experimental measurements and field performance that relative permeability of the gas can be significantly impacted by capillary number (Singh and Whitson 2010). For small capillary numbers, the capillary forces dominate and traditional "immiscible" relative permeabilities is found Figure 9.1. For large capillary numbers, the viscous forces dominate giving relative permeabilities approaching the straight line or "miscible-like" behavior (A → B → C is increasing in capillary number) (Whitson, Fevang, and Sævareid 1999).

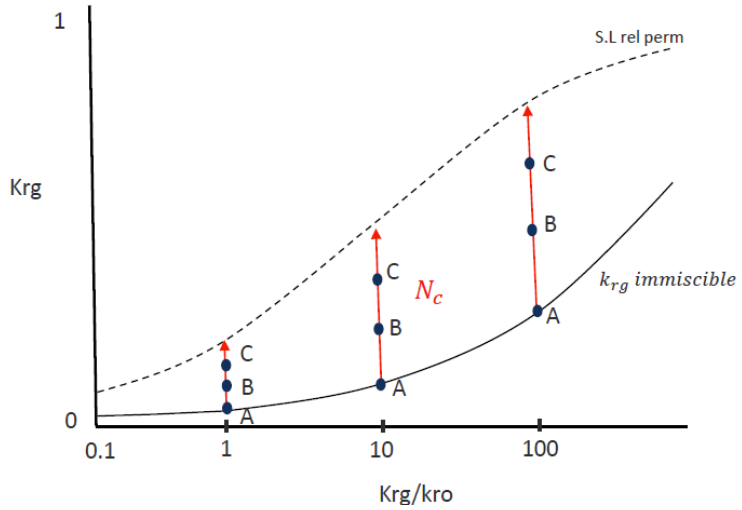

Figure 9.1 Capillary number dependent relative permeability schematic

- Non-Darcy effects study cases. While capillary numbers tend to increase the well deliverability, non-Darcy effects tends to reduce well deliverability. Near the wellbore both high capillary numbers and non-Darcy flow effects can be expected depending on the nature of the reservoir and well rate (Singh and Whitson 2010). The Forchheimer equation is often used for modelling non-Darcy effects.

- All the results presented in this master thesis is conducted on vertical wells. Performing study cases with horizontal wells is also desirable since the wells that was in the planning for Field A was horizontal wells. Condensate blockage is also happening in these cases, where k_v/k_h is most likely to play a bigger part than it did in this study.

Acronyms and Nomenclature

Acronyms

BHFP Bottom hole flowing pressure
CCE Constant composition expansion
CGR Condensate/Gas ratio
CVD Constant volume depletion
EOS Equation of state
GOR Gas/oil ratio
HCPV Hydrocarbon pore volume
IFIP Initial Fluids in place
ICIP Initial Condensate in Place
MW Molecular weight
OBM Oil-based mud
RMS Root mean square
SCN Single carbon number
QC Quality Control

Nomenclature

B_{gd} = dry gas formation volume factor
B_{gw} = wet gas formation volume factor
b_i = component repulsion parameter in Peng Robinson EOS
B_o = oil formation volume factor
c = unit conversion factor
C = gas rate constant
C_f = Soreide constant
c_i = temperature dependent component volume shift factor, PVTsim
C_{og} = conversion factor of gas-equivalent of surface oil
C_{pen} = temperature independent volume correction PVTsim
C_{penT} = temperature dependent volume correction PVTsim
C_{7+} = heptanes-plus
D_x = grid block x-dimension
D_y = grid block y-dimension
G = initial gas in place
h = reservoir/layer thickness
K = Kelvin
k = absolute permeability
k_{rg} = relative permeability of gas
k_{rgro} = relative permeability of gas at $S_o = S_{org}$
k_{ro} = relative permeability of oil
k_x = permeability in x-direction

k_y = permeability in y-direction

k_z = permeability in z-direction

$m(p)$ = total gas + oil pseudopressure function, $m_t(p)$

M = molecular weight

M_i = molecular weight of component i

N_C = capillary number

n = moles

n_d = moles at initial dewpoint pressure

n_p = produced moles

N = initial oil in place

p = pressure

p_{ci} = component Critical pressure

p_{CVD}= pressure at CVD test stage

p_d = dewpoint pressure

p_G = well-grid cell average pressure

Δp = pressure drop

Δp_p = delta pseudopressure

p_R = reservoir pressure

p_{SC} = pressure at surface conditions

p_{wf} = BHFP

p^* = dewpoint of the producing wellstream

V = volume

V_d = dewpoint volume

V_{rel} = relative volume

V_{roCCE} = CCE oil relative volume, V_o/V_{tot}

V_{roCVD}= CVD oil relative volume, V_o/V_d

w = mass fraction

$w_{a,i}$ = component mass fraction in analytical model

q = flow rate

R = universal gas constant

R_p = Producing gas/oil ratio

R_s = solution gas/oil ratio

r_s = solution oil/gas ratio

r_e = external drainage radius

r_o = pressure equivalent radius

r_w = wellbore radius

r_2 = outer radius of radial grid block

s = skin factor

s_i = component volume shift factor PhazeComp

S_{gc} = critical gas saturation

SG = specific gravity

S_o = oil saturation

S_{org} = critical oil saturation in gas at connate water saturation

S_w = water saturation

S_{wc} = connate water saturation

T_{ci} = component critical temperature

T_R = temperature at reservoir conditions

T_{SC} = temperature at surface conditions

$x_{m,i}$ = component mass fraction of OBM

y_{7+} = C_{7+} composition in the produced gas

z = total mole fraction

Z = Z-factor

Z_d = dewpoint pressure Z-factor

Z_2 = two-phase Z-factor

β_s = surface gas mole fraction in wellstream (or gas volume fraction in black oil simulators)

λ = mobility

μ = viscosity

ρ = density

θ = segment connection with the well in radians

γ = specific gravity

γ_i = specific gravity for component

Subscripts

d = property at initial dewpoint

D = Depletion

g = Gas phase

$\bar{g}$ = Surface gas phase

$\bar{g}g$ = Surface gas phase from reservoir gas

i = Initial

k = pressure step in CVD

new = synthetic reservoir model

$n+$ = C_n and heavier components

old = original reservoir model

o = Oil phase

$\bar{o}$ = Surface oil phase

$\bar{o}g$ = Surface oil phase from reservoir gas

t = total (e.g. mobility)

w = well stream

References

CALSEP. Methode Documentation PVTsim 13. 28-30.

Fetkovich, M. D., Guerrero, E. T., Fetkovich, M. J. et al. 1986. Oil and Gas Relative Permeabilities Determined From Rate-Time Performance Data. Presented at the SPE Annual Technical Conference and Exhibition, New Orleans, Louisiana. 1986/1/1/. https://doi.org/10.2118/15431-MS.

Fevang, Øivind. 1995. *Gas Condensate - Flow Behavior and Sampling*. PHD, The Norwegian Institute of Technology, Trondheim (October).

Fevang, Øivind and Whitson, C. H. 1996. Modeling Gas-Condensate Well Deliverability. *SPE Reservoir Engineering* **11** (04): 221-230. https://doi.org/10.2118/30714-PA.

Fevang, Øivind and Whitson, Curtis H. 1995. Modeling Gas Condensate Well Deliverability. *SPE 30714*.

Mott, Robert. 1999 Calculating Well Deliverability in Gas Condensate Reservoirs *EAGE - 10th European Symposium on Improved Oil Recovery, Brighton*.

Schlumberger. 2017a. ECLIPSE Reference Manual Version 2017.2.

Schlumberger. 2017b. ECLIPSE Technical Description Version 2017.2.

Schlumberger. 2019. Schlumberger Oilfield Glossary: absolute permeability, https://www.glossary.oilfield.slb.com/en/Terms/a/absolute_permeability.aspx (accessed 3/12 2019).

Singh, Kameshwar and Whitson, Curtis H. 2010. Gas-Condensate Pseudopressure in Layered Reservoirs. *SPE Reservoir Evaluation & Engineering* **13** (02): 203-213. https://doi.org/10.2118/117930-PA.

Torheim, Erlend. 2019. PVT Analysis for Condensate Blockage - A study of gas condensate samples from the Norwegian Continental shelf. **1**.

Whitson, C. H. and Fevang, Oivind. 1997. Generalized Pseudopressure Well Treatment in Reservoir Simulation

Whitson, Curtis H. and Brulé, Michael R. 2000. *Phase Behaviour* Vol. 20.

Whitson, Curtis H. , Fevang, Øivind, and Yang, Tao. 1999. Gas Condensate PVT - What's Really Important and Why? (in English).

Whitson, Curtis H., Fevang, Øivind, and Sævareid, Aud. 1999. Gas Condensate Relative Permeability for Well Calculations. Presented at the SPE Annual Technical Conference and Exhibition, Houston, Texas. 1999/1/1/. https://doi.org/10.2118/56476-MS.

Whitson, Curtis H. and Mott, Robert E. 2005. *Gas-Condensate-Course-Overheads-All* (Reprint).

Yang, Tao, Fevang, Oivind, Christoffersen, K. R. et al. 2007. LBC Viscosity Modeling of Gas

Condensate to Heavy Oil. Presented at the SPE Annual Technical Conference and Exhibition, Anaheim, California, U.S.A. 2007/1/1/. https://doi.org/10.2118/109892-MS.

Younus, Bilal, Whitson, Curtis, Alavian, Ahmad et al. 2019. Field-Wide Equation of State Model Development. Presented at the SPE/AAPG/SEG Unconventional Resources Technology Conference, Denver, Colorado, USA. 2019/7/31/. https://doi.org/10.15530/urtec-2019-551.

Appendix A

A.1 Black Oil Table Comparison Reservoir Zone 2

The reservoir pressure in reservoir zone 2 is 374.3 bara and the temperature are 115.2 °C.

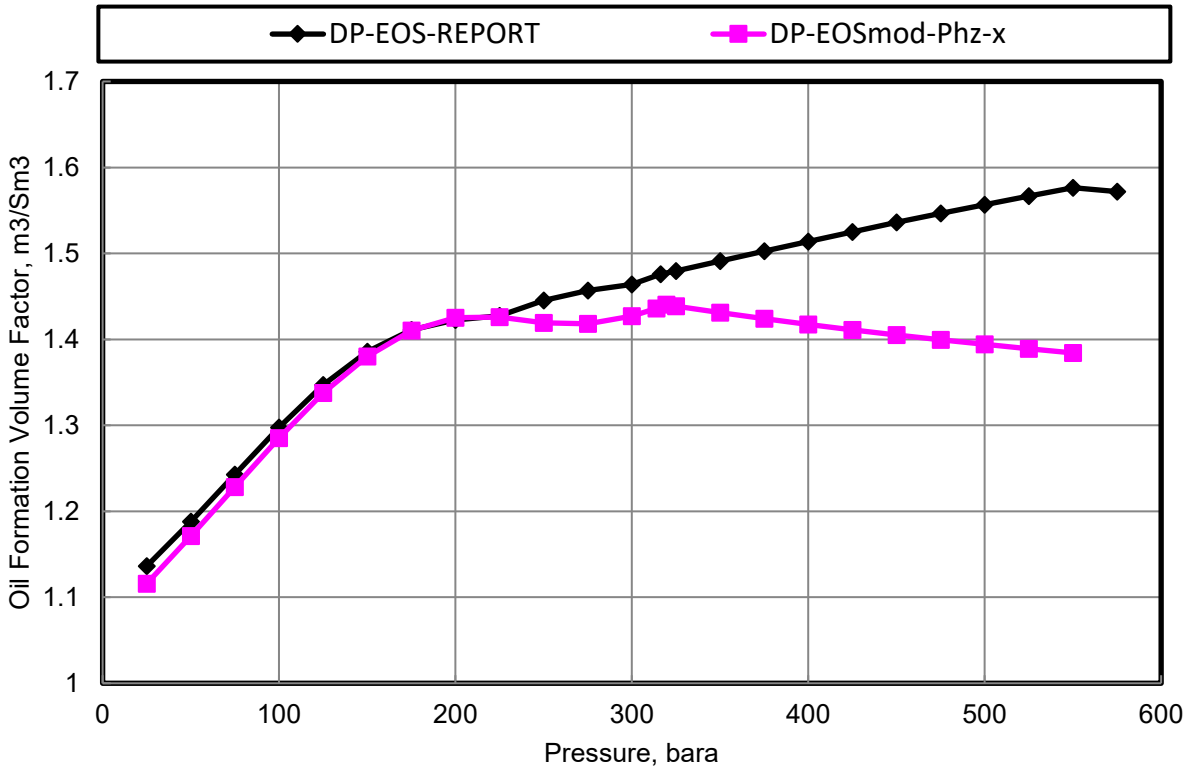

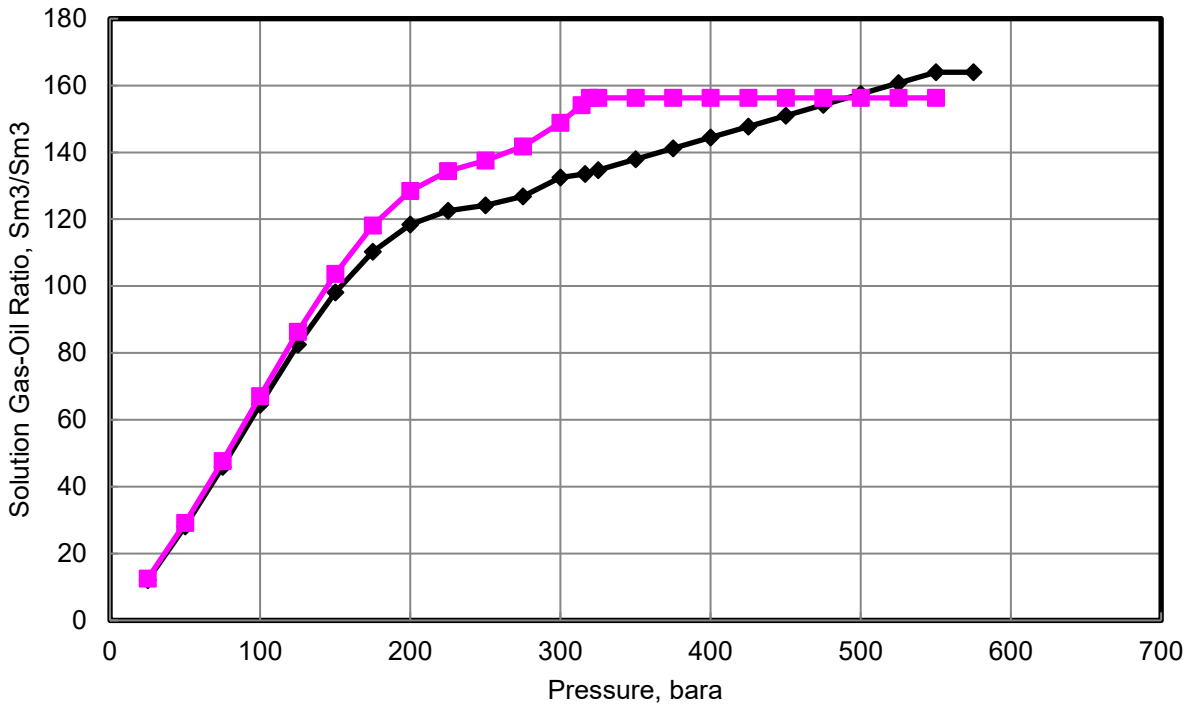

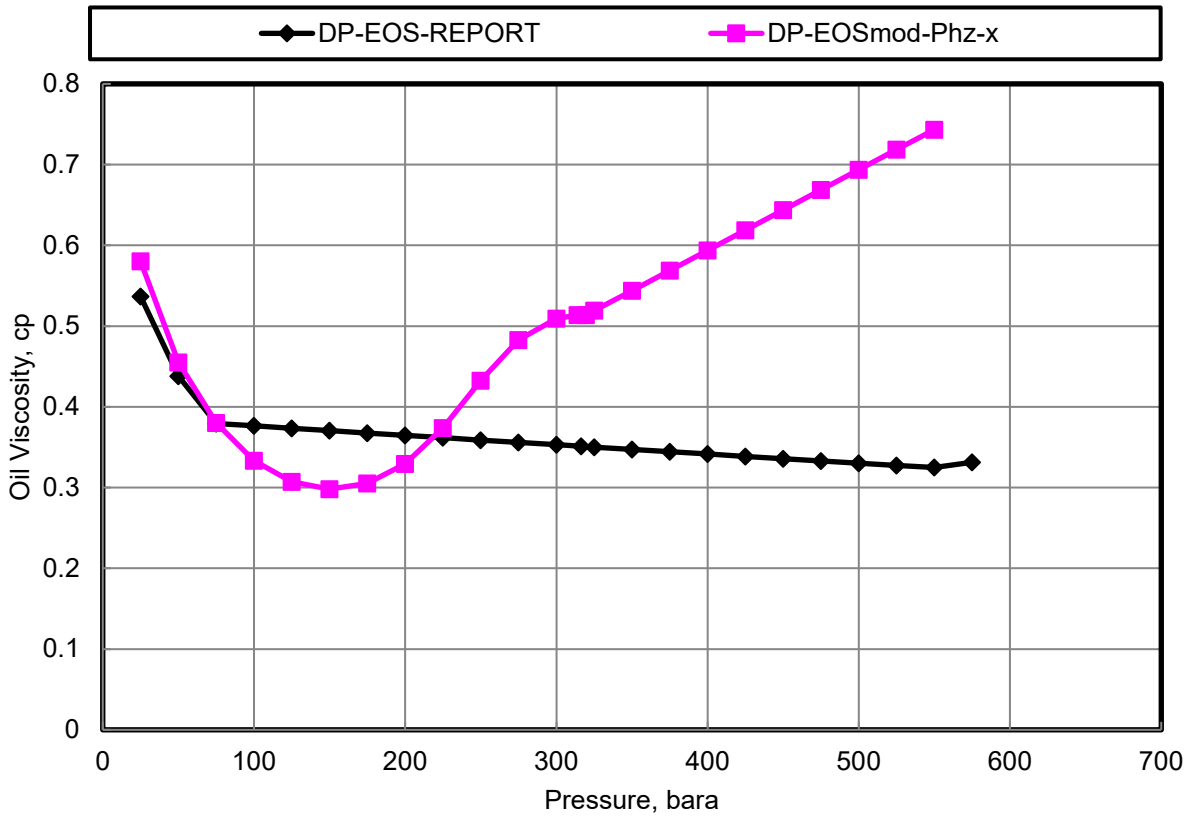
DP-EOS-REPORT
DP-EOSmod-Phz-x
Oil Viscosity, cp
0.8
0.7
0.6
0.5
0.4
0.3
0.2
0.1
0
0
100
200
300
400
500
600
700
Pressure, bara

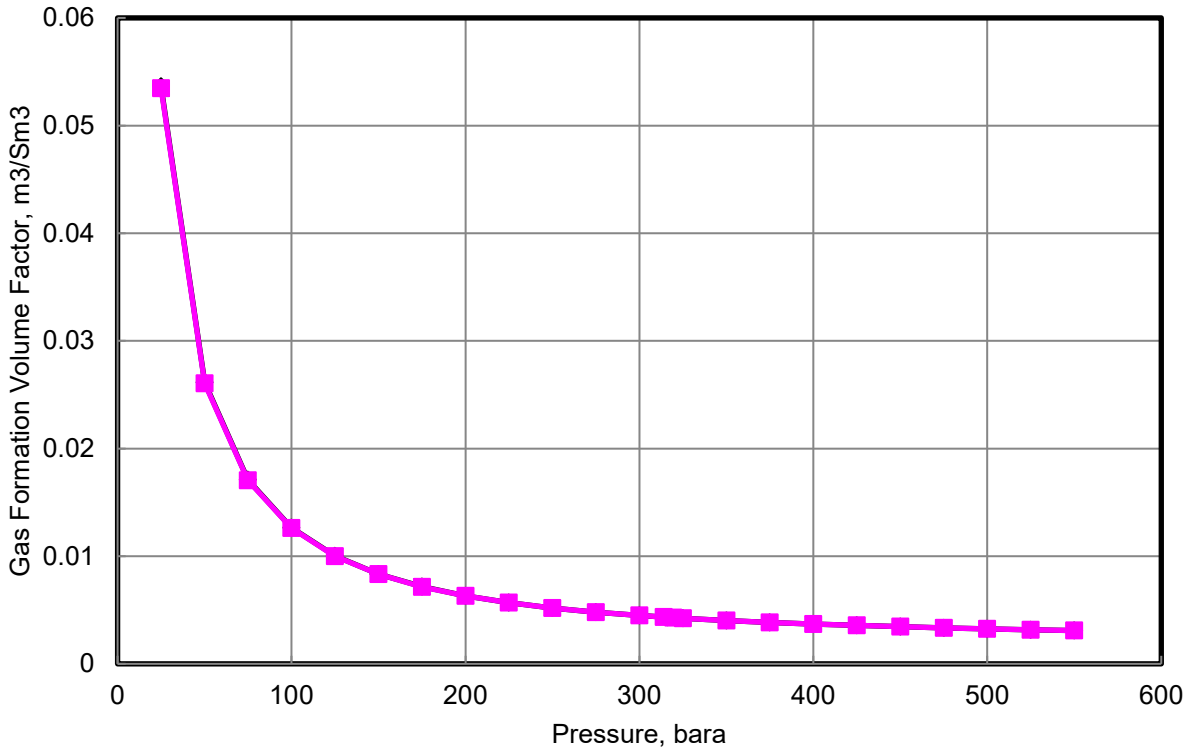
Gas Formation Volume Factor, m3/Sm3
0.06
0.05
0.04
0.03
0.02
0.01
0
0
100
200
300
400
500
600
Pressure, bara

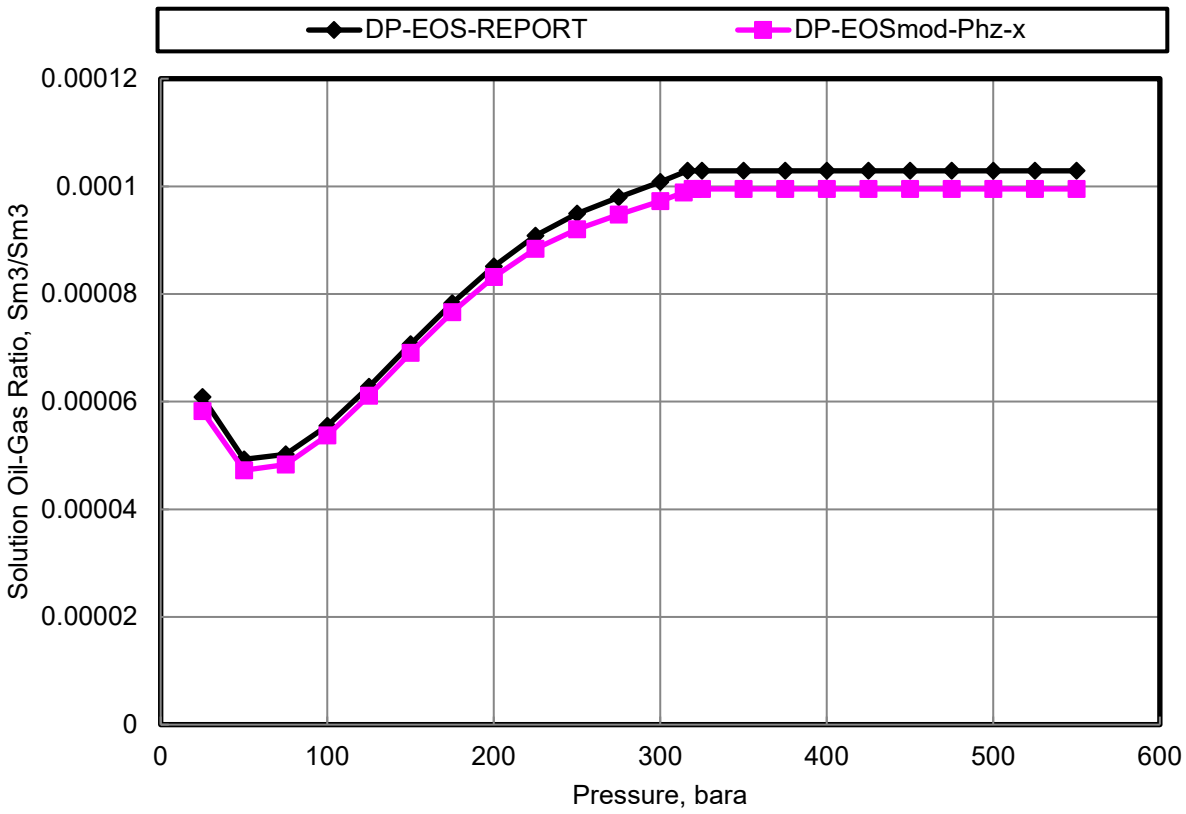
DP-EOS-REPORT
DP-EOSmod-Phz-x
Solution Oil-Gas Ratio, Sm3/Sm3
0.00012
0.0001
0.00008
0.00006
0.00004
0.00002
0
0
100
200
300
400
500
600
Pressure, bara

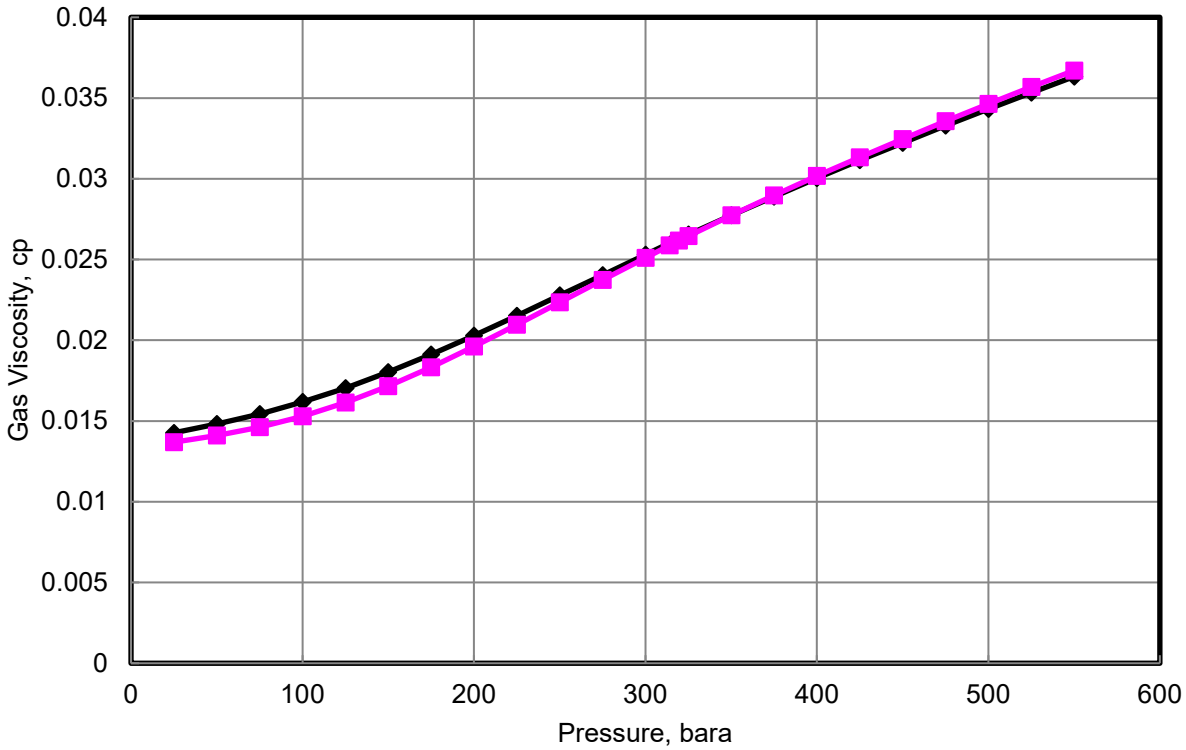
Gas Viscosity, cp
0.04
0.035
0.03
0.025
0.02
0.015
0.01
0.005
0
0
100
200
300
400
500
600
Pressure, bara

A.2 Black Oil Table Comparison Reservoir Zone 3

The reservoir pressure in reservoir zone 3 is 385.7 bara and the temperature are 121.2 °C.

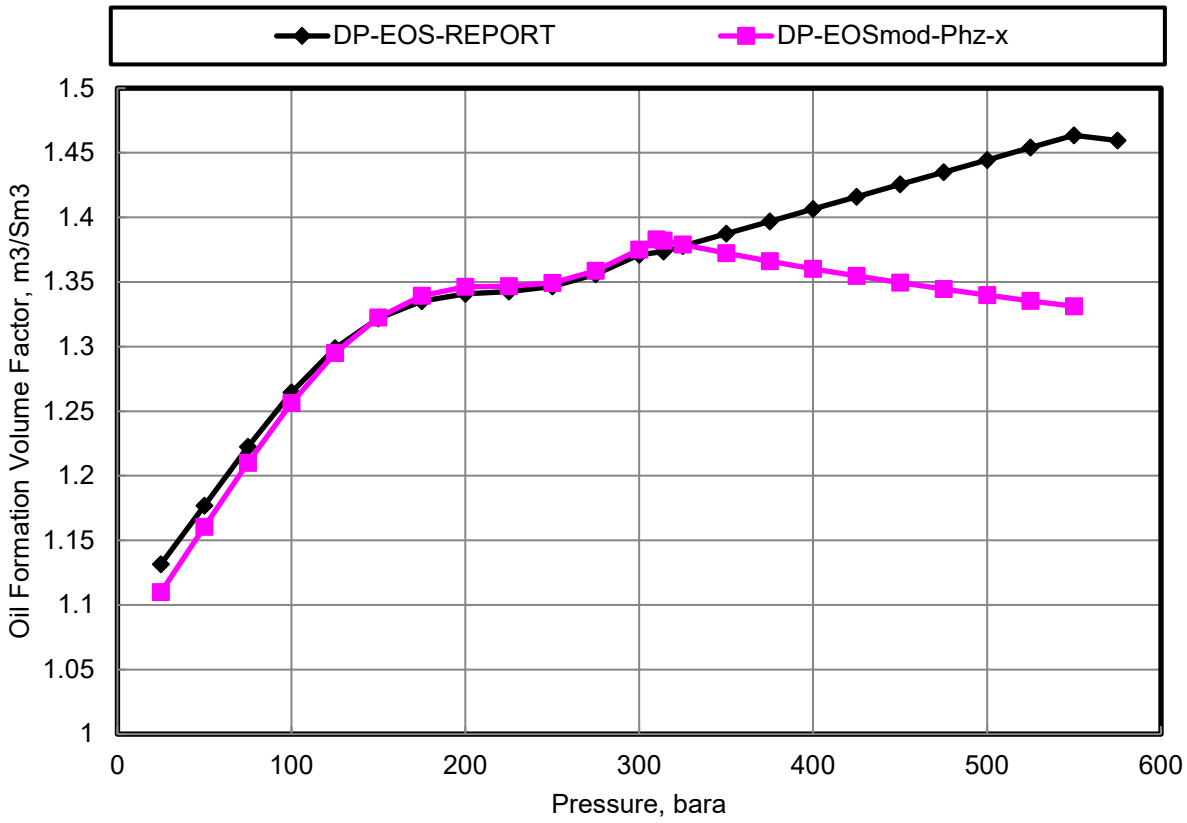

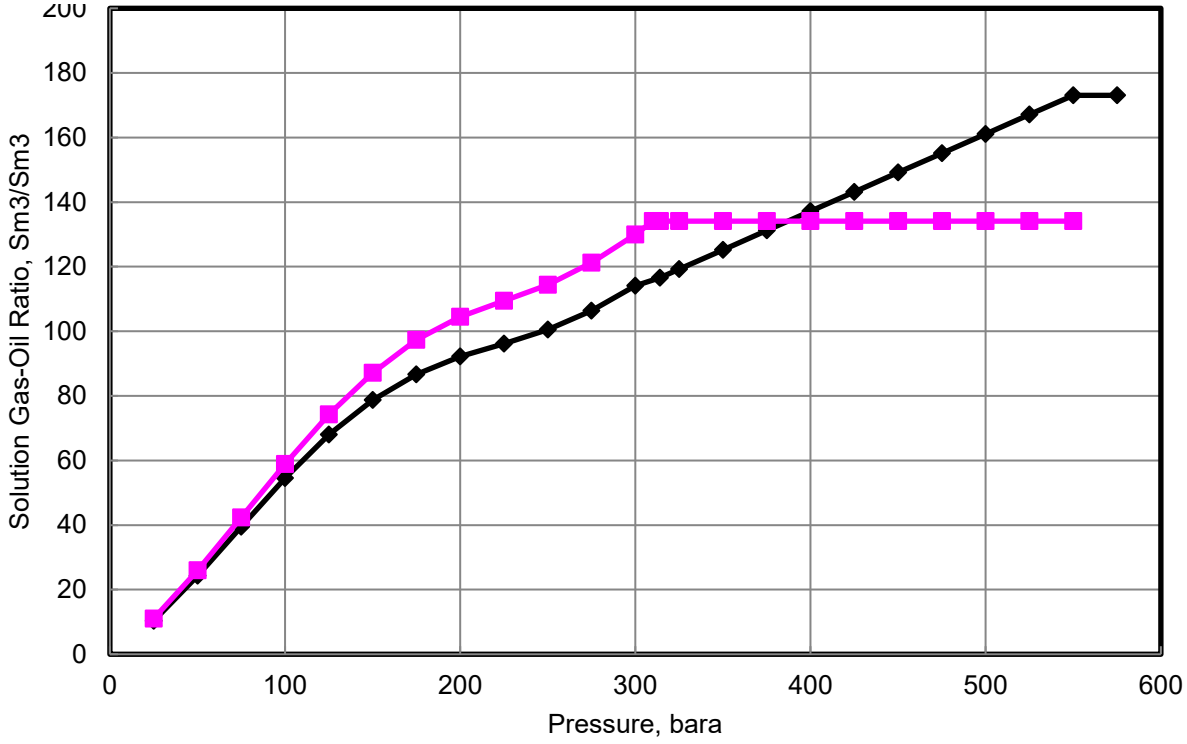

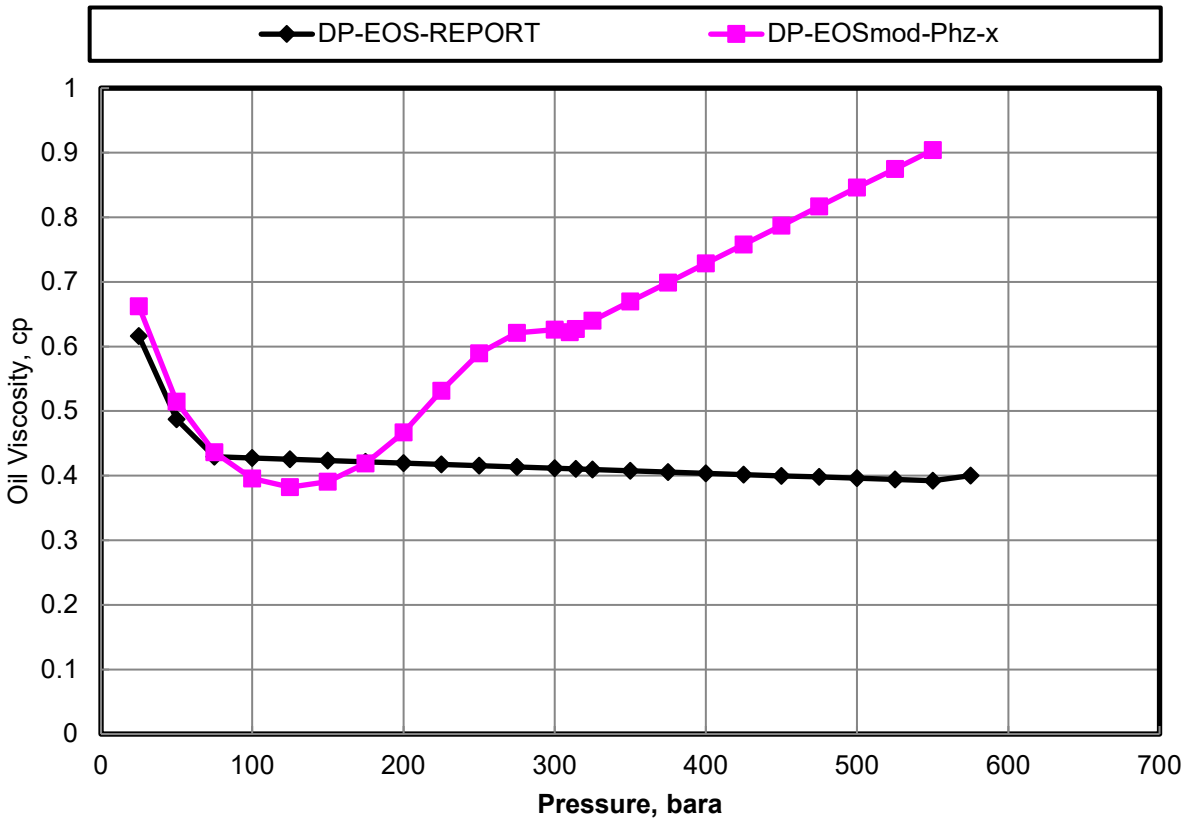
DP-EOS-REPORT
DP-EOSmod-Phz-x
Oil Viscosity, cp
0
0.1
0.2
0.3
0.4
0.5
0.6
0.7
0.8
0.9
1
0
100
200
300
400
500
600
700
Pressure, bara

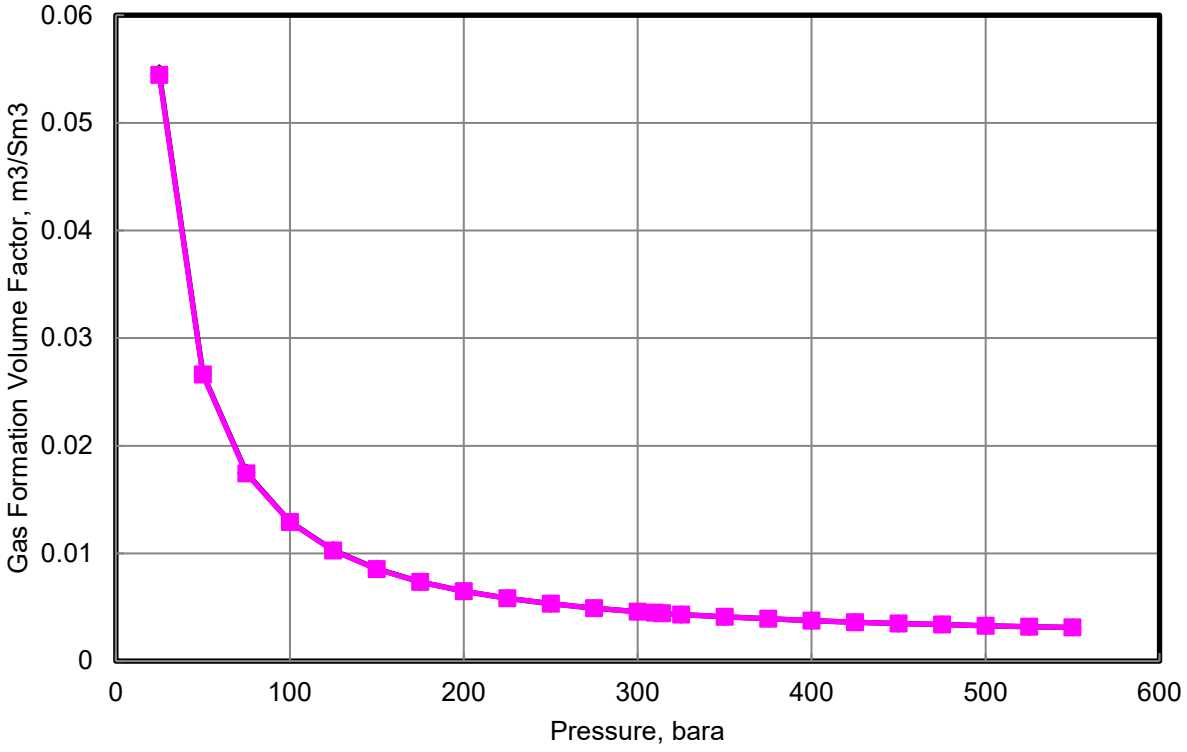
Gas Formation Volume Factor, m3/Sm3
0
0.01
0.02
0.03
0.04
0.05
0.06
0
100
200
300
400
500
600
Pressure, bara

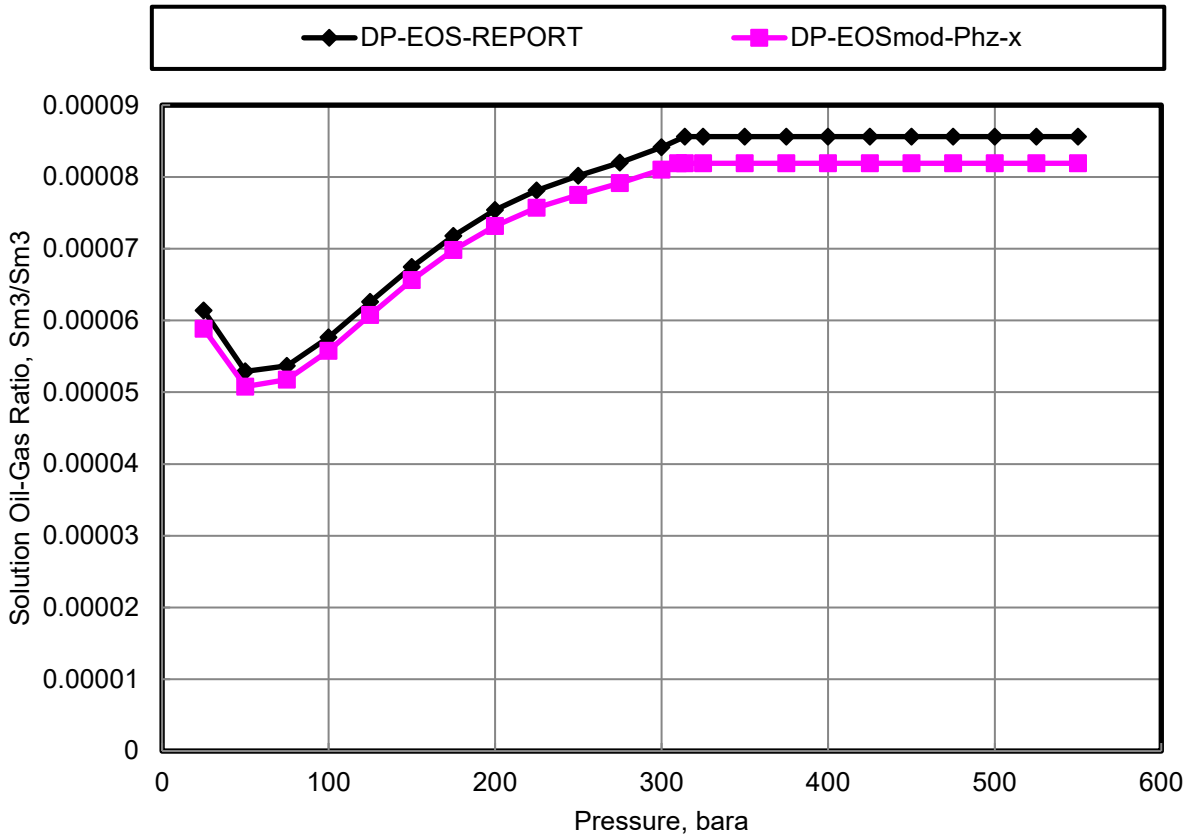
DP-EOS-REPORT
DP-EOSmod-Phz-x
Solution Oil-Gas Ratio, Sm3/Sm3
0.00009
0.00008
0.00007
0.00006
0.00005
0.00004
0.00003
0.00002
0.00001
0
0
100
200
300
400
500
600
Pressure, bara

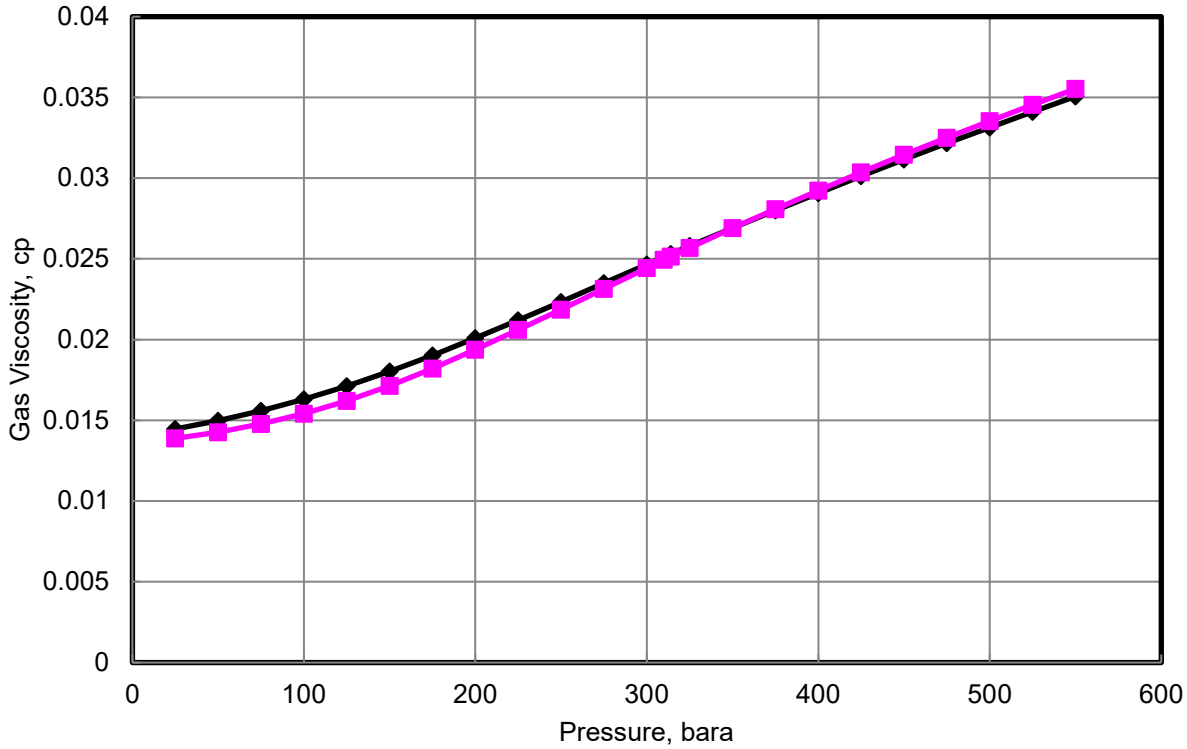
Gas Viscosity, cp
0.04
0.035
0.03
0.025
0.02
0.015
0.01
0.005
0
0
100
200
300
400
500
600
Pressure, bara

Appendix B

B.1 Porosity vs Relative Reservoir Depth

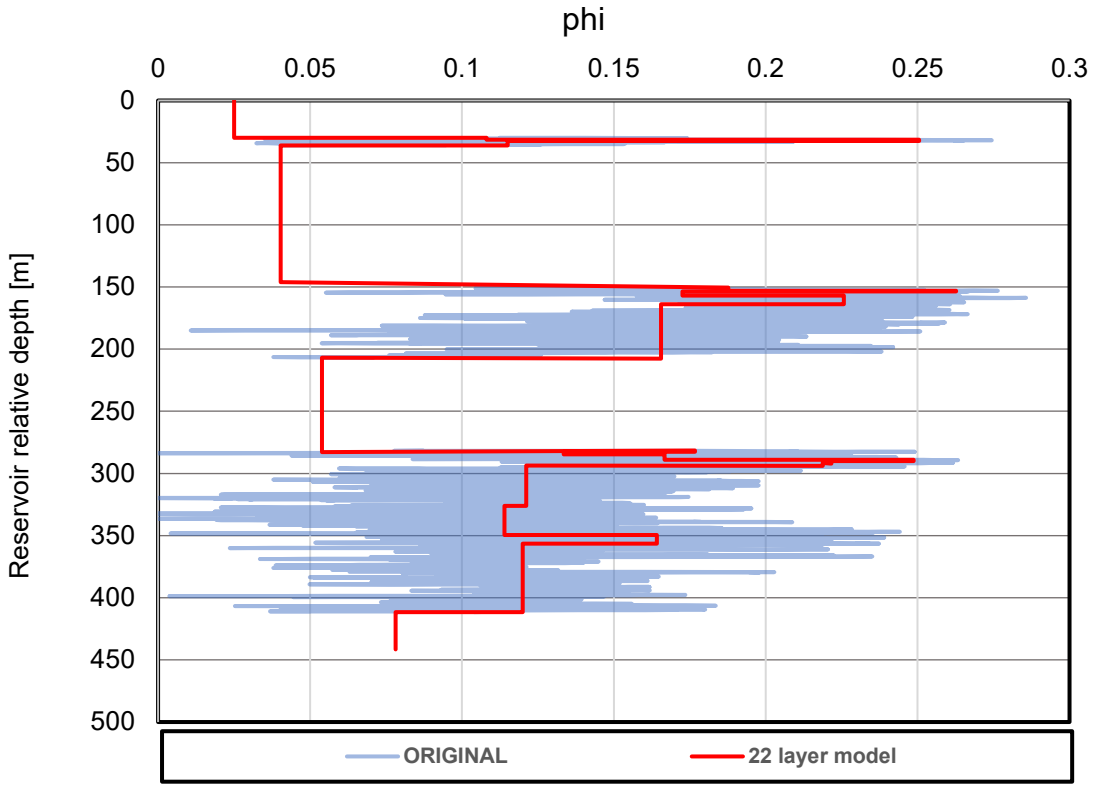

B.2 SWL vs Relative Reservoir Depth

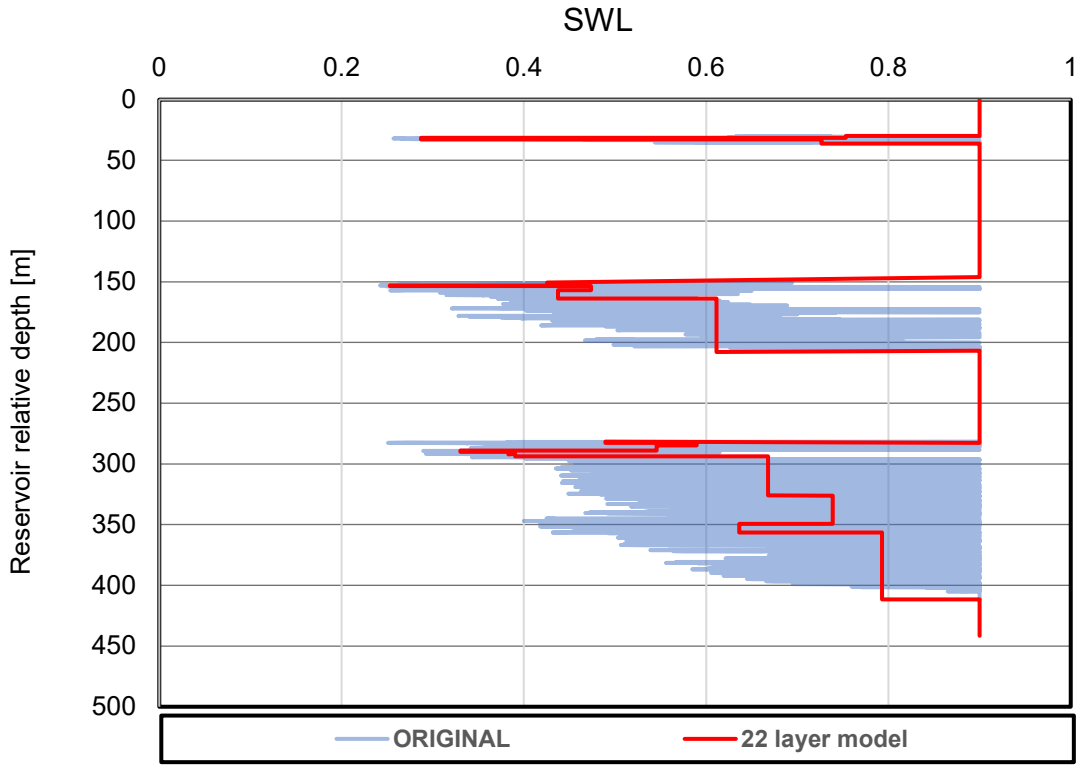

B.3 SWCR vs Relative Reservoir Depth

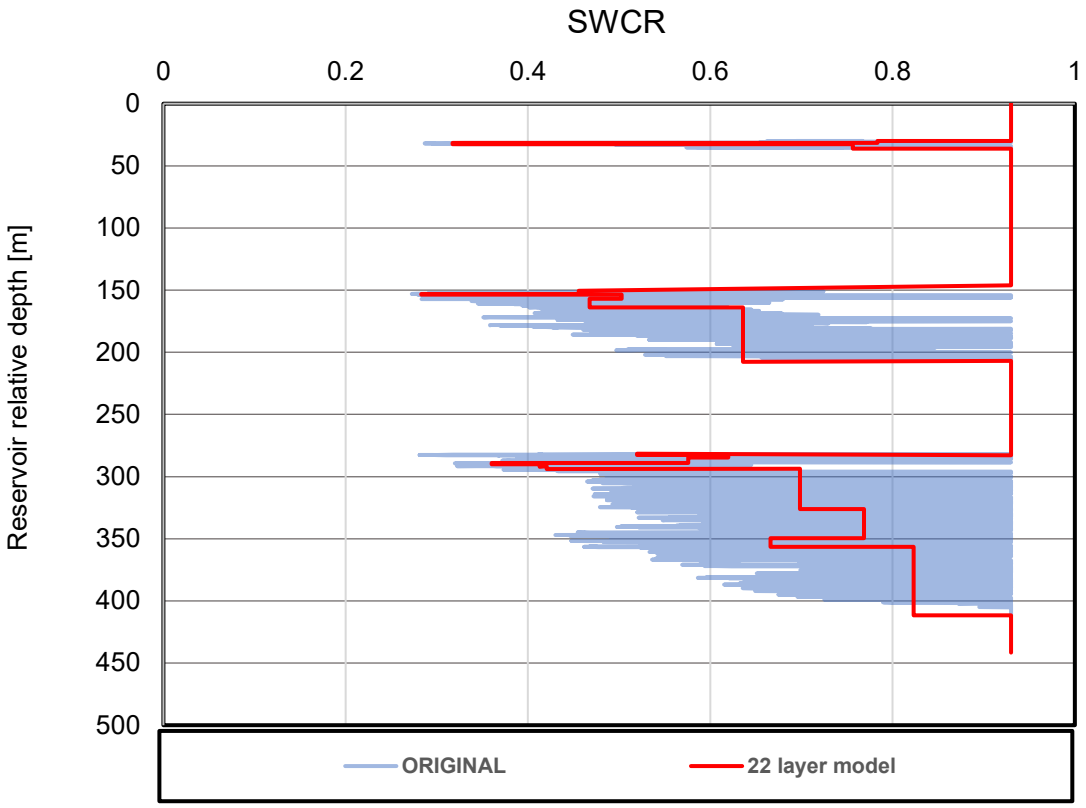

B.4 SGU vs Relative Reservoir Depth

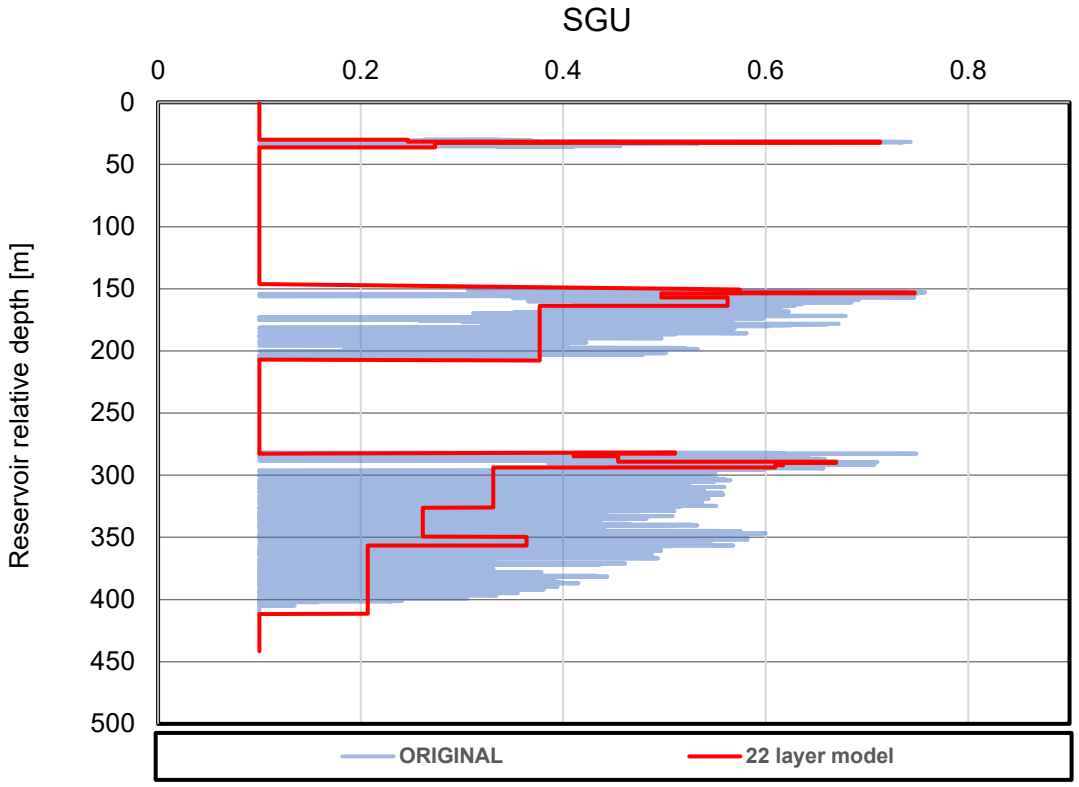

B.5 SGCR vs Relative Reservoir Depth

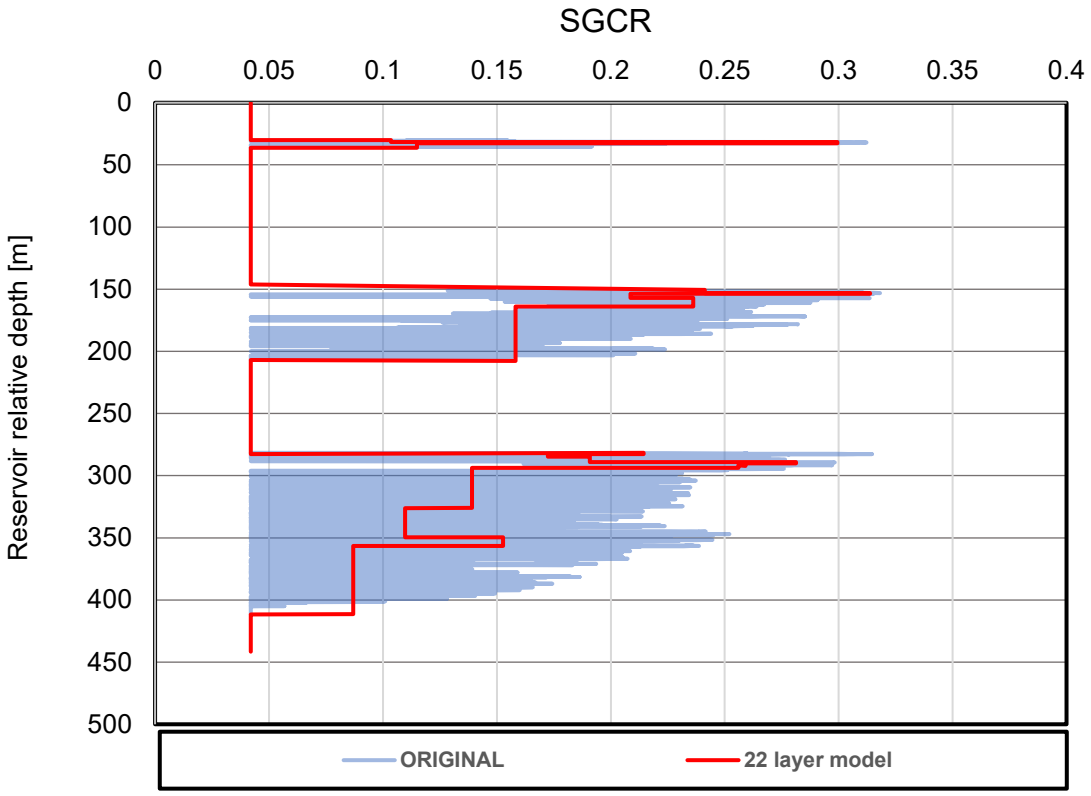

Appendix C

C.1 TPG4560 Project Report

Project Report

Student:
Erlend Torheim

TPG4560 Petroleum Engineering, Specialization Project

PVT Analysis for Condensate Blockage
A study of gas condensate samples from the Norwegian Continental shelf

Trondheim, December 17th, 2019.

NTNU
Norwegian University of Science and
Technology Faculty of Engineering
Department of Geoscience and Petroleum

NTNU
Norwegian University of
Science and Technology

Preface

The following paper is the final part of the TPG4560 Petroleum Engineering Specialization project, which is a part of the master's degree program in petroleum engineering at the Department of Geoscience and Petroleum at the Norwegian University of Science and Technology (NTNU)

Related to my work, I would like to thank Wintershall DEA, with special notice to my supervisor in the company Gerardo Seri, for providing me with knowledge and support when needed and the necessary data related to do this study. Also deserving a big thanks is the helpful employees at Whitson AS for guidance, motivation and educational discussions.

Among my co-students, I would like to thank Markus Hays Nielsen, Madelene Skintveit and Sindre Forsetløkken, for good discussions, brainstorming and knowledge sharing.

Last, but most importantly, I would like to thank my advisor at NTNU Dr. Curtis H. Whiston for supporting me throughout this process, providing the knowledge needed, excellent mentorship, motivation and support. It has been a privilege working with such an inspiring and recognized professional.

Abstract

Condensate blockage is a phenomenon important to understand related to field development of a gas condensate field. Well deliverability can be greatly reduced due to blockage in the near-wellbore region and can lead to an increase in number of wells needed. The pressure drop due to condensate blockage must be weighed relatively to the total pressure drop in the production system. Modelling the pressure drop in the near-wellbore region, using a three-region modelling concept developed by Fevang and Whitson (Fevang and Whitson 1995), is an effective method to get an idea of the relative importance of the condensate blockage. However, before the modelling can be done a basic understanding of the mechanisms and fluid behavior related to the blockage is required.

Having an equation of state (EOS) predicting the correct fluid behavior is crucial for modelling the condensate blockage correctly. Reservoir engineers often work with an EOS developed by a third part or co-worker. It can be difficult to directly understand the process behind the EOS and often the quality of the EOS is unknown. Therefore, a quality control (QC) is important. Younus et al. provides a recommended validation process that can be applied to any EOS model (Younus et al. 2019). Such a QC will make sure that the EOS predicts reliable (at least physical) properties.

If the EOS is converted from one PVT software to another, problems might occur. The importance of doing a QC in this case is shown in this report, as the EOS discussed in this study is converted from PVTsim to PhazeComp developed by Zick Technologies.

Once a trusted EOS model is obtained it can be used for predicting important properties related to condensate blockage. The major pressure drop due to condensate blockage is in the near-wellbore region (region 1 in the three-region model) and is an effect of reduction in the relative permeability of gas, krg. In this region both oil and gas flows and krg can be described as a function of the krg/kro-ratio in the region. Therefore krg/kro-ratios at different stages of depletion is obtained using the EOS to design core flooding experiments to be done on a set of cores with different absolute permeabilities (going from low to high relative for the field). The core experiments will provide relevant relative permeability data input to the reservoir model and the condensate blockage can be simulated.

Table of Contents

List of Figures

List of Tables

1 Introduction

1.1 Reservoir introduction

Field A is a potential field development in Wintershall DEA's portfolio. The development is in an early stage where studying different challenges that might occur is important. One of these challenges is condensate blockage as the fluid in the reservoir is a gas condensate.

The Field A discovery was made in March 2018 in three separate reservoir zones. Table 1.1 indicates that the porosity in the sandstone reservoir zones is good, but that the permeability is variable ranging from an average of 12.67 mD in zone 1 to 0.35 mD for zone 3. The purpose of including this table is to get an idea of the characteristics of the reservoir studied in this paper.

Table 1.1 Petrophysical parameters net reservoir (cutoffs: Vcl < 40%, PHIE > 8%)

Reservoir	Gross Thickness, m TVD	Net Thickness, m TVD	NTG, %	Av. PHIE, %	Av. Sw, %	Av. Vcl, %	Av. perm, mD
Zone 1	6.36	4.39	69.1	17.6	37.9	14.6	12.67
Zone 2	56.31	50.33	89.2	18.6	53.9	19.8	2.98
Zone 3	129.35	93.59	72.5	15.0	67.1	22.9	0.35

1.2 Samples

The samples discussed in this report are real gas condensate samples from Field A. An exploration well was drilled in the Norwegian sea, and open hole samples were collected using the modular formation dynamic tester (MDT). A total of ten samples were collected. The samples were later sent to Core Laboratories (CoreLab) where compositional analysis was done. Two constant composition expansion (CCE) experiments on two of the samples was also conducted. The two samples come from zone 1 and 2 in the reservoir.

The exploration well was drilled with oil-based mud (OBM), resulting in OBM contaminated samples. This means that the samples are "cleaned" using mathematical techniques for decontamination, based on knowledge of the OBM used in the drilling process.

1.3 Potential Condensate Blockage issues

Condensate blockage is the stabilization of a two phase gas/oil flow region near the wellbore when the bottom hole flowing pressure (BHFP) drops below the dewpoint pressure (Whitson et al. 1999). Due to this the relative permeability of the gas may drop and the well deliverability is lowered accordingly. This

effect is always present in a gas condensate reservoir, when the BHFP drops below the dewpoint. The question to be answered is how important the effects due to this phenomenon are in context of the field development.

To evaluate the importance of the condensate blockage, the potential pressure-drop over the blockage region must be compared with the pressure drop in the rest of the production system (pipe and tubing). Understanding the behavior of the fluid in the near-wellbore region is the first step in the process of determining the impact of the condensate blockage.

1.4 Study Objective

The study for this report is part one of a study of potential condensate blockage issues for the field development of field A. There are two main objectives in this study. One is to perform a quality control of the equation of state (EOS) provided by Wintershall DEA and making sure that the PVT is understood properly. Related to the quality control of the EOS is the understanding of the samples and compositional analysis. Secondly, "design curves" of gas-oil relative permeability ratio as a function of pressure is made using the EOS to be used for designing a lab experiment obtaining relevant relative permeability data needed in modelling of the condensate blockage.

The existing EOS made by Consultant A was built in PVTsim. For this project the EOS was transferred to PhazeComp where the quality control was performed. Consultant A is a third-party company delivering consultancy to the oil and gas industry and is given an anonymous name for confidentiality reasons.

1.5 Scope of Work

This report is divided into four main parts. The first part is a literature review related to understanding which PVT properties are most important for condensate blockage and why, as well as researching the theory behind the modelling of condensate blockage. The second part is dedicated to the samples from the exploration well. Quality control of the data including reviewing sampling methods used, going from the measured mass fractions to mole fractions and examine the decontamination processes. The third part covers a quality control of the EOS made by Consultant A and potential changes made. The last part will cover deliverables for further work i.e. the "design curves" of krg/kro as a function of pressure for designing a low-pressure gas condensate relative permeability test.

It should be emphasized that the work done and discussed in this report is meant to be a preparation for the following Master Thesis, where the main goal is to study the effect condensate blockage will have on the field development of Field A.

2 Gas Condensates & Blockage

This section is a literature study of gas condensate reservoir management with special notice to condensate blockage. The purpose of this section is to give insight into what the EOS discussed in this study will be used for and to determine the deliverables for further work related to modelling condensate blockage.

2.1 Introduction to Gas Condensates

A reservoir fluid is formally classified as a gas condensate if the reservoir temperature is less than the cricondentherm (where the fluid will never enter a two-phase region) and greater than the critical temperature (Whitson and Brulé 2000). Figure 2.1 shows this graphically.

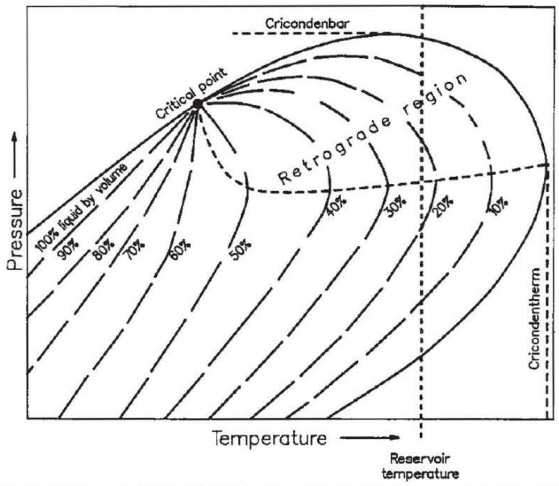

Figure 2.1 Hypothetical p-T diagram for a gas condensate showing isothermal retrograde region (Whitson and Brulé 2000).

Typical retrograde gas condensate reservoirs present a gas/oil ratio (GOR) ranging from 3000 to 150000 scf/STB (535 to 26720 Sm3/Sm3). This corresponds to a condensate/gas ratio (CGR) of 350 to 5 STB/MMscf (0.002 to 0.00003 Sm3/Sm3). Liquid gravities range typically between 40 to 60° API.

Gas condensate engineering is for the most part regular gas engineering, with some extent of additional engineering due to surface condensate production and retrograde condensate left in the reservoir. It can be argued that gas condensate engineering is 80% traditional gas engineering and 20% "extra" engineering (Whitson et al. 1999). The main characteristics of a gas condensate can be summarized as follows (Whitson and Mott 2005):

1. The already mentioned retrograde condensation happening in the reservoir. This liquid phase usually has no or very low mobility, except from in the near well bore region.

2. Surface condensate production may lead to a significant increase in the income of a gas condensate field. Processing methods and optimization at surface will decide the "extra" income from the surface condensate.
3. Recoveries by depletion will typically range from 60-80% for gas and 20-40% for condensate.
4. Gas cycling is a potential method for increasing the condensate recoveries but will require injection gas. The injection gas can either be the produced gas or purchased injection gas. (Gas cycling will not be covered in detail in this report).
5. Condensate blockage can become a significant contributor to pressure drop and thus well deliverability after the BHFP falls below the dewpoint pressure. This is an important consideration for low and medium permeability gas condensate reservoirs.

2.2 Gas Condensate PVT

As mentioned in the previous section there are extra issues needed to be handled for a gas condensate reservoir compared to a traditional "dry" gas reservoir. How the condensate "yield" varies with time and how the two-phase gas/oil flow affect the gas productivity are the most important issues. PVT properties are strongly connected to these issues. In addition to Z-factor and gas viscosity (traditional gas engineering) the compositional (C_{7+}) variation with pressure, oil viscosity and liquid dropout are crucial to understand and quantify.

2.2.1 PVT Experiments

There are mainly two PVT experiments performed on gas condensate samples:

1. CCE (Constant Composition Expansion)
2. CVD (Constant Volume depletion)

The CCE experiment is utilized for measuring dewpoint pressure, single-phase gas Z-factor and liquid dropout curve (oil relative volume). A PVT cell is charged with a sample of reservoir fluid. Usually the PVT cell has a window for visual observation. The cell is brought to reservoir temperature and a pressure high enough to ensure that the sample is single phase. Pressure is declined by increasing cell volume, keeping the temperature constant. When the pressure is decreased enough for a liquid droplet to form, and to be detected through the glass window, the dewpoint is found. Oil relative volume is found by monitoring cell and liquid volume from the initial reservoir pressure down to a low pressure. Volumetric data is often reported as relative volume, $V_{rel} = V/V_{Sat}$ (i.e. volume at indicated pressure per volume at dew point pressure), retrograde liquid volume as a percentage of the volume at the dewpoint and retrograde liquid volume as a percentage of the volume at the indicated pressure.

CVD experiments monitor the phase and volumetric changes of a reservoir gas sample as the pressure drops below the dewpoint and equilibrium gas phase is removed. It can be argued that CVD tests simulates closely the actual behavior of pressure depletion of a gas condensate reservoir and the results obtained can be used to quantify recoveries of surface gas and condensate below the dewpoint as a function of pressure (Whitson et al. 1999). The experiment is conducted by lowering the pressure below the dewpoint, with an associated increase in cell volume. After equilibrium is reached at every pressure step the original cell volume at the dewpoint is obtained by removing equilibrium gas from the top of the cell. The removed gas is analyzed in terms of amount, composition and Z-factor. The volume of the remaining oil is measured and reported.

A "two-phase" Z-factor is reported to be used in the traditional gas material balance below the dewpoint. This Z-factor is given in Eq. 2.1 and is a not-physical property. This pseudo property is calculated assuming that the gas-condensate reservoir is depleting according to the dry (traditional) gas material balance and the initial conditions of the reservoir is at the dewpoint (Whitson and Brulé 2000).

$$Z_2 = \frac{P_{CVD}}{\frac{P_d}{Z_d}\left[1 - \frac{n_p}{n}\right]} \tag{2.1}$$

In Eq. 2.1 n_p/n represents G_{pw}/G_w, which is reported in a CVD report. Here G_{pw} = cumulative wet gas produced and G_w = initial wet gas in place at dewpoint pressure. Wet gas indicates that condensate is produced at surface from the gas. The moles produced, n_p, is calculated from the measured properties $\Delta V_{\bar{o}}$, $\Delta V_{\bar{g}}$, $\rho_{\bar{o}}$, $\rho_{\bar{g}}$ and $M_{\bar{o}}$ of the surface gas and condensate (Whitson and Brulé 2000). Combining the single-phase Z-factor from the CCE test and data obtained in the CVD prediction of depletion behavior from initial pressure to abandonment can be obtained.

2.2.2 Initial Fluids in Place and Depletion Recovery

Initial fluids in place (IFIP) can be calculated from knowing reservoir properties (i.e. hydrocarbon pore volume (HCPV) and initial pressure) and PVT properties. For calculating initial gas in place (IGIP), HCPV, initial pressure and Z-factor are the properties needed. Initial condensate in place (ICIP) is dependent on IGIP and the liquid composition i.e. C_{n+} mole fraction that will become sellable oil at surface. This is dependent on the surface processing. Two equations can be defined for describing IGIP and ICIP:

$$IGIP = \frac{HCPV_g}{B_{gdi}} \tag{2.2}$$

$$ICIP = IGIP * r_{si} = HCPV_g * \frac{r_{si}}{B_{gdi}} \tag{2.3}$$

5

Here, B_{gdi} is referring to the initial dry gas formation volume factor, which is defined as the volume of reservoir gas divided by the volume of surface gas resulting after separation of the reservoir gas. This is shown in Eq. 2.4.

$$B_{gd} = \frac{V_g}{V_{\bar{g}g}} \tag{2.4}$$

It is important to emphasize that B_{gd} is not equal to the traditional wet gas formation volume factor B_{gw} given by Eq. 2.5. In Eq. 2.4 $V_g = n_g ZRT_R/P_R$ and $V_{\bar{g}g} = n_{\bar{g}g} RT_{SC}/P_{SC}$, where n_g is moles reservoir gas and $n_{\bar{g}g}$ is moles surface gas from the reservoir gas.

$$B_{gw} = \frac{P_{sc}}{T_{sc}} * \frac{T_R}{P_R} * Z \tag{2.5}$$

As a result, Eq. 2.4 can be written as Eq. 2.6:

$$B_{gd} = B_{gw} * \frac{n_g}{n_{\bar{g}g}} \tag{2.6}$$

Typically, $n_{\bar{g}g}/n_g$ i.e. mole fraction of reservoir gas that remains gas at surface conditions, will vary depending on the richness of the of the gas condensate and the surface process. The range may go from 85% for a rich gas condensate to 99% for lean gas systems. $n_{\bar{g}g}/n_g$ can be approximated by Eq. 2.7 where z_{n+} refers to the approximate mole fraction of the reservoir gas becoming oil at surface.

$$\frac{n_{\bar{g}g}}{n_g} = 1 - z_{n+} \tag{2.7}$$

The r_{si} term in Eq. 2.3 is referring to the initial solution oil gas ratio. An equation for approximating the OGR is defined in Eq. 2.8.

$$r_s = \frac{V_{\bar{o}g}}{V_{\bar{g}g}} = \frac{z_{n+}(M/\rho)_{n+}}{(1 - z_{n+})(RT_{sc}/P_{sc})} \tag{2.8}$$

In the equations above HCPV is given from geological and petrophysical research. B_{gdi} and r_{si} are PVT properties found in PVT experiments as a function of the initial reservoir composition z_i and surface processing.

Before the reservoir pressure drops below the dewpoint pressure, the gas and condensate recovery factors are the same. This is because all the condensate in place in the gas is brought to surface. Since

the recoveries are proportional to Z_i/Z in the gas material balance equation (Eq. 2.9 shows the *straight-line* material balance), the Z-factor is an important property to predict correctly.

$$\frac{P}{Z} = \left(\frac{P}{Z}\right)_i \left(1 - \frac{Gp}{G}\right) \tag{2.9}$$

Equation 2.9 can be rewritten in terms of recovery factor as in Eq. 2.10:

$$RF_g = \frac{G_p}{G} = \left(1 - \frac{P/Z}{P_i/Z_i}\right) \tag{2.10}$$

Straight line material balance represents pressure depletion with no extra pressure support due to aquifer influx, water expansion etc. Recovery factor of condensate RF_o equals recovery factor of gas, RF_g, at pressures greater than the dewpoint pressure. This can be shown by defining the initial OGR, r_{si}, as the ratio of surface oil produced from the reservoir gas, versus surface gas produced initially ($V_{\bar{o}gi}/V_{\bar{g}gi} = OGR_i = r_{si}$). As the composition of the produced gas does not change before the dewpoint is reached, r_s does not change and the surface oil produced can be written as shown in Eq. 2.11 i.e. that above the dewpoint pressure the producing OGR, r_p, equals the initial solution OGR, r_{si} (assuming that BHFP is above dewpoint pressure also).

$$N_p = \int_{P_{Ri}}^{P_d} r_p dG_p = r_{si} * G_p \tag{2.11}$$

This leads to Eq. 2.12 , which is as mentioned valid for $P > P_d$

$$RF_{\bar{o}} = \frac{N_p}{N} = \frac{G_p * r_{si}}{G * r_{si}} = RF_{\bar{g}} \tag{2.12}$$

As the reservoir pressure drops below the dewpoint pressure, retrograde condensate will be left in the reservoir. This leads to compositional variation during depletion. From this point on Eq. 2.12 is not valid as the producing OGR, r_p, will vary from solution OGR r_s. This is emphasized in more detail in section 2.3 about condensate blockage.

An approximation of the effect compositional variation has on depletion below the dewpoint can be made using the data from a CVD experiment directly. For the purpose of this simplification C_{7+} is the assumed surface condensate produced from the wellstream. First the oil rate versus time is defined approximately by Eq 2.13, where $q_g(t)$ is the surface gas rate production profile:

$$q_o(t) \cong \mathrm{q_g(t)} * \frac{(\mathrm{y_{7+}})_{CVD}}{1-(\mathrm{y_{7+}})_{CVD}} * \frac{(\mathrm{M_{7+}/\rho_{7+}})_{\mathrm{CVD}}}{\mathrm{RT_{sc}/P_{sc}}} \tag{2.13}$$

The surface gas equivalent of one surface oil volume, C_{og} is defined in Eq 2.14. The property is dependent on the molecular weight and density of C_{7+} and will in theory change for every reported CVD depletion step. For simplicity the property is often assumed constant as it does not change drastically.

$$C_{og} = \frac{RT_{sc}}{P_{sc}} * \left(\frac{\rho_{7+}}{M_{7+}}\right)_{CVD} \tag{2.14}$$

The CVD properties are dependent on time and must be correlated to wet gas cumulative volumes produced, G_{PW}, as follows:

$$G_{pw} = \int q_w dt \tag{2.15}$$

where $q_w = q_g + q_o * C_{og}$. The rate profile and cumulative wet gas produced can be translated into cumulative wellstream produced form the CVD test. $(n_p/n_d)_{CVD}$ is defined in Eq. 2.16. and is valid from pressures equal to or below the dewpoint.

$$\frac{n_p}{n_d} = \frac{G_{pw}}{G_w} - \left[1 - \frac{(P/Z)_d}{(P/Z)_i}\right] \tag{2.16}$$

The approximate recoveries can be calculated from the initial reservoir pressure to the abandonment using Eq 2.17. and Eq. 2.18. below. These recovery factors are used for making sure that the reservoir model, with the PVT model, is matching exactly the PVT experiments done on in the lab. These equations do not consider the near wellbore effects discussed in section 2.3.

$$RF_{oD} = \left(1 - \frac{(P/Z)_d}{(P/Z)_i}\right) + \frac{(P/Z)_d}{(P/Z)_i} \sum_{k=1}^{N} \left(\frac{\Delta n_p}{n_d}\right)_k \frac{(z_{7+} M_{7+}/\rho_{7+})_{CVD,k}}{(z_{7+} M_{7+}/\rho_{7+})_{CVD,i}} \tag{2.17}$$

$$RF_{gD} = \left(1 - \frac{(P/Z)_d}{(P/Z)_i}\right) + \frac{(P/Z)_d}{(P/Z)_i} \sum_{k=1}^{N} \left(\frac{\Delta n_p}{n_d}\right)_k \frac{(1 - z_{7+})_{CVD,k}}{(1 - z_{7+})_{CVD,i}} \tag{2.18}$$

The above equations can be rewritten as Eq. 2.19 and Eq. 2.20:

$$RF_{oD} = \left(1 - \frac{(P/Z)_d}{(P/Z)_i}\right) + \frac{(P/Z)_d}{(P/Z)_i} \sum_{k=1}^{N} \left(\frac{\Delta n_p}{n_d}\right)_k \frac{(1/r_{si} + C_{og})}{(1/r_{sk} + C_{og})} \tag{2.19}$$

$$RF_{gD} = \left(1 - \frac{(P/Z)_d}{(P/Z)_i}\right) + \frac{(P/Z)_d}{(P/Z)_i} \sum_{k=1}^{N} \left(\frac{\Delta n_p}{n_d}\right)_k \frac{(1 + r_{si} * C_{og})}{(1 + r_{sk} * C_{og})} \tag{2.20}$$

8

where C_{og} is as mentioned above assumed constant and r_s is calculated from Eq. 2.8.

It can also be important to a gas condensate field development to consider the compositional variation with depth. The effect of compositional variation as a result of gravitational segregation is that a gas condensate gets richer (i.e. for practical purposes more C_{7+}) with greater depths (Whitson et al. 1999). As a results calculation of initial surface condensate in place will vary depending on the depth where the sample is collected.

2.3 Condensate Blockage

Condensate blockage is the stabilization of a two phase gas/oil flow region near the wellbore when the BHFP drops below the dewpoint pressure (Whitson et al. 1999). From a field development point of view the well deliverability reduction due to condensate blockage is only important when the BHFP reaches a minimum and the well is forced to go on decline (Fevang and Whitson 1995). This is when the field will have problems delivering the rates required. Therefor the condensate blockage will have an important role in the field development strategy i.e. number of wells etc. In the big picture the pressure drop due to condensate blockage must be compared with the pressure drop in the rest of the production system. The method for calculating gas condensate well deliverability studied in this report is the three-region model presented by Fevang and Whitson in 1995.

2.3.1 Condensate Blockage Modelling Theory

To understand the effect condensate blockage has on well deliverability the gas condensate rate equation must be introduced. Equation 2.21 and 2.22 describe the general volumetric rate equation for a gas condensate well with a compositional formulation and in terms of black-oil PVT respectively.

$$q_g = C\left(\frac{RT_{sc}}{p_{sc}}\right)\beta_s \int_{P_{wf}}^{P_R}\left(\frac{\rho_o k_{ro}}{M_o \mu_o} + \frac{\rho_g k_{rg}}{M_g \mu_g}\right) dp \tag{2.21}$$

$$q_g = C\int_{P_{wf}}^{P_R}\left(\frac{k_{ro}}{B_{o\mu_o}} R_s + \frac{k_{go}}{B_g \mu_g}\right) dp \tag{2.22}$$

In the two equations above the gas rate constant C includes the basic reservoir properties,

$$C = \frac{2\pi a_1 kh}{ln(r_e/r_w) - 0.75 + s} \tag{2.23}$$

where a_1 varies depending on the units. β_s in Eq. 2.21 is the surface gas mole fraction in wellstream. It

is also important to notice that relative permeabilities k_{rg} and k_{ro} are defined relative to absolute permeability i.e. the ability to flow fluid through a rock when only one phase is present in the rock (Schlumberger 2019).

The three-region model is an accurate model for well deliverability of a gas condensate well undergoing depletion. One, two or all three regions may exist depending on the producing condition. An important assumption is that the flow condition in the three regions is pseudo-steady state, i.e. steady-state conditions at a given time, but the steady state condition changes during depletion. Figure 2.2 shows the three regions:

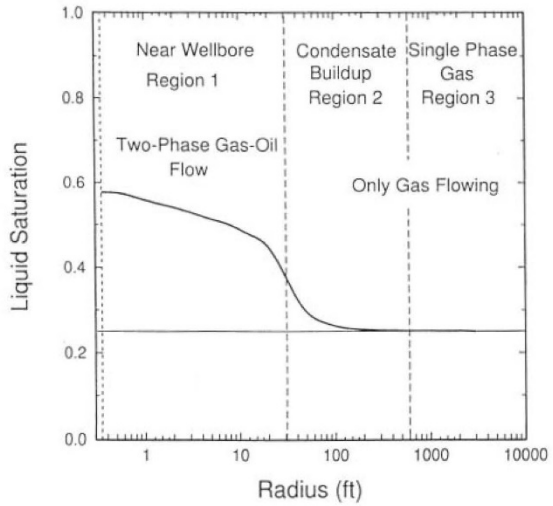

Figure 2.2 The three regions of flow behavior in Fevang and Whitson's three-region model (Fevang and Whitson 1996)

The three-region model is based on decomposing the pseudopressure integral in Eq. 2.21 and 2.22 into three parts representing the pressure drop in the three different regions. These integrals will be defined further down under the description of each region (Fevang and Whitson 1995):

Region 1 is the region where both gas and condensate flow simultaneously. Because of the reduction in relative permeability of gas, region 1 is the main source of reduction in well deliverability. This region will always exist if the BFHP is less than the dewpoint. The GOR is constant, meaning that the single-phase gas entering the region has the same composition as the produced wellstream mixture. The condensate saturation is determined as a function of radius to ensure that all liquid that condenses from the single-phase gas entering Region 1 has high enough mobility to flow through and out of the region without any net accumulation. The *solution* OGR decreases with pressure, and since pressure decreases towards the wellbore the liquid saturation increases towards the wellbore (see figure 2.2)

(Fevang 1995). Region 1 will increase with time and the outer boundary moves outwards as a result. The liquid saturation closest to the wellbore will also decrease with time, as the gas entering the region gets leaner throughout production.

Equation 2.24 shows the pseudopressure integral of region 1 in terms of black-oil PVT properties.

$$\Delta P_{p1} = \int_{P_{wf}}^{P^*} \left(\frac{k_{ro}}{B_o \mu_o} R_s + \frac{k_{rg}}{B_g \mu_g} \right) dp \tag{2.24}$$

The integral ranges from the BHFP, P_{wf}, to the dewpoint of the producing wellstream P^*. This dewpoint will be lower than the initial dewpoint p_d. The equation is solved using the modified Evinger-Muskat approach modified for gas condensates. The producing GOR and PVT properties are needed. Equation 2.25 describes the producing GOR (Fetkovich et al. 1986),

$$R_P = R_S + \left(\frac{k_{rg}}{k_{ro}} \right) \left(\frac{\mu_o B_o}{\mu_g B_{gd}} \right) (1 - r_s R_p) \tag{2.25}$$

which is the modified version of the producing GOR defined by Evinger and Muskat for an oil reservoir in Eq. 2.26 (Whitson 1984).

$$R_P = R_S + \left(\frac{k_{rg}}{k_{ro}} \right) \left(\frac{\mu_o B_o}{\mu_g B_{gd}} \right) \tag{2.26}$$

Rearranging Eq. 2.25 yields k_{rg}/k_{ro} given in Eq. 2.27 as a function of pressure as the PVT properties are functions of pressure. The derivation of Eq. 2.25 can be found in Appendix A.

$$\frac{k_{rg}}{k_{ro}}(P) = \left(\frac{R_p - R_S}{1 - r_S R_P} \right) \frac{\mu_g B_{gd}}{\mu_o B_o} \tag{2.27}$$

Relative volume from CCE data can be used to express Eq. 2.27 as a function of $V_{ro} = V_o/V_{tot}$ at each pressure in the CCE experiment as shown in Eq. 2.28.

$$\frac{k_{rg}}{k_{ro}}(P) = \left(\frac{1}{V_{roCCE}} - 1 \right) \frac{\mu_g}{\mu_o} \tag{2.28}$$

When both oil and gas phases are mobile, as it is in region 1, k_{rg} and k_{ro} can be expressed directly as a function of the ratio defined in Eq. 2.28. This is equivalent to saying that k_{rg} and k_{ro} can be evaluated directly as a function of pressure, $k_{rg}(P) = f[k_{rg}/k_{ro}(P)]$ and $k_{ro}(P) = f[k_{rg}/k_{ro}(P)]$. Section 5 describes in more detail the plots of $k_{rg}/k_{ro}(P)$ used for designing the relative permeability experiments needed to model the reduction in well deliverability due to condensate blockage.

Region 2 will always co exists with region 1 after reservoir pressure drops below the dewpoint pressure (no region 3). All three regions will exist if the reservoir is slightly undersaturated and BHFP is less than the dewpoint pressure, while region 2 may be neglectable for highly undersaturated reservoirs. Region 2 is the region where only gas is flowing i.e. oil mobility is practically zero, while condensate starts to accumulate. The condensate saturation can be approximated by the liquid dropout curve of a CVD experiment, corrected for water saturation. According to Fevang and Whitson the size and importance of Region 2 is greater for lean gas condensates (Fevang and Whitson 1995).

Equation 2.29 show the pseudopressure integral for region 2.

$$\Delta P_{p2} = \int_{p^*}^{P_d} \frac{k_{rg}}{B_g \mu_g} dp \tag{2.29}$$

The relative permeability of gas is a function of oil saturation $k_{rg}(S_o)$, where S_o is estimated as a function of CVD relative oil volumes. $V_{roCVD}(P) = V_o(P)/V_d$ will give $S_o(P) = [V_{roCVD}(P)](1 - S_w)$, where $(1 - S_w)$ is the correction for the present water saturation. There is also accumulation of condensate due to the gas flowing in region 2 (i.e. the condensate coming out of solution as the pressure decreases closer towards region 1). When CVD relative volume data are missing, it can be calculated from the equation below (Fevang and Whitson 1995):

$$(V_{roCVD})_k = \frac{N_{k-1} - G_{k-1}(r_s)_k}{1 - (r_s R_s)_k} (B_o)_k \tag{2.30}$$

where k is the current pressure step. N_{k-1} and G_{k-1} is defined as flows

$$N_{k-1} = \left(\frac{V_{roCVD}}{B_o} + \frac{1 - V_{roCVD}}{B_{gd}} r_s \right)_{k-1} \tag{2.31}$$

$$G_{k-1} = \left(\frac{V_{roCVD}}{B_o} R_s + \frac{1 - V_{roCVD}}{B_{gd}} \right)_{k-1} \tag{2.32}$$

Region 3 is existing if the reservoir is undersaturated and will exist if the reservoir pressure is above the dewpoint pressure. As gas is the only phase present only PVT properties are relevant. Equation 2.33 show the pseudopressure integral of region 3 which is the traditional single phase pseudopressure function.

$$\Delta P_{p3} = k_{rg}(S_{wi}) \int_{P_d}^{P_R} \frac{1}{B_{gd} \mu_g} dp \tag{2.33}$$

2.3.2 Viscosity

The importance of having correct oil and gas viscosity is emphasized in section 2.3.1. Compared to gas viscosity, it can be argued that oil viscosity is more important for modeling of condensate blockage. Region 1 blockage discussed in the section above is highly dependent on the oil viscosity. Usually oil viscosity is low in condensate reservoirs, with values ranging from 0.1 to 1 cP in the near wellbore region. Typical values for gas viscosities will vary from 0.02 to 0.03 cP for all pressure conditions. This means that the gas viscosity does not vary greatly for a given gas system. In most cases gas viscosities are within 5-10% of predicting the viscosity correctly.

It is important to notice that viscosity of condensate measured from a CVD test usually reports higher viscosities to the reality is. The difference may be a factor of 2-3 (Whitson et al. 1999). Laboratories do not normally make measurements of viscosity in routine tests, and difficulties obtaining large enough oil volumes from lean condensate prevent tests from being done. This is the case for the samples studied in this report. Correlations for calculating oil viscosities can be unreliable in predicting low viscosities like what is often found in lean gas condensates. Section 4.2.4 describes a method predicting reliable viscosities in lack of sample measured viscosities.

3 Samples

Wintershall DEA drilled a successful exploration wildcat well on Field A. The target for the drilling was three separate sandstone reservoirs of Formation A. Table 1.1 summarizes net reservoir petrophysical properties. Oil-based mud was used in the drilling of the well, leading to contaminated samples.

Three MDT samples were retrieved from the hydrocarbon columns in Zone 1 and 2 and four samples from Zone 3. Table 3.1 includes an overview of the samples. The samples marked in blue are the samples CoreLab used for CCE experiments.

Table 3.1 Overview of the samples from the exploration well.

Reservoir zone	Sample ID	[redacted]	%-Contaminated
Zone 1 **Temp = 109.9 °C**	24583 - IB		4
	34423 - IB		3
	21364 - IB		3
Zone 2 **Temp = 115.2 °C**	24582 - IB		7
	34428 - IB		5
	34430 - IB		5
Zone 3 **Temp = 121.2 °C**	24592 - IB		14
	24577 - IB		13
	34434 - IB		11
	28346 - IB		9

3.1 Analysis Methods – CoreLab

According to CoreLab, integrity of the samples was maintained by measuring the opening pressure of the open-hole gas condensate samples at ambient temperatures, before heating the samples to 93.3 °C and stabilizing them at 656.0 bara. This ensures homogeneity of the samples, before any sample removal. This section will cover a summary of the compositional analysis CoreLab did on the samples and an overview of the CCE experiments.

3.1.1 Compositional Analysis Summary

Cryogenic distillation and gas chromatography techniques were used to determine the compositions of the samples. The process is described by CoreLab as follows:

1. The samples were pumped into pre-weighed flasks submerged in liquid nitrogen and were condensed.
2. The condensed gas phase was then gradually allowed to return to ambient temperature.
3. Residual condensates and evolved gases were collected separately, weighed and then analyzed using gas chromatography.
4. The compositions were than combined mathematically, to the measured gas-liquid weight ratios to calculate the recombined fluid compositions.

The liquid samples were introduced to temperature programmed high resolution capillary gas chromatography, giving the stabilized liquid compositions. Gas compositions were determined using extended gas chromatography with a temperature program to provide optimum detection and resolution of the C7+ components.

The molar compositions and residual fraction properties are calculated entities. Using the measured weight % (wt %) distribution and pseudo component molecular weight and density properties taken from published property tables (Katz and Firoozabadi) the mole % is calculated.

To quantify the amount of contamination present in the sample compositional analysis was done on a portion of mud filtrate extract. Comparisons of the mud composition and the composition of the contaminated gas condensate samples leads to a log-plot of contaminated sample wt % versus carbon number plotted together with the mud filtrate in order to highlight the area of contamination. Assuming a linear relationship the approximate level of contamination was calculated from the deviation of the linear plot. Calculation of the uncontaminated reservoir fluid was then performed.

3.1.2 CCE - PVT Experiment

CoreLab together with Wintershall DEA decided to use zone 1 open-hole gas condensate sample 21364-IB and zone 2 sample 34428-IB for CCE experiments. The experiments were carried out in a specialized 400cc CoreLab PVT cell. Portions of the samples were charged to the cell at reservoir temperature. The experiment was performed during which the dewpoint pressure was determined as well as pressure-volume data for the single and two-phase fluid. Table 3.2 summarizes the data gathered from the experiment. See Appendix B for more details around the CCE experiments. It is important to keep in mind the samples used in the experiments are OBM contaminated samples and will therefore not represent the in-situ reservoir fluids.

Table 3.2 Summary of PVT data obtained by CCE experiments.

CCE properties			Sample: 21364-IB T_R = 109.9 °C P_R = 362.7bara	Sample: 34428-IB T_R = 115.2 °C P_R = 374.3 bara
Saturation pressure	P_d	[bara]	346.6	335.6
Z-factor @	P_R		1.019	1.027
Z-factor @	P_d		1.000	0.984
Density @	P_R	[kg/m3]	253.1	244.6
Density @	P_d	[kg/m3]	246.3	228.6

3.2 Quality Control of Samples

This section is dedicated to a QC of the reported data in the CoreLab report. This includes checking that the claimed molecular weights (in the CoreLab report) are used when calculating the molar composition from the measured weight composition, and a review and discussion of the decontamination process. A full overview of calculated mole % of sample 21364-IB and 34428-IB is found in Appendix C

3.2.1 Mole Fraction Calculated from Measured Mass Fraction

CoreLab states specifically in the report that molar composition is "calculated from pseudo component data using properties taken from published property tables (katz and Firoozabadi)". An easy check of this can be done by inputting the weight % and molecular weights to PhazeComp (or excel) for the samples studied and calculate the mole %.

The reported mole % is accurately calculated from this method. It is clear that the reported mole % in the CoreLab report suffers from poor resolution in significant digits in the heavier components. For instance, mole % of C35 is reported as 0.000, while the calculated value from PhazeComp is 0.0005 for sample 21364-IB (see table 3.3). Thus, inputting the lab measured weight fractions to an equation of state PVT software or model instead of copying the mole fractions directly from a lab report, seems to be a better option.

The C36+ molecular weight in table 3.3 is a calculated property and it differs from the different samples. Laboratories often provide these "calculated" properties. It has become more seldom that the residue properties (i.e C_{n+} n = 7, 11, 20, 36 etc.) are calculated from measured "flashed" properties, but instead based on measured w_i and assumed Mi and γ_i – e.g. Katz and Firoozabadi or in-house methods (Younus et al. 2019). Equation 3.1 describes the calculation of C_{n+} molecular weight if the average molecular weight had been measured by the lab. In the equation $w_{\bar{o}i}$ is the mass fraction of components in the stabilized oil, i represents $n-1$ and lighter components.

Table 3.3 Comparison of contaminated sample mole % reported in the CoreLab report and calculated from mass % in PhazeComp for sample 21364-IB and 34428-IB

All components	Sample 21346-IB			Sample 34428-IB		
	CoreLab Appendix	CoreLab Reported	PhazeComp Calculated	CoreLab Appendix	CoreLab Reported	PhazeComp Calculated
	MW	mole %	mole %	MW	mole %	mole %
N2	28.013	0.551	0.551	28.013	0.480	0.480
CO2	44.010	1.83	1.83	44.010	2.28	2.28
C1	16.043	84.849	84.847	16.043	85.718	85.718
:	:	:	:	:	:	:
:	:	:	:	:	:	:
C29	402	0.005	0.0048	402	0.002	0.0018
C30	416	0.003	0.0035	416	0.001	0.0015
C31	430	0.002	0.0024	430	0.001	0.0012
C32	444	0.002	0.0016	444	0.001	0.0010
C33	458	0.001	0.0011	458	0.001	0.0008
C34	472	0.001	0.0007	472	0.001	0.0006
C35	486	0.000	0.0005	486	0.001	0.0006
C36+	529	0.001	0.0012	565	0.004	0.0039
sum		100.00	100.00		100.00	100.00

$$M_{n+} = \frac{w_{n+}}{\frac{1}{M_{\bar{o}}} - \sum \frac{w_{\bar{o}i}}{M_i}} \tag{3.1}$$

In the case of the gas condensate samples studied in this paper cyanogenic flash is the process used for compositional analysis by the lab. This involves that the reservoir gas is cooled with liquid nitrogen before the temperature is brought up to room temperature and the gas has bled of into a container. The gas collected represents the “flashed gas” and the remaining liquid is the “flashed oil” used to calculate the recombined fluid compositions. These “flashed” samples are not in thermodynamic equilibrium after such a process (Younus et al. 2019). It is important to consider that plus fraction average properties from the lab can lead to uncertain and incorrect C_{n+} characteristics.

3.2.2 Contaminated to Decontaminated Samples

The log plot mentioned in section 3.1.1 was recreated for sample 21364-IB and 34428-IB. Figure 3.1 and 3.2 include these plots. Included in these plots are the results of the decontamination process described in this section (“calculated wt% decon”) and the decontaminated samples CoreLab reports (“CoreLab decon”). The OBM reported in the CoreLab report is also included as “OBM” and the original contaminated wt % is plotted as “Contaminated”.

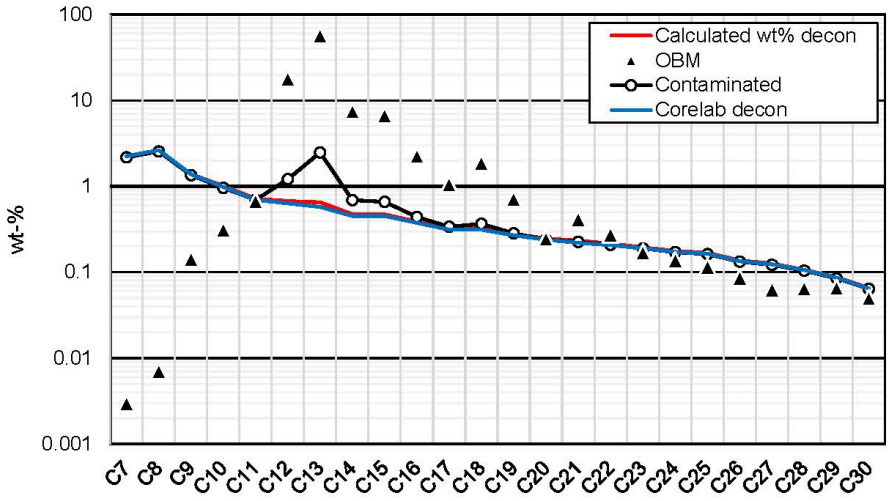

Figure 3.1 Sample 21364-IB decontamination comparison

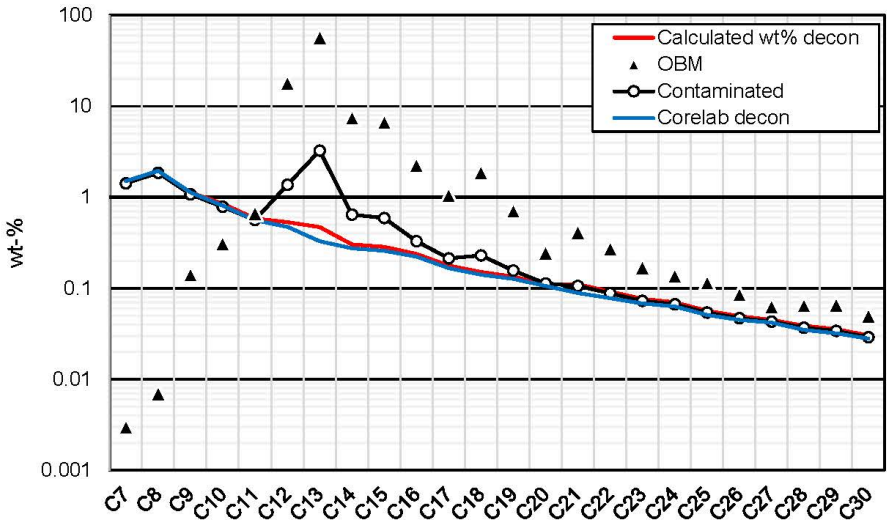

Figure 3.2 Sample 34428-IB decontamination comparison

The approach used for decontaminating in this study is the "subtraction" method (Gozalpour et al. 2002). The method relies on knowledge of the OBM composition which CoreLab reports. Weight fraction will be the basis for this calculation, instead of mole fraction, as wt % is the measured quantity in the lab. For C7 to C10 the single carbon number (SCN) has been lumped together from the reported C7 to C10 "groups" in the CoreLab report. Consequently, a weighted average approach to the molecular weights of the component in the "groups" has been chosen to estimate the molecular weights

of the “groups”. Table 3.4 shows this lumping of the groups.

Table 3.4 Averaging of molecular weights used in SCN decontamination of samples

Components groups	MW	SCN	Weighted average MW
Me-Cyclo-Pentane	84.16	C7	91.55
Benzene	78.11		
Cyclo-Hexanes	84.16		
C7*	100.2		
Me-Cyclo-Hexane	98.19	C8	104.87
Toluene	92.14		
C8*	114.23		
Ethyl-Benzene	106.17	C9	119.77
Meta/Para-xylene	106.17		
Ortho-xylene	106.17		
C9*	128.26		
Tri-Me-Benzene	120.19	C10	140.00
C10*	142.28		

An amount of OBM, f_M, is subtracted from the original mass fraction of 1 mole contaminated sample in the region where the composition can be fitted to an analytical model. Equation 3.2 shows this. Typically, the region of interest is in the range of C7-C20. For the case of this recreation an exponential model is assumed and made using the LOGEST function in excel. This means that a linear trend is assumed for a decontaminated sample when plotted against molecular weight.

$$w_{MDT,i} = f_M * x_{m,i} + (1 - f_M) * w_{R,i} \tag{3.2}$$

In the equation above $w_{MDT,i}$ is the mass fraction of the contaminated MDT sample component, $x_{m,i}$ is the mass fraction of the OBM component i and $w_{R,i}$ is the decontaminated component mass fraction. The equation can be written as:

$$w_{R,i} = \frac{w_{MDT,i} - f_M * x_{wt,i}}{1 - f_M} \tag{3.3}$$

The amount of OBM is defined as $f_M = \frac{mass\ of\ OBM}{mass\ of\ reservoir\ fluid + mass\ of\ OBM}$. The amount of f_M is quantified by finding the minimized sum of the squares of the relative error of mass fraction in SCN components. Since a fraction of the original amount is removed, a normalization is done to bring the decontaminated sample to summarize to 1. The error function is defined in Eq. 3.4 (Mott et al. 2003)

$$E = \sum \left(\frac{w_i}{w_{a,i}} - 1 \right)^2 \tag{3.4}$$

where w_i is the mass fraction of SCN component i in the decontaminated sample, and $w_{a,i}$ is the mass fraction in the analytical model. Each component is weighted the same, regardless of the magnitude of the mass fraction.

CoreLab does not report directly how the decontaminated samples were calculated, but there are clear indications that the calculated decontaminated quantities are fitted to an exponential or gamma model. In the calculations done in this study C10 to C20 components were assumed to fit an exponential (linear on semi log plot) model when molecular weight is plotted against weight fractions. The resulting decontamination of the samples are not matching 100% to the CoreLab reported decontaminated samples but are not far off. For sample 21364-IB the total difference in composition is less than 1% and for sample 34428-IB just above 1%. The difference between CoreLab and calculated decontaminated samples in this report is a result of mainly three factors (Mott et al. 2003) described under.

The first issue is the choice of which components to include in the fitting process. The number of components CoreLab has included in their fitting is unknown. As mentioned, the components from C10 to C20 were used in the fitting for the calculations done in this report. Secondly, the choice of molecular weights of the SCN fractions could have an impact on the results. For this study the molecular weights reported in the appendix of the CoreLab report were used. Lastly, there is a question of how to define the “best fit” to the analytical model. The error function used her might not necessarily be the optimal.

The key takeaway from this study is that CoreLab has used some sort of analytical model in their fitting of the decontaminated sample calculation. An exponential (linear on log plot) approach used with molecular weights reported by CoreLab fitting mass factions for C10 to C20 to the exponential approach model gives a fair estimate of the decontaminated sample with small compositional differences compared with CoreLab. If CoreLab’s reported decontaminated samples is more representative of the in-situ reservoir fluid compared to the decontaminated sample found in this study remains unknown. Figure 3.3 includes the whole range of wt-% from C1-C36+ for sample 21364-IB.

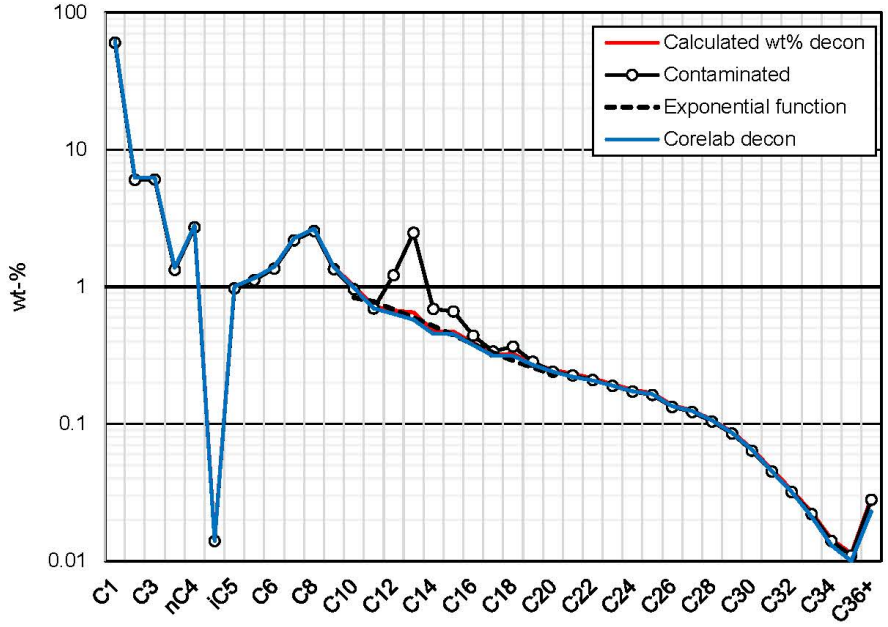

Figure 3.3 Overview of sample 21364-IB component weight %

21

4 EOS considerations

Consultant A was provided with the laboratory report from CoreLab and made two EOS models based on the data and PVT experiments. There is a 22-component model and a 10-component model. The main goal of this section is to perform a quality control of the EOS models. The original EOS is made using PVTsim. For the purpose of this study the equation of state-PVT-package PhazeComp by Zick Technologies was used. The Peng Robinson EOS with temperature dependent volume correction is used by Consultant A.

The composition of the two different EOS models, as defined by Consultant A, is given in table 4.1. The molecular weights are also included in the table. The 22-component EOS is the one discussed further in the report.

Table 4.1 Component lumping definition for the two EOS models made by Consultant A

22-Componet EOS	MW	10-component EOS	MW
N2	28.01	N2-C1	16.113
CO2	44.01	CO2-C2	34.384
C1	16.04	C3-N-C4	48.449
C2	30.07	I-C5-C6	77.067
C3	44.10	C7	96.000
I-C4	58.12	C8	107.000
N-C4	58.12	C9	121.000
I-C5	72.15	C10-C12	146.471
N-C5	72.15	C13-C15	182.925
C6	86.18	C16-C80	290.861
C7	96.00		
C8	107.00		
C9	121.00		
C10	134.00		
C11-C12	154.80		
C13	175.00		
C14	190.00		
C15	206.00		
C16	222.00		
C17-C18	243.76		
C19-C23	285.12		
C24-C80	401.36		

4.1 Check of samples used in EOS

It has been noticed that the lumped composition of the samples used both as in-situ and contaminated

fluids in the EOS does not match in the heavier components with a lumping done in PhazeComp. Table 4.2 and 4.3 include a comparison of the Consultant A defined in-situ and contaminated fluid for the 22-compoent system and the corresponding lumping of the composition in table C.2 (in Appendix C) done in PhazeComp. This is shown for both contaminated and decontaminated composition. Appendix D includes the full versions as well as the same tables for the 10-component system.

Table 4.2 Comparison of composition used by Consultant A and composition lumped in PhazeComp form C36+ composition reported by CoreLab. 22 component system. *Decontaminated* samples

Component	21364-IB		34428-IB	
	Consultant A mole %	PhazeComp mole %	Consultant A mole %	PhazeComp mole %
N2	0.5540	0.5535	0.483	0.483
CO2	1.8340	1.8344	2.291	2.291
C1	85.2050	85.2028	86.248	86.247
C2	4.5660	4.5665	5.008	5.008
:	:	:	:	:
:	:	:	:	:
C15	0.0480	0.0481	0.026	0.026
C16	0.0370	0.0372	0.021	0.021
C17-C18	0.0560	0.0566	0.027	0.026
C19-C23	0.0950	0.0864	0.036	0.034
C24-C80	0.0510	0.0586	0.019	0.021

Table 4.3 Comparison of composition used by Consultant A and composition lumped in PhazeComp form C36+ composition reported by CoreLab. 22 component system. *Contaminated* samples

Component	21364-IB		34428-IB	
	Consultant A mole %	PhazeComp mole %	Consultant A mole %	PhazeComp mole %
N2	0.5510	0.5514	0.4800	0.4800
CO2	1.8270	1.8268	2.2770	2.2770
C1	84.8540	84.8473	85.7250	85.7177
C2	4.5470	4.5474	4.9770	4.9772
:	:	:	:	:
:	:	:	:	:
C15	0.0730	0.0727	0.0620	0.0620
C16	0.0450	0.0449	0.0320	0.0320
C17-C18	0.0650	0.0653	0.0390	0.0393
C19-C23	0.0920	0.0908	0.0300	0.0409
C24-C80	0.0530	0.0601	0.0280	0.0267

What can be seen from the tables is that something is going on in the C19-C23 and C24-C80 composition of the Consultant A defined fluid for the 22-component EOS. This does not follow a normal lumping as is done in PhazeComp where the components are simply just added together. Why this

compositional “tweak” has been done is unknown, but a likely reason could be that the composition has been changed to fit the EOS calculated CCE data to the experimental data.

To quantify the effect of the compositional difference in the heavier components, a comparison of the liquid dropout curve was made from a CCE experiment in PhazeComp. Figure 4.1 shows this graphically and table 4.4 include the PhazeComp reported root-mean-square error (RMS) from the experimental data for the two samples.

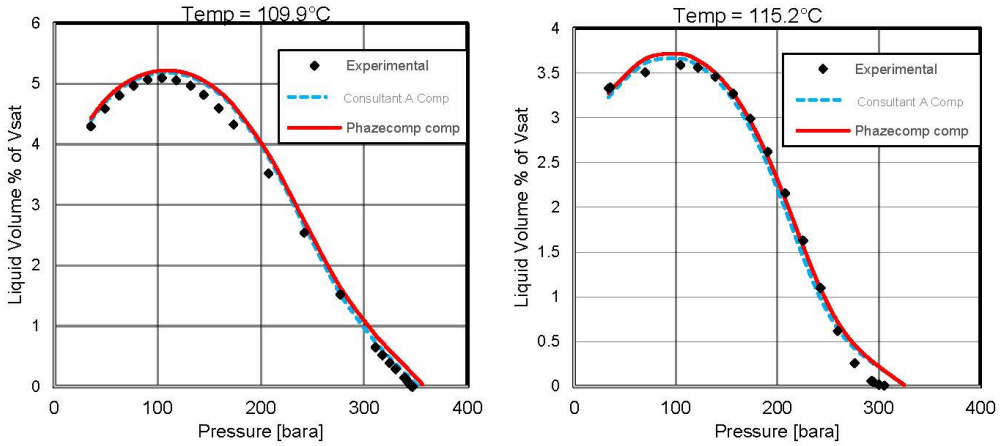

Figure 4.1 Sample 21364-IB and 34428-IB liquid dropout curve comparing Consultant A reported and PhazeComp calculated composition

Table 4.4 RMS % error from experimental data comparing calculations dine with compositions in table 4.3

	Sample 21364-IB - contaminated		**Sample 34428-IB – contaminated**	
	Consultant A comp	PhazeComp comp	Consultant A comp	PhazeComp comp
RMS % Err	**2.56**	**3.95**	**3.76**	**3.48**

The results presented in the table above indicate that the difference in composition makes a difference in the liquid dropout curve. For sample 21364-IB the Consultant A defined composition matches the experimental data better than the composition lumped in PhazeComp. For sample 34428-IB the situation is opposite.

The dewpoint is another other measured property that can be checked to quantify what difference the composition make. Table 4.5 summarizes the dewpoint calculated by the EOS for the different sample compositions and the measured dewpoint form the lab CCE experiments. In this case both the dewpoints calculated with the Consultant A reported compositions are closer to the measured dewpoint. The two checks done her can be an indication that Consultant A has allowed the composition to change to better match the liquid drop out curve and dewpoint for the contaminated sample.

Table 4.5 Consultant from CCE experiment compared with calculated dewpoint from EOS

	Sample 21364-IB - contaminated			Sample 34428-IB – contaminated		
	Experimental	Consultant A comp	PhazeComp comp	Experimental	Consultant A comp	PhazeComp comp
p_d [bara]	**346.6**	**352.2**	**358.3**	**335.6**	**327.5**	**326.9**

4.2 Quality control of EOS

This section focuses on the quality control of the EOS made by Consultant A. Undergoing this process, it was observed that the temperature dependent volume shifts converted from PVTsim to PhazeComp were giving unrealistic specific gravities and thus had to be replaced. This is described throughout the sections under. Whether the unrealistic densities are a problem only appearing when the EOS is converted from PVTsim to PhazeComp, or if the actual EOS itself predicts "wrong" densities in PVTsim, is unknown and should be checked.

4.2.1 Volume shifts and density calculations.

The volume shift in PVTsim is temperature dependent and is expressed in the EOS parameter table as two constants C_{pen} and C_{penT} with units [cm3/mol] and [cm3/mol °C] respectively. These constants are used in calculating the temperature dependent volume shift constant c_i for each component using Eq. 4.1. T_{ref} in the equation is 288.15 K according to the PVTsim user manual (CALSEP).

$$c_i = C_{peni} + C_{penTi}(T_R - T_{ref}) \tag{4.1}$$

PhazeComp accepts only volume shift factors on a dimensionless from. The volume shifts given by Eq. 4.1 were converted to dimensionless form following Eq. 4.2

$$s_i = \frac{c_i}{b_i} \tag{4.2}$$

where b_i is the "repulsion" parameter in the Peng-Robinson equation defined in Eq. 4.3. The constant Ω_{bPR} = 0.07780 for Peng-Robinson.

$$b_i = \frac{RT_{ci}}{P_{ci}}\Omega_{bPR} \tag{4.3}$$

Since the EOS is used to describe three different reservoirs zones for Field A, where the temperature is different, three sets of volume shifts were generated using an excel sheet and the equations above. Surface calculations are also done during the QC making it necessary to calculate a fourth set of s_i values. The volume shift factors are summarized in table 4.6.

Table 4.6 Volume shift factors calculated from Consultant A temperature dependent volume shift parameters

	Zone 1	Zone 2	Zone 3	Surface
Components	$s_i, T = 109.9°C$	$s_i, T = 115.2°C$	$s_i, T = 121.2°C$	$s_i, T = 15.56°C$
N2	-0.1156384	-0.1156384	-0.1156384	-0.1156384
CO2	-0.0262189	-0.0254241	-0.0245394	-0.0403652
C1	-0.1275705	-0.1275705	-0.1275705	-0.1275705
C2	-0.0941191	-0.0941191	-0.0941191	-0.0941191
C3	-0.0740996	-0.0740996	-0.0740996	-0.0740996
I-C4	-0.0652217	-0.0652217	-0.0652217	-0.0652217
N-C4	-0.0589489	-0.0589489	-0.0589489	-0.0589489
I-C5	-0.0463196	-0.0463196	-0.0463196	-0.0463196
N-C5	-0.0373888	-0.0373888	-0.0373888	-0.0373888
C6	0.0062866	0.0062866	0.0062866	0.0062866
C7	0.0402566	0.0399132	0.0395308	0.0463700
C8	0.0858920	0.0858556	0.0858151	0.0865394
C9	0.1175318	0.1174116	0.1172777	0.1196723
C10	0.1370805	0.1368481	0.1365893	0.1412178
C11-C12	0.4828728	0.4823886	0.4818496	0.4914918
C13	0.4914140	0.4907610	0.4900340	0.5030379
C14	0.4854910	0.4846774	0.4837717	0.4999727
C15	0.4746504	0.4736391	0.4725133	0.4926522
C16	0.1405623	0.1393904	0.1380859	0.1614217
C17-C18	0.1290148	0.1275174	0.1258505	0.1556682
C19-C23	0.1136106	0.1118631	0.1099178	0.1447156
C24-C80	0.0751516	0.0728627	0.0703147	0.1158936

The volume shift factors given above was used for calculating component densities at reservoir conditions and surface and plotted in figure 4.2.

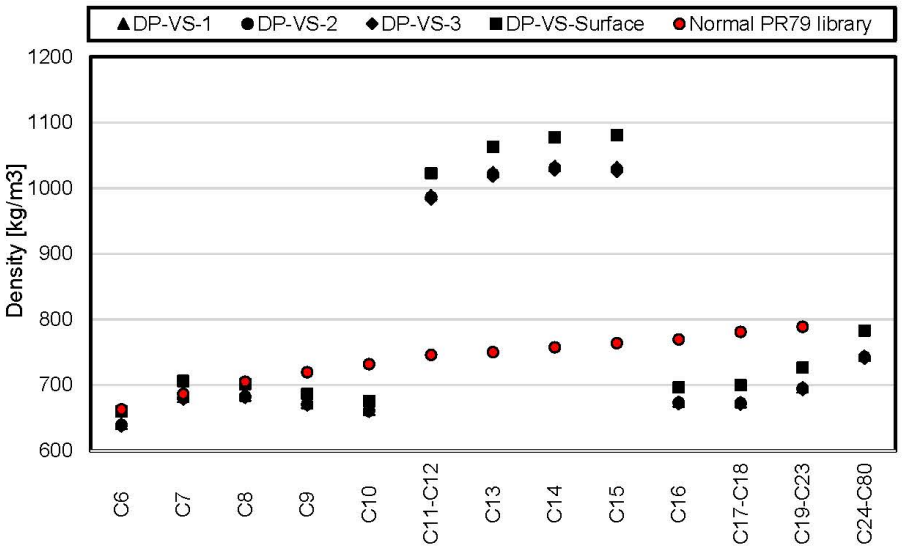

Figure 4.2 Monotonicity check for component densities at reservoir and surface conditions. "DP-VS-1" = Consultant A volume shift for reservoir zone 1 conditions

"Normal PR79 library" is the surface densities calculated from the specific gravities reported for the normal component (i.e. N-C10, N-C14 etc...) in the Peng Robinson library in PhazeComp and was plotted to compare surface densities of the components calculated with the volume shift factors in table 4.6. The lumped components are average values of the normal component specific gravities for the compositions in the lump. A plot of component densities should increase monotonically with carbon number which is clearly not the case in figure 4.2. Corrections had to be done at this point to get realistic densities in further calculations.

The Soreide correlation (Ghasemi et al. 2011) given in Eq 4.4 with PhazeComp default constants (C_f = 29 and n = 13) was used to estimate realistic specific gravities for the C6+ components based on the molecular weights in table 4.1. Volume shifts were than calculated based on the specific gravities and assumed to be equal for every reservoir zone (i.e. only one set of volume shift factors needed).

$$\gamma_i = 0.2855 + C_f(M_i - 66)^n \tag{4.4}$$

Figure 4.3 summarize the new component densities graphically, where the densities are increasing monotonically and will provide physical realistic densities. There are no density measurements on a sample available in the CoreLab report which make density matching to a measured value impossible.

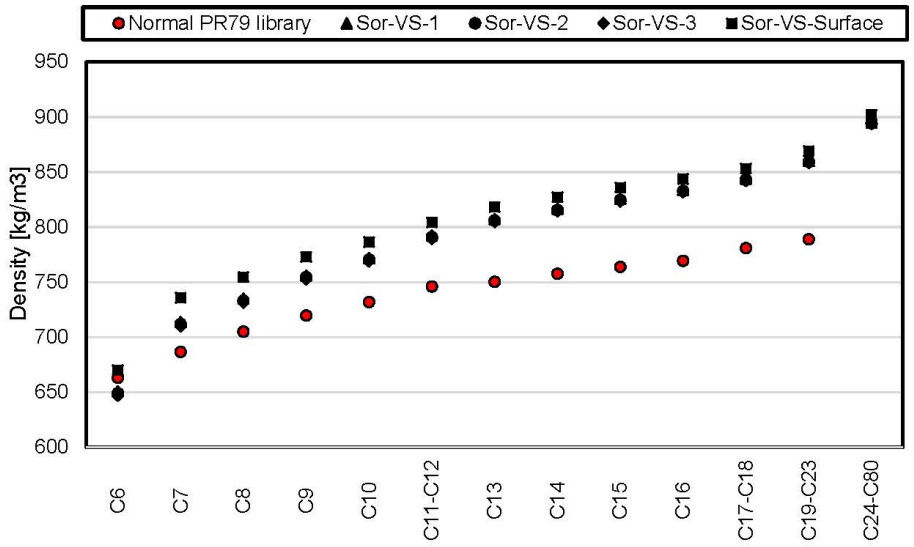

Figure 4.3 Monotonicity check for component densities at reservoir and surface conditions. "Sor-VS-1" = Soreide calculated volume shift for reservoir zone 1 conditions

Reservoir liquid densities are plotted in figure 4.4 and 4.5 for decontaminated samples 21364-IB and 34428-IB. In the figures "DP-VS-Consultant A" is referring to the volume shifts from table 4.6 with the

Consultant A reported sample composition in table 4.2, "DP-VS-PhazeComp" refers to the same volume shifts but using the composition lumped in PhazeComp. "Sor-VS-Consultant A" and "Sor-VS-PhazeComp" use the volume shifts generated by PhazeComp when using the Soreide correlation to estimate specific gravities as explained above.

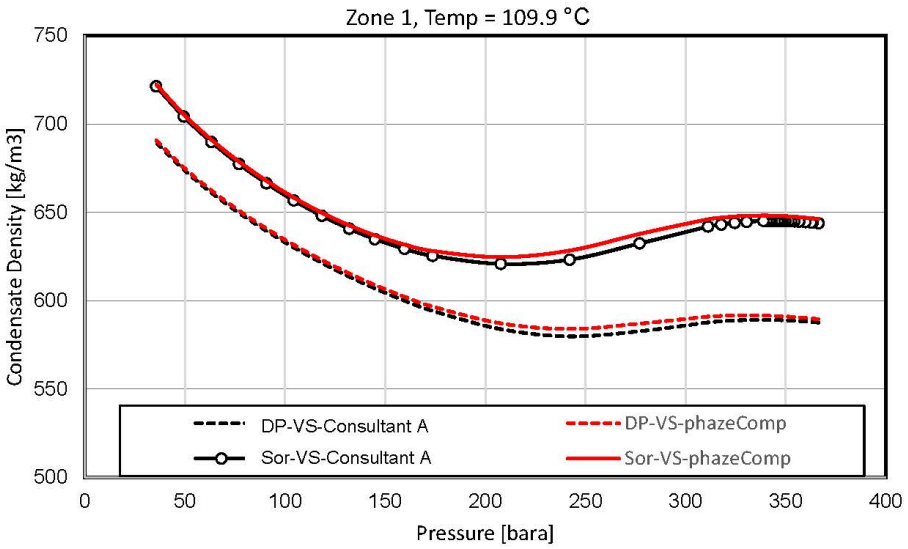

Figure 4.4 Reservoir liquid densities calculated for reservoir zone 1

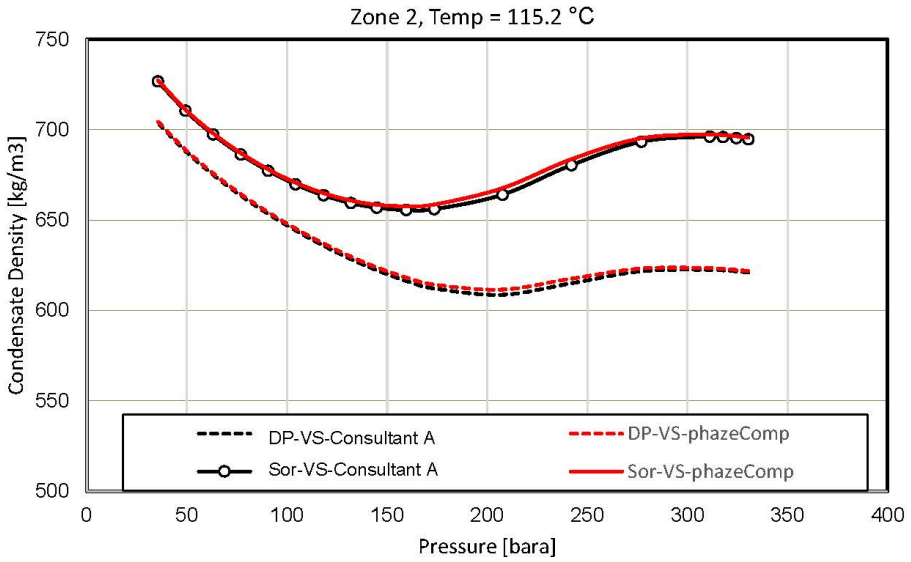

Figure 4.5 Reservoir liquid densities calculated for reservoir zone 2

The densities plotted in the figures above show that the composition "tweaks" done by Consultant A have some effect. *For further calculations the Soreide generated specific gravities and corresponding volume shifts are used together with compositional lumping done in PhazeComp.*

4.2.2 K-value QC

A plot of EOS calculated K-values versus the normal boiling point temperature used in the EOS characterization table should yield a monotonic trend (Younus et al. 2019). Figure 4.6 displays this plot where the trend is monotonically decreasing. The values were calculated from a saturation pressure calculation in PhazeComp at reservoir temperature for the different zones. Sample 21364-IB represents zone 1, sample 34428-IB represents zone 2 and sample 28346-IB represents zone 3.

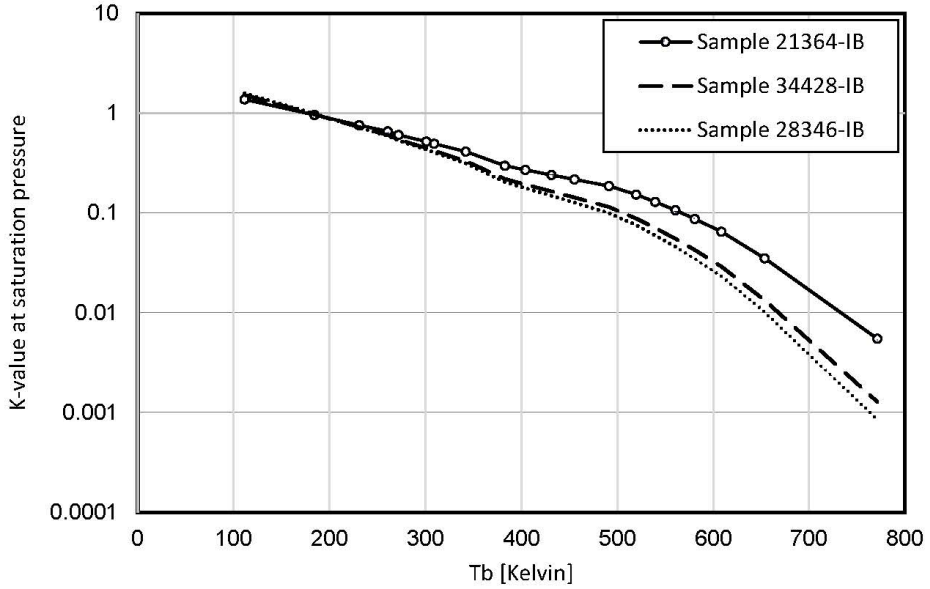

Figure 4.6 Component K-value plotted against normal boiling point temperature at saturation pressure for checking monotonicity.

The monotonic trend shown in the plot above should guarantee that the K-values do not cross in a plot of component K-values versus pressure ranging from atmospheric pressure to saturation pressure. K-value crossing could be an indication that the binary interaction parameters (BIPs) where modified inconsistently for neighboring components. The effect is greater for larger pressures (Younus et al. 2019). Figure 4.7 includes a plot of K-values versus pressure ranging from atmospheric pressure to saturation pressure and a "zoomed in" resolution of higher-pressure range, for sample 21364-IB. The K-values were calculated from a CCE experiment in PhazeComp. As expected from the monotonic trend in the plot in Figure 4.6 the K-values does not cross. The same result applies to sample 34428-IB and 28346-IB.

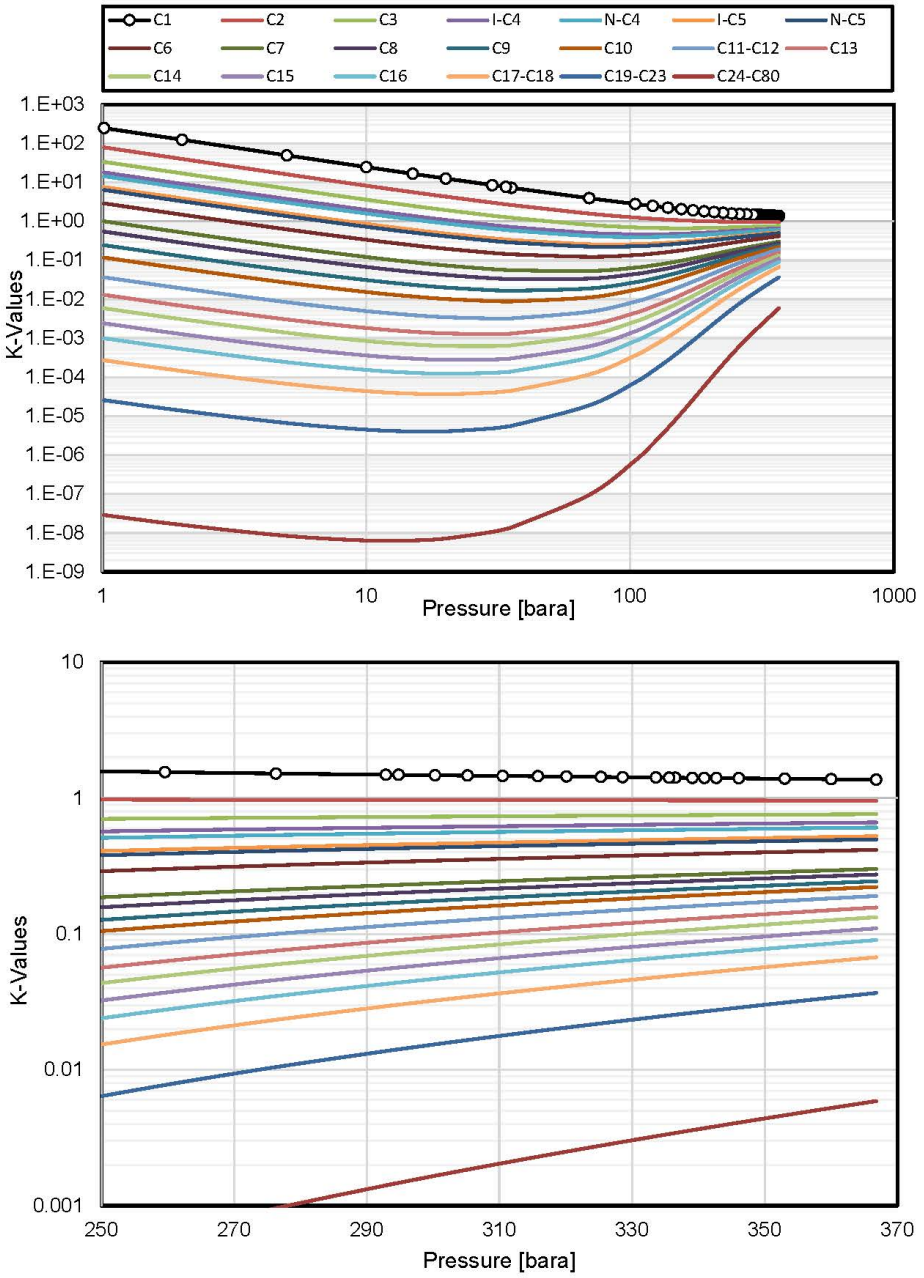

Figure 4.7 Non-crossing K-value QC by plotting K-Values for pressures ranging from atmospheric pressure to saturation pressure. K-Values calculated with a CCE experiment in PhazeComp for sample 21364-IB.

30

4.2.3 EOS parameters in characterized compositions

Consultant A states in the explanation of the EOS tuning that the molecular weight could change up to +/- 5% during the initial tuning of the saturation pressure. Further, the critical temperature, critical pressure and acentric factor were adjusted where the critical temperature was adjusted for the four heaviest components. The process described under was done to check that unrealistic component parameters was avoided during the tuning. Initially the specific gravities were not monotonically increasing (section 4.2.1).

A consistency check of the parameters in the table over the characterized compositions in the EOS was done by plotting the critical pressure and temperature, specific gravities and acentric factor against the molecular weight in table 4.1 for C6+ components. The results are presented in figure 4.8 where all the trends are monotonic. This indicates that Consultant A's tuning of the EOS, with the fixed specific gravities, does not exceed unrealistic component property boundaries.

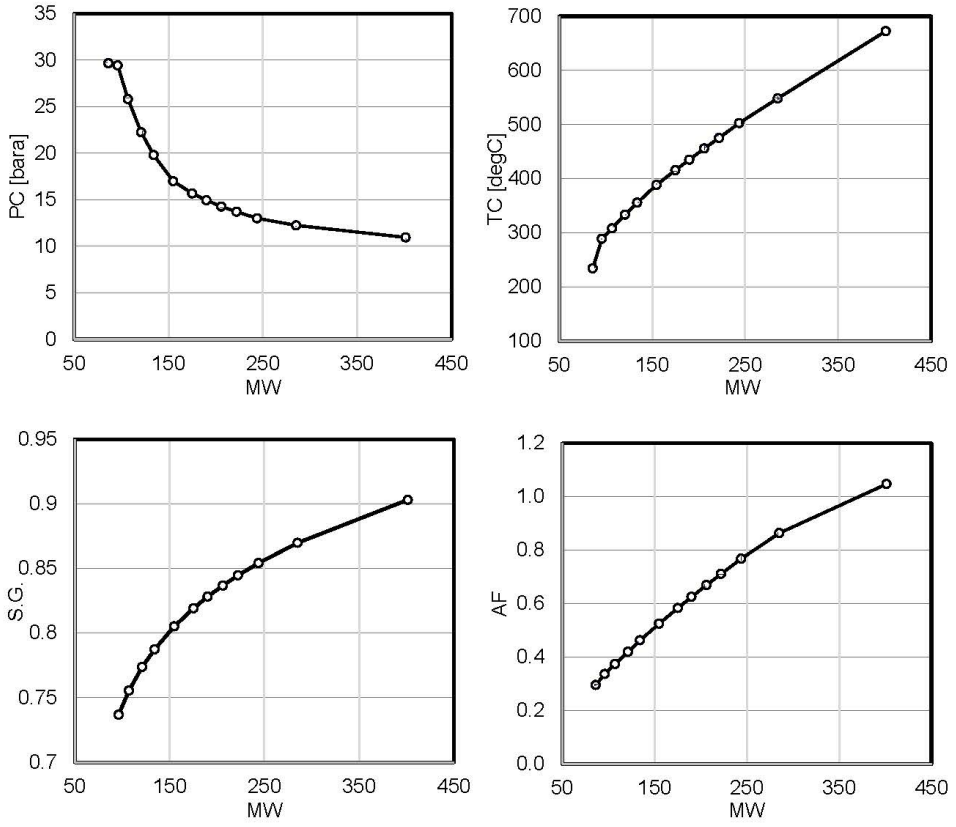

Figure 4.8 Critical pressure and temperature, specific gravity and acentric factor plotted against molecular weight as a consistency check of the EOS

31

4.2.4 Viscosity modelling

Predicting reliable condensate viscosities is important for the two-phase flow region near the well bore in the condensate blockage model described in section 2.3.1. It is usually straight forward to get a reasonable viscosity description of the single-phase gas, regardless of the viscosity model used; the problem is predicting reasonable condensate viscosities below the dewpoint (Yang et al. 2007). For the samples discussed in this study, the only reported viscosity data is calculated single-phase gas viscosities using the method of Lee, Gonzales and Eakin (Lee et al. 1966) form the two CCE experiments.

Consultant A states in their report that the last part of the EOS tuning was to fit the corresponding state principle viscosity model (CSP), which is the Pedersen model in this case. As calculated gas viscosities is the only reported viscosity data, it is reasonable to assume that this is the data the CSP model was fitted to. There is no reported tuning of the viscosity model to known viscosity correlations or condensate samples. The reason for this could be that Consultant A assumes that the CSP method predicts the oil viscosity well enough. It is in fact known that the CSP method shows better prediction capability for oil viscosity compared to the LBC correlation, but the LBC correlation is the most widely used model due to the simplicity and flexibility (Yang et al. 2007). The CSP method is not implemented in PhazeComp meaning that the LBC model is used.

Because the default LBC correlation predicts unrealistic oil viscosities the model must be tuned to reliable viscosity data. As mentioned, there are no available separator oil viscosity data. This leads to tuning of the LBC model based on calculated viscosity data from other viscosity correlations. The process used is as follows;

1. The method of Orrick and Erbar (Poling et al. 1987) is used to estimate reliable component liquid viscosities at atmospheric pressure and reservoir temperature in an excel sheet. In this case 109.9 °C is chosen (temperature of reservoir zone 1).
2. The estimated component viscosities are then inputted to PhazeComp in separate CCE experiments at surface pressure and reservoir temperature for each component starting from C_7.
3. The "ZC" parameter in PhazeComp (i.e. the critical Z-factor) is allowed to change under regression to match exactly the inputted component viscosities.
4. The new set of ZC values obtained from this process is used for the rest of the mixture calculations.

A result of the process described above should be that the component viscosities increase monotonically when plotted against the molecular weight. Figure 4.9 includes this plot and as expected the trend is monotonic increasing fort the calculated component viscosities.

32

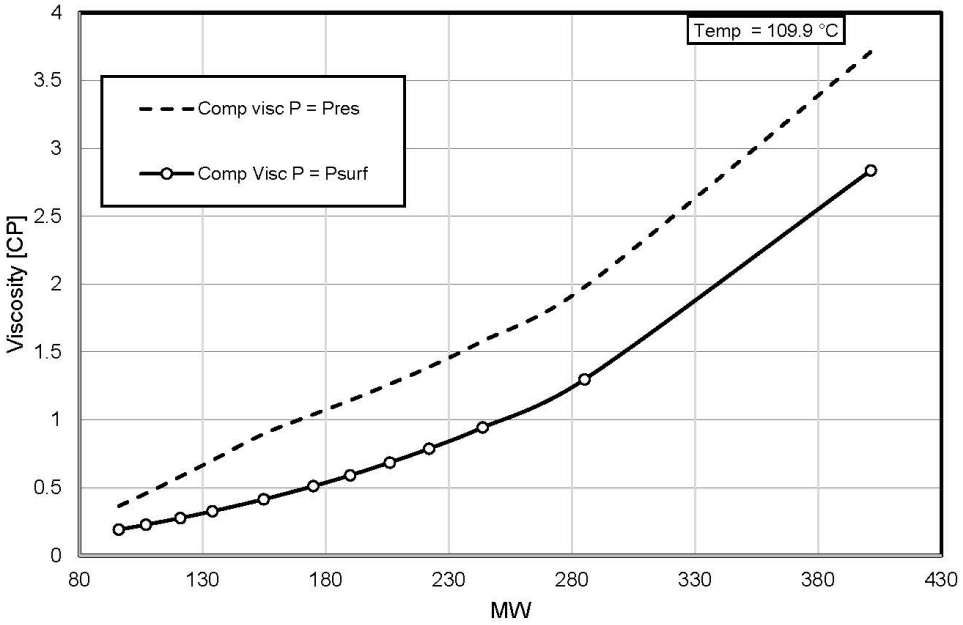

Figure 4.9 Monotonicity QC of component viscosity plotted against molecular weight at surface and reservoir pressure, keeping the temperature equal to reservoir temperature.

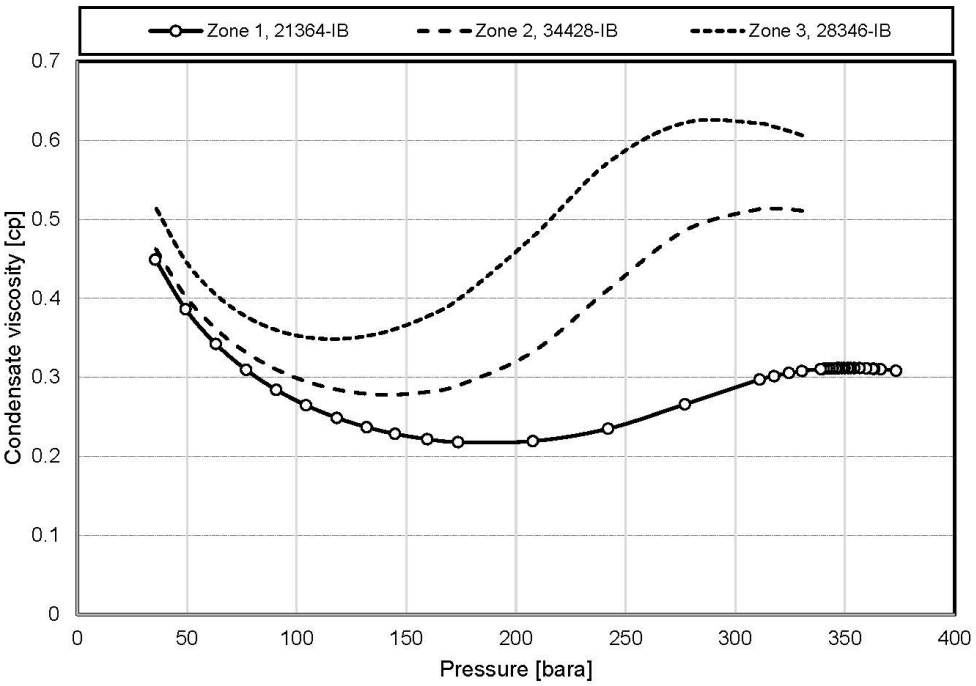

Figure 4.10 Calculated condensate viscosities for the three reservoir zones using a CCE experiment in PhazeComp at the respective reservoir temperature.

After the tuning described above, condensate viscosities were calculated from a CCE experiment in PhazeComp. Fluids from all three different zones were used. The results are presented in figure 4.10. The calculated viscosities are as expected low and lays in the range of 0.1 to 1 cp, which is a normal range found in gas condensate reservoirs (Whitson et al. 1999).

4.3 EOS calculations

This section aims to verify that the EOS modified in PhazeComp estimates the reported data from the CCE experiments and calculates PVT properties for the cleaned samples closely to the calculated properties in the Consultant A report. Some deviation is expected in the calculated PVT properties as the PhazeComp EOS has been modified with new temperature independent volume shift factors and uses the LBC approach for modelling viscosities.

4.3.1 CCE experiment EOS calculation match

The results of this comparison are best expressed graphically and by reporting the RMS for the different parameters. The samples used were contaminated samples reported in table D.2 from Appendix D. The following figures show the results graphically:

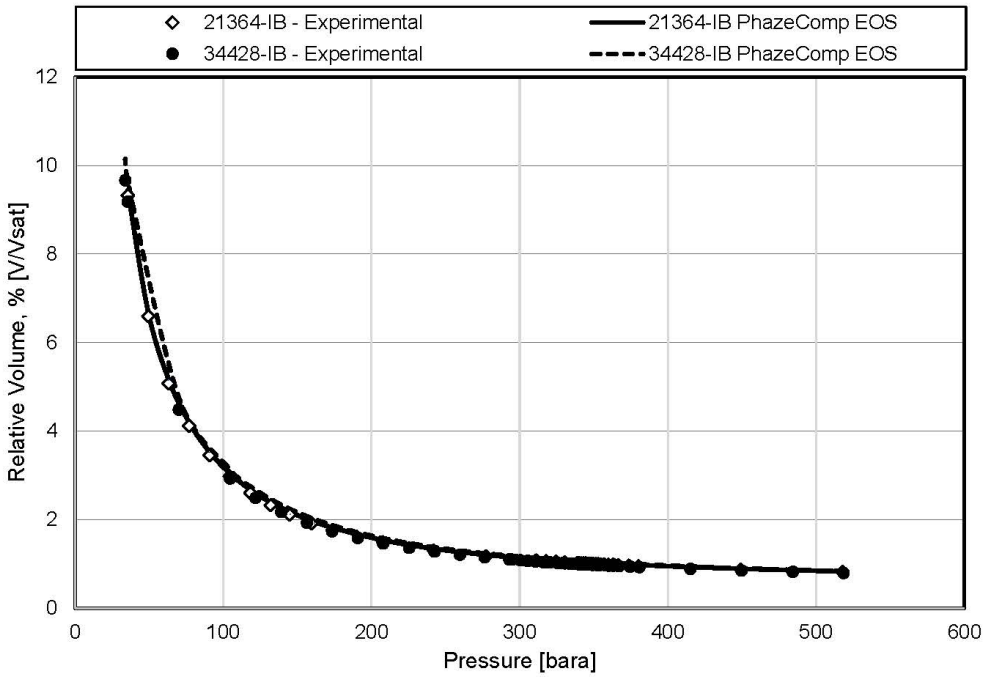

Figure 4.11 Match to relative volumes in CCE experiment

34

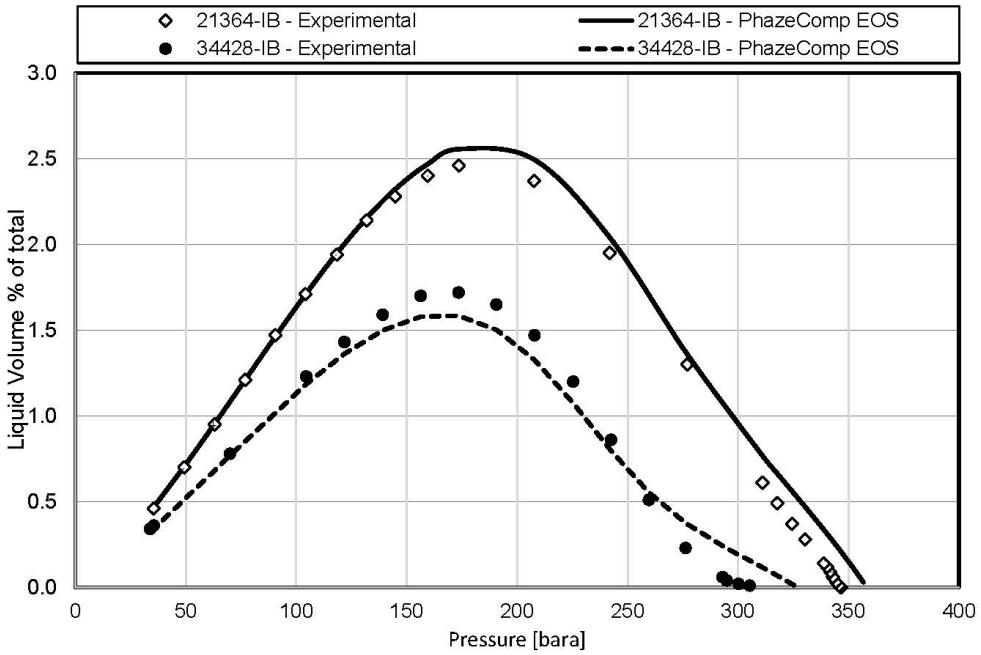

Figure 4.12 Match to liquid drop out volumes in CCE experiment relative to total volume

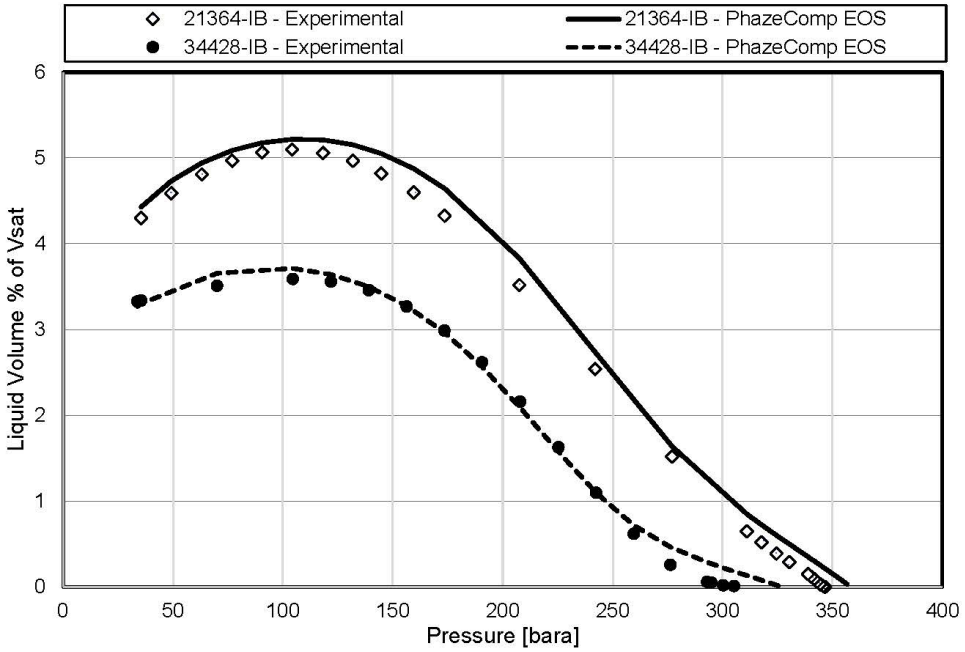

Figure 4.13 Match to liquid drop out volumes in CCE experiment relative to volume at saturation pressure

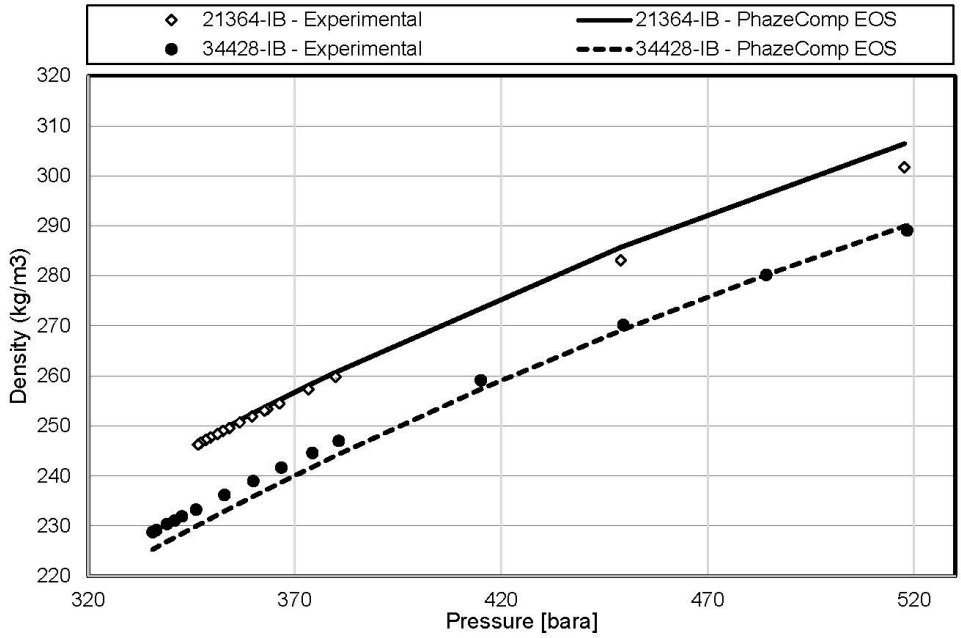

Figure 4.15 Match of gas densities in CCE experiment

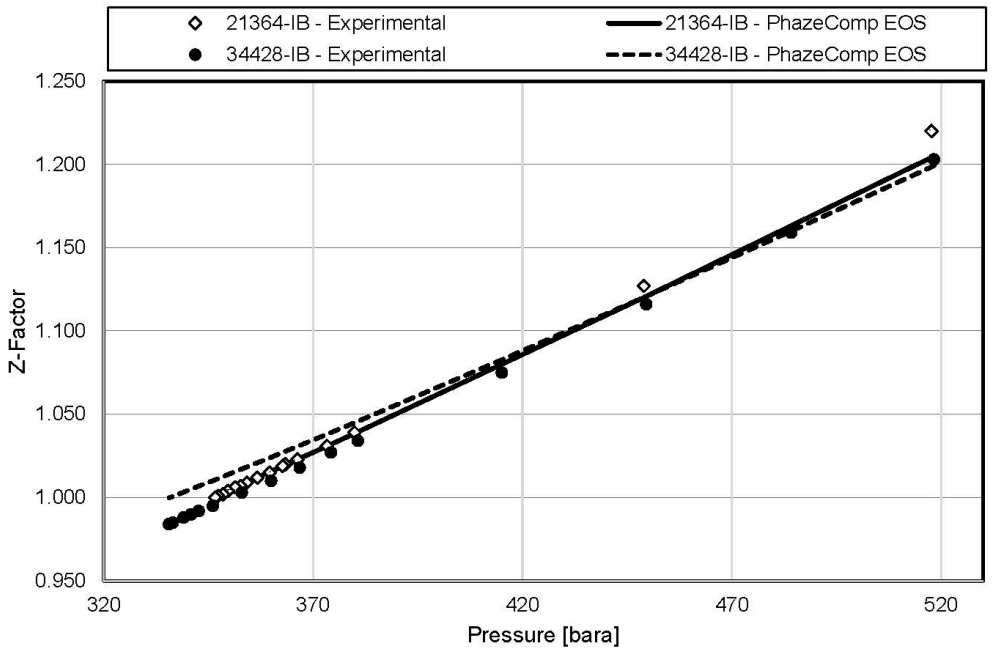

Figure 4.14 Match of gas z-factors in CCE experiment

36

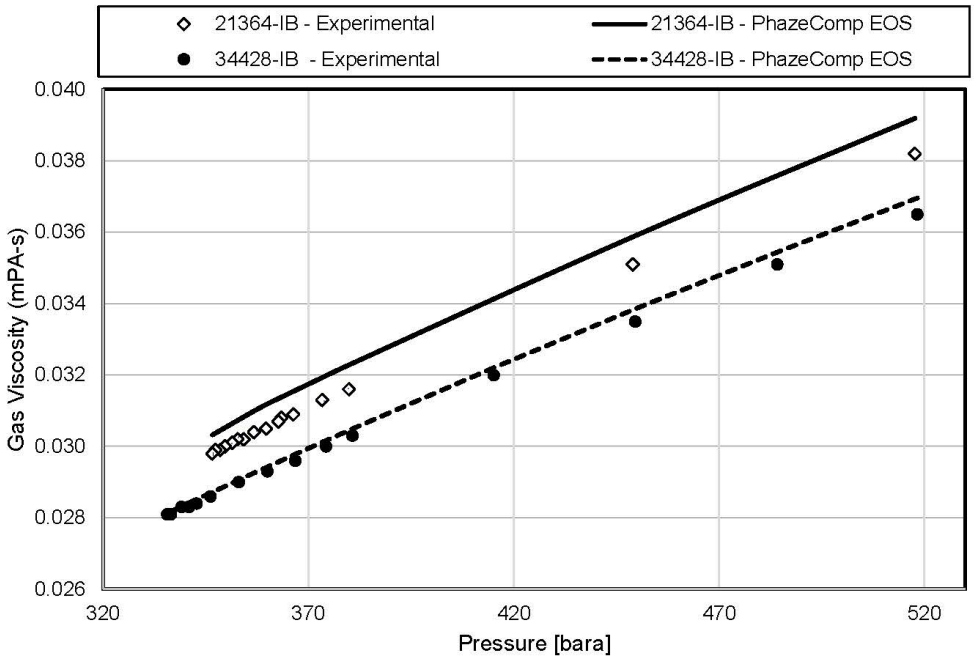

Figure 4.16 Match of gas viscosities from CCE experiment

Table 4.7 and 4.8 reports the RMS % error for the different parameters calculated by PhazeComp compared to the experimental values. This is a good indication of how well the EOS calculated parameter data match to the lab reported data. As can be seen from the tables the largest differences are in the liquid drop out curves. It is important to keep in mind that the samples used in the CCE experiments are contaminated with OBM.

Table 4.7 Sample 21364-IB RMS % error for the parameters from CCE calculations in PhazeComp

	Sample 21364-IB - contaminated					
	V_{rel}	Liq. Drop out Vtot	Liq. Drop out Vsat	ρ_g	Z-factor	μg
RMS % Err	**0.54**	**5.53**	**3.95**	**0.48**	**0.36**	**1.66**

Table 4.8 Sample 34428-IB RMS % error for the parameters from CCE calculations in PhazeComp

	Sample 34428-IB - contaminated					
	V_{rel}	Liq. Drop out Vtot	Liq. Drop out Vsat	ρ_g	Z-factor	μg
RMS % Err	**1.54**	**6.90**	**3.48**	**0.98**	**1.05**	**0.57**

4.3.2 Calculated PVT properties

Consultant A reports calculated PVT properties for the three different reservoir zones using what they consider representative in situ samples. These are the samples discussed in section 4.1 named Consultant A in table 4.1 plus sample 28346-IB (not discussed in detail in this report but has the same "tweaked" trend as discussed for the other two samples) representing the third reservoir zone.

As some changes were made to the EOS going from PVTsim to PhazeComp (explained earlier), there are some differences in the calculated PVT properties compared to the Consultant A reported data. The properties were also calculated for both the Consultant A reported sample compositions and the composition given from lumping the components in PhazeComp, resulting in differences in the properties. Table 4.9 summarizes the calculated PVT properties. The Consultant A reported calculated data is included.

Table 4.9 Calculated PVT properties for the three reservoir zones

		Consultant A report	PhazeComp EOS	
			Consultant A-Comp	PhazeComp-Comp
		Sample 21364-IB Temp = 109.9 °C		
P_d	[bar]	356	355.9	362.6
ρ_{gi}	[kg/m3]	246.2	245.7	245.8
μgi	[cP]	0.0306	0.0304	0.0305
R_s*	[Sm3/Sm3]	7424	7742.8	7716.0
ρ_{STO}*	[kg/m3]	768.6	798.4	799.0
		Sample 34428-IB Temp = 115.2 °C		
P_d	[bar]	316.3	315.3	319.5
ρ_{gi}	[kg/m3]	230.8	230.0	230.0
μgi	[cP]	0.0289	0.0289	0.0289
R_s *	[Sm3/Sm3]	13813	14236.0	14214.0
ρ_{STO}*	[kg/m3]	775.2	795.6	795.8
		Sample 28346-IB Temp = 121.2 °C		
P_d	[bar]	314.0	313.5	309.96
ρ_{gi}	[kg/m3]	225.8	225.0	224.93
μgi	[cP]	0.0285	0.0286	0.0286
R_s *	[Sm3/Sm3]	17386	18054	18140
ρ_{STO}*	[kg/m3]	767.0	793.2	792.7

There are clear differences in the density of stock tank oil. These differences are expected because of the changes done to the EOS discussed in section 4.2.1. CoreLab does not report measured densities of the condensate, but there are reported calculated densities of C_{7+} at standard conditions which could be used as an indication of what densities could be expected if C_{7+} is assumed to be the components

* Single stage flash separation

becoming oil at surface. For sample 21364-IB the reported calculated C_{7+} density is 786.4 kg/m3, for sample 34428-IB calculated density = 778.6 kg/m3 and for sample 28346-IB the calculated density = 777.3 kg/m3. If a 3-stage separation test is used instead of a single stage flash, the calculated liquid densities are closer to the C_{7+} densities reported in CoreLab.

The compositions used in the calculations also play a role in the calculated dewpoint pressures. Gas viscosities are as expected almost exactly equal as viscosity models are precise in the modelling of gas viscosity.

5 Deliverables for further work

5.1 Designing relative permeability experiments.

The modelling of well deliverability for a gas condensate well as discussed in section 2.3.1 is important to get correctly. For region 1 this is done by measuring k_{rg} at relevant k_{rg}/k_{ro} ratios. The EOS discussed in section 4 is used to make plots of $k_{rg}/k_{ro}(P)$ for different stages of depletion. These plots are used for designing relative permeability experiments to secure relevance of the measurements done in the lab. All ten decontaminated samples have a plot made and can be found in Appendix E. The following plots are three samples representing the three reservoir zones.

For the cores available from the Field A exploration well it preferred to do experiments on three standard core plugs; a 1-md core, 10-md core and 50-md core approximately. The flow near the wellbore is as discussed, a steady-state process where, at any radius, the mixture entering a volume element is the same mixture leaving (Fevang and Whitson 1995). This means that steady state flow experiments through a core with different mixtures representing different krg/kro ratios would represent the volume element at different times of depletion. Five of these mixtures should be run through each core with two different flow tests representing a lower and higher rate. The krg/kro ratio for the tests should range approximately from a maximum of 50 to the minimum value calculated from Eq. 2.28 in section 2.3.1 (Fevang and Whitson 1995). From the figures following the lowest value is found in zone 1 (figure 5.1), where krg/kro is approximately 5.

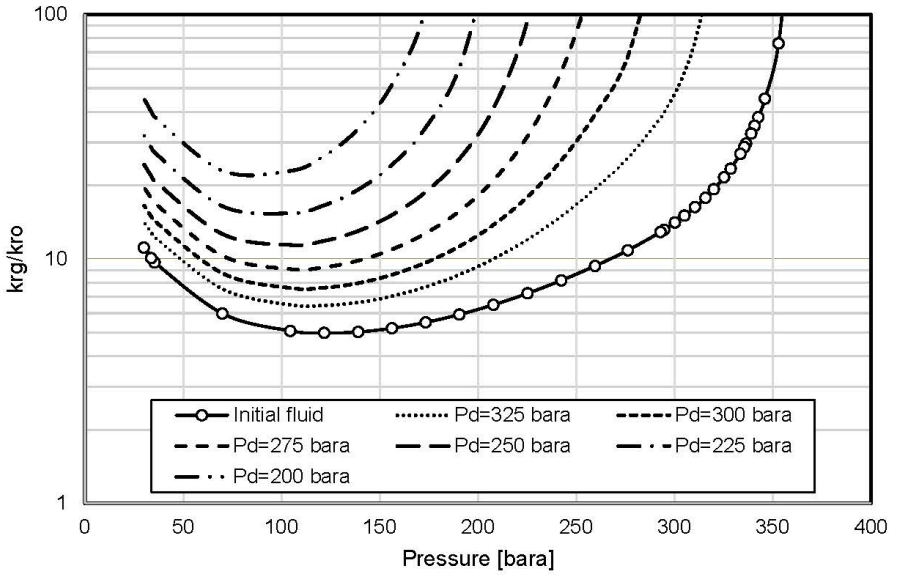

Figure 5.1 krg/kro for sample 21364-IB from reservoir zone 1. T_R = 109.9 °C and P_{Ri} = 362.7 bara

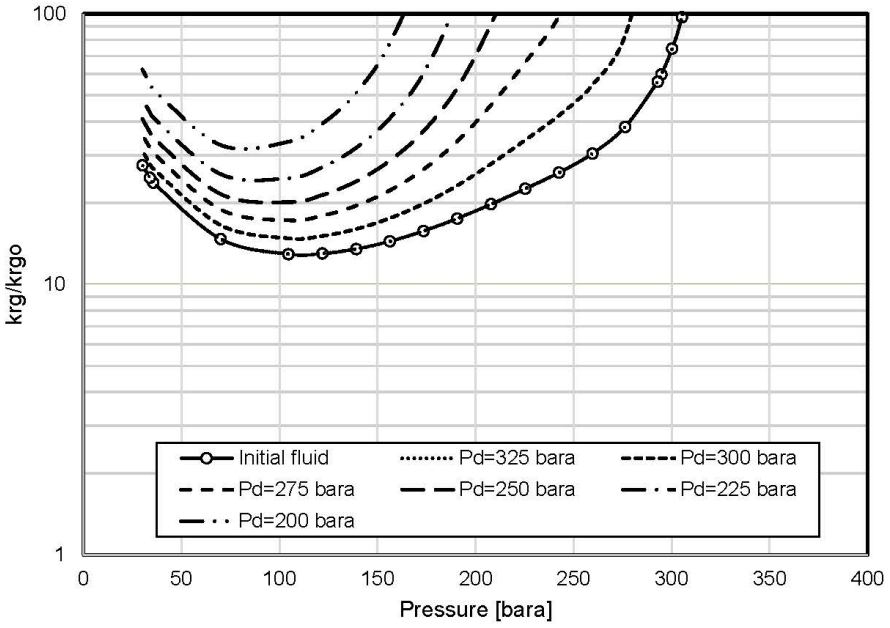

Figure 5.2 krg/kro for sample 34428-IB from reservoir zone 2. T_R = 115.2 °C and P_{Ri} = 374.3 bara

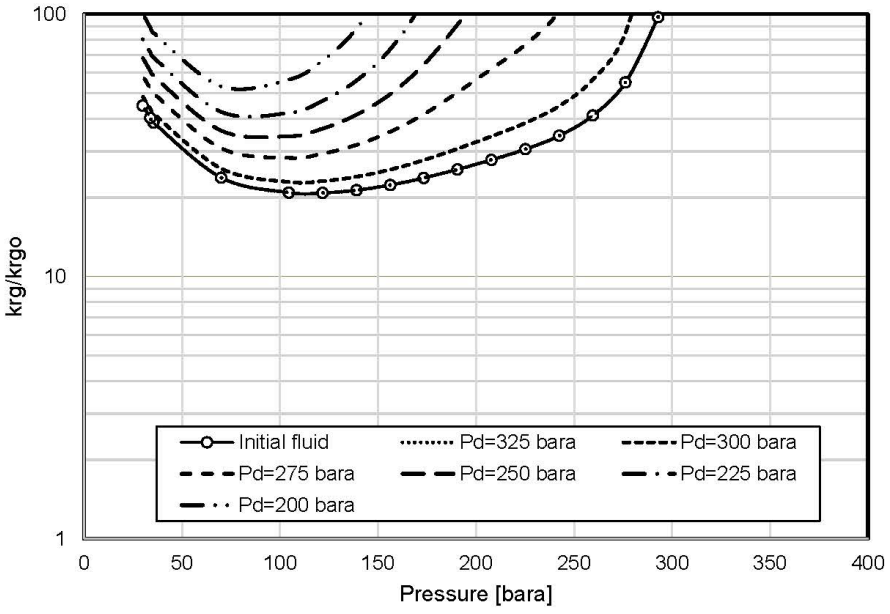

Figure 5.3 krg/kro for sample 28346-IB from reservoir zone 3. T_R = 121.2 °C and P_{Ri} = 385.7 bara.

6 Conclusions

- From the literature study of condensate blockage, it is clear that the main reduction in well deliverability occurs in the near well-bore region (region 1). It is important to understand this region and model the well deliverability reduction. One method for modeling is the three-region model presented by Fevang and Whitson in 1995. To model region 1 correctly it is important to have a trustworthy EOS that predicts reasonable viscosities and liquid drop out curves, as this is what is used in the equation calculating the krg/kro relationship

- The mole % reported in the lab report for each sample is calculated directly from the measured weight % of the different components, using properties taken from published tables (Katz and Firoozabadi)

- The open hole MDT samples were OBM-contaminated, thus CoreLab has used a method for decontaminating the samples. To understand the process of decontaminating samples, a "subtraction" method was used based on the knowledge of the samples to create decontaminated versions of the samples and compare the results with the reported decontaminated samples from CoreLab. Similar results were obtained, however the decontaminated samples reported by CoreLab were used further on.

- The EOS was originally made in PVTsim and had to be converted to PhazeComp as that is the software used for the QC. The EOS could not be used directly as volume shifts and viscosity are handled differently in PhazeComp compared to PVTsim.
    - New specific gravities were generated using the Soreide correlation
    - The LBC viscosity model were introduced and tuned to atmospheric component viscosities at reservoir temperatures for C7+ component calculated by a known correlation, to give reliable liquid viscosities.

- Different consistency checks were performed making sure that EOS is predicting component properties with monotonic trends, following a validating process described by Younus et al. in the paper called "Field-wide Equation of State Model Development" (Younus et al. 2019).

- The match to the CCE experiment conducted on contaminated samples is good using the current EOS. The highest deviation is in the liquid drop out volumes. It is important to keep in mind that the samples used for this part are contaminated samples which are not directly representative of the in-situ reservoir fluid.

- As EOS parameters were changed compared to the original EOS the calculated PVT properties differ from the reported by Consultant A. As Consultant A also uses a “tweaked” composition compared to just normal lumping, there are differences in the calculated data from PhazeComp using the C reported compositions to the normal lumping in PhazeComp.
- krg/kro was plotted using the EOS for the ten different samples from the three reservoir zones to be used for further work. The plots have similar trends for the corresponding reservoir zones.

7 Recommendations for further work

- The LBC viscosity model used in PhazeComp could be tuned against other correlations known to be better for predicting oil viscosity data, other than the method already used and described in section 4.2.4. This could for instance be the CSP method or the Standing correlation. It would be even better to get measured viscosity data from the lab on the condensate oil dropping out at different pressures for fitting the LBC model. When new measured sample data is obtained in the future, updating the EOS to match the measured oil densities and viscosities.

- To verify that the EOS being used in the reservoir models predicts reliable PVT properties a similar QC should be performed using PVTsim. This will verify if there is a problem with the EOS itself, or if the problems related to the EOS occurring in this study was only related to the conversion from PVTsim to PhazeComp. If there are problems with the EOS after the QC it should be fixed and updated immediately.

- A relative permeability experiment designed based on the krg/kro ratios from this study should be done to make sure that the relevant krg data is obtained for modeling the condensate blockage in a reservoir simulator.

Acronyms and Nomenclature

Acronyms

BHFP Bottom hole flowing pressure
CCE Constant composition expansion
CGR Condensate/Gas ratio
CVD Constant volume depletion
EOS Equation of state
GOR Gas/oil ratio
HCPV Hydrocarbon pore volume
IFIP Initial Fluids in place
IGIP Initial Gas in Place
ICIP Initial Condensate in Place
MW Molecular weight
OBM Oil-based mud
RMS Root mean square
SCN Single carbon number
QC Quality Control

Nomenclature

B_{gd} = dry gas formation volume factor
B_{gw} = wet gas formation volume factor
b_i = component repulsion parameter in Peng Robinson EOS
B_o = oil formation volume factor
C = gas rate constant
C_f = Soreide constant
c_i = temperature dependent component volume shift factor, PVTsim
C_{og} = conversion factor of gas-equivalent of surface oil
C_{pen} = temperature independent volume correction PVTsim
C_{penT} = temperature dependent volume correction PVTsim
C_{7+} = heptanes-plus
E = Error function
f_M = amount of OBM in contaminated sample
G = initial gas in place
G_p = cumulative gas produced
G_{pw} = cumulative wet gas produced
G_w = initial wet gas in place
h = reservoir thickness
k = absolute permeability
kr_g = relative permeability of gas
kr_o = relative permeability of oil
M = molecular weight
M_i = molecular weight of component i
n = moles
n_d = moles at initial dewpoint pressure
n_p = produced moles
N = initial oil in place

N_p = cumulative oil produced

P = pressure

P_{ci} = component Critical pressure

P_{CVD}= pressure at CVD test stage

P_d = dewpoint pressure

ΔP_p = pseudopressure

P_R = reservoir pressure

P_{SC} = pressure at surface conditions

P_{wf} = BHFP

P^* = dewpoint of the producing wellstream

V = volume

V_{rel} = relative volume

V_{roCCE} = CCE oil relative volume, V_o/V_{tot}

V_{roCVD}= CVD oil relative volume, V_o/V_d

w = mass fraction

$w_{a,i}$ = component mass fraction in analytical model

$w_{MDT,i}$ = component mass fraction from contaminated MDT sample

$w_{R,i}$ = component mass fraction of "Reservoir" decontaminated fluid.

$w_{\bar{o}i}$ = mass fraction of stabilized oil of component i.

q = flow rate

R = universal gas constant

RF = recovery factor

R_p = Producing gas oil ratio

R_s = solution gas oil ratio

r_s = solution oil/gas ratio

r_e = external drainage radius

r_w = wellbore radius

s = skin factor

s_i = component volume shift factor PhazeComp

S_o = oil saturation

S_w = water saturation

T_{ci} = component critical temperature

T_R = temperature at reservoir conditions

T_{SC} = temperature at surface conditions

$x_{m,i}$ = component mass fraction of OBM

y_{7+} = C_{7+} composition in the produced gas

z = total mole fraction

Z = Z-factor

Z_d = dewpoint pressure Z-factor

Z_2 = two-phase Z-factor

β_s = surface gas mole fraction in wellstream

μ = viscosity

ρ = density

γ = specific gravity

γ_i = specific gravity for component

Type equation here.

Subscripts

d = property at initial dewpoint

D = Depletion

g = Gas phase

$\bar{g}$ = Surface gas phase

$\bar{g}g$ = Surface gas phase from reservoir gas

i = Initial

k = pressure step in CVD

$n+$ = C_n and heavier components

o = Oil phase

$\bar{o}$ = Surface oil phase

$\bar{o}g$ = Surface oil phase from reservoir gas

w = well stream

References

CALSEP. Methode Dokumentation PVTsim 13. 28-30.

Fetkovich, M. D., Guerrero, E. T., Fetkovich, M. J. et al. 1986. Oil and Gas Relative Permeabilities Determined From Rate-Time Performance Data. Presented at the SPE Annual Technical Conference and Exhibition, New Orleans, Louisiana. 1986/1/1/. https://doi.org/10.2118/15431-MS.

Fevang, Øivind. 1995. *Gas Condensate - Flow Behavior and Sampling*. PHD, The Norwegian Institute of Technology, Trondheim (October).

Fevang, Øivind and Whitson, C. H. 1996. Modeling Gas-Condensate Well Deliverability. *SPE Reservoir Engineering* **11** (04): 221-230. https://doi.org/10.2118/30714-PA.

Fevang, Øivind and Whitson, Curtis H. 1995. Modeling Gas Condensate Well Deliverability. *SPE 30714*.

Ghasemi, Mohammad, Alavian, Sayyed Ahmad, and Whitson, Curtis Hays. 2011. C7+ Characterization of Heavy Oil Based on Crude Assay Data. Presented at the SPE Heavy Oil Conference and Exhibition, Kuwait City, Kuwait. 2011/1/1/. https://doi.org/10.2118/148906-MS.

Gozalpour, F., Danesh, A., Tehrani, D. H. et al. 2002. Predicting Reservoir Fluid Phase and Volumetric Behavior From Samples Contaminated With Oil-Based Mud. *SPE Reservoir Evaluation & Engineering* **5** (03): 197-205. https://doi.org/10.2118/78130-PA.

Lee, Anthony L., Gonzalez, Mario H., and Eakin, Bertram E. 1966. The Viscosity of Natural Gases. *Journal of Petroleum Technology* **18** (08): 997-1000. https://doi.org/10.2118/1340-PA.

Mott, Robert, Whitson, Curtis H., and Fevang, Øivind. 2003. Oil-Base Mud Contamination in Gas-Condensate Samples. *Unublished*.

Poling, B. E., Prausnitz, J. M., and O'Connell, J. P. 1987. *The Properties of Gases and Liquids*, Fifth edition edition, 510-512.

Schlumberger. 2019. Schlumberger Oilfield Glossary: absolute permeability, https://www.glossary.oilfield.slb.com/en/Terms/a/absolute_permeability.aspx (accessed 3/12 2019).

Whitson, C. H. 1984. Reservoir Well Performance and Predicting Deliverability. 20.

Whitson, Curtis H. and Brulé, Michael R. 2000. *Phase Behaviour* Vol. 20.

Whitson, Curtis H. , Fevang, Øivind, and Yang, Tao. 1999. Gas Condensate PVT - What's Really Important and Why? (in English).

Whitson, Curtis H. and Mott, Robert E. 2005. *Gas-Condensate-Course-Overheads-All* (Reprint).

Yang, Tao, Fevang, Oivind, Christoffersen, K. R. et al. 2007. LBC Viscosity Modeling of Gas Condensate to Heavy Oil. Presented at the SPE Annual Technical Conference and Exhibition, Anaheim, California, U.S.A. 2007/1/1/. https://doi.org/10.2118/109892-MS.

Younus, Bilal, Whitson, Curtis, Alavian, Ahmad et al. 2019. Field-Wide Equation of State Model Development. Presented at the SPE/AAPG/SEG Unconventional Resources Technology Conference, Denver, Colorado, USA. 2019/7/31/. https://doi.org/10.15530/urtec-2019-551.

Appendix A

A.1 Derivation of Equation 2.25

This is the derivation of Eq. 2.25 in section 2.3.1. This derivation is found in the paper by Fetkovich et al. called "Oil and Gas Relative Permeabilities Determined From Rate-Time Performance Data" (Fetkovich et al. 1986). It uses a modified version of the producing GOR defined by Evinger and Muskat for oils, by including the OGR.

First oil and gas rates are defined by the following equations.

$$q_o = q_{o,free} + q_{g,free} * r_s \tag{A.1}$$

$$q_g = q_{g,free} + q_{o,free} * R_s \tag{A.2}$$

The producing GOR is then defined as

$$R_p = \frac{q_g}{q_o} = \frac{q_{g,free} + q_{o,free} * R_s}{q_{o,free} + q_{g,free} * r_s} \tag{A.3}$$

Following is algebra:

$$R_p = \frac{\frac{q_{g,free}}{q_{o,free}} + R_s}{1 + \frac{q_{g,free}}{q_{o,free}} * r_s} \tag{A.4}$$

$$R_p \left(1 + \frac{q_{g,free}}{q_{o,free}} * r_s\right) = \frac{q_{g,free}}{q_{o,free}} + R_s \tag{A.5}$$

$$R_p - R_s = \frac{q_{g,free}}{q_{o,free}} \left(1 - R_p * r_s\right) \tag{A.6}$$

Which leads to Eq. 2.25:

$$R_P = R_S + \left(\frac{k_{rg}}{k_{ro}}\right)\left(\frac{\mu_o B_o}{\mu_g B_{gd}}\right)\left(1 - r_s R_p\right) \tag{A.7}$$

Appendix B

B.1 Core Lab CCE experiment data.

B.1.1 Sample 21364-IB

Table B.1: CCE experiment for sample 21364-IB

Temperature = 109.9°C

Pressure [Bara]	Relative Volume (1)	Retrograde Liquid Volume % (2)	Retrograde Liquid Volume % (3)	Density [kg/m3]	Deviation Z-factor	Calculated Gas Viscosity (mPa*s) (4)
517.7	0.8162			301.7	1.22	0.0382
449	0.8698			283.1	1.127	0.0351
379.9	0.9479			259.8	1.039	0.0316
373.3	0.9572			257.3	1.031	0.0313
366.3	0.9675			254.5	1.023	0.0309
363.4	0.9718			253.4	1.02	0.0308
362.7	0.973			253.1	1.019	0.0307
359.7	0.9778			251.9	1.015	0.0305
356.7	0.9825			250.7	1.012	0.0304
354.2	0.9867			249.6	1.009	0.0302
352.7	0.9892			249	1.007	0.0302
351.4	0.9914			248.4	1.006	0.0301
349.7	0.9944			247.7	1.004	0.03
348.5	0.9964			247.2	1.002	0.0299
347.3	0.9987			246.6	1.001	0.0299
346.6	1	0	0	246.3	1	0.0298
345.8	1.0013	0.01	0.01			
344.4	1.0038	0.03	0.03			
343	1.0063	0.06	0.06			
341.7	1.0087	0.09	0.09			
340.3	1.0113	0.12	0.12			
338.9	1.0138	0.15	0.14			
330.4	1.0302	0.29	0.28			
324.5	1.0424	0.39	0.37			
317.7	1.0572	0.52	0.49			
311.1	1.0722	0.65	0.61			
277	1.1664	1.52	1.3			
242	1.2999	2.54	1.95			
207.6	1.4874	3.52	2.37			
173.6	1.7618	4.33	2.46			
159.5	1.9161	4.6	2.4			
144.8	2.1125	4.82	2.28			
131.9	2.3253	4.97	2.14			
118.3	2.6046	5.06	1.94			
104.2	2.9761	5.1	1.71			
90.6	3.4549	5.07	1.47			
76.9	4.1158	4.97	1.21			
63.1	5.0751	4.81	0.95			
49.3	6.598	4.59	0.7			
35.5	9.3273	4.3	0.46			

B.1.2 Sample 34428-IB

Table B.2 CCE experiment for sample 34428-IB

Temperature = 115.2°C

Pressure [Bara]	Relative Volume (1)	Retrograde Liquid Volume % (2)	Retrograde Liquid Volume % (3)	Density [kg/m3]	Deviation Z-factor	Calculated Gas Viscosity (mPa*s) (4)
518.3	0.7913			289.1	1.203	0.0365
484.2	0.8165			280.2	1.159	0.0351
449.6	0.8469			270.2	1.116	0.0335
415.1	0.8829			259.1	1.075	0.032
380.7	0.9263			247	1.034	0.0303
374.3	0.9354			244.6	1.027	0.03
366.8	0.9466			241.7	1.018	0.0296
360.0	0.9572			239	1.01	0.0293
353.0	0.9686			236.2	1.003	0.029
346.1	0.9806			233.3	0.995	0.0286
342.7	0.9866			231.9	0.992	0.0284
340.9	0.9900			231.1	0.99	0.0283
339.1	0.9932			230.4	0.988	0.0283
336.5	0.9982			229.2	0.985	0.0281
335.6	1.0000	0.00	0.00	228.8	0.984	0.0281
333.6	1.0038	trace	trace			
328.6	1.0136	trace	trace			
325.3	1.0204	trace	trace			
320.1	1.0315	trace	trace			
315.8	1.0410	trace	trace			
310.5	1.0531	trace	trace			
305.2	1.0658	0.01	0.01			
300.3	1.0782	0.02	0.02			
294.8	1.0927	0.05	0.04			
292.9	1.0981	0.06	0.06			
276.3	1.1473	0.26	0.23			
259.6	1.2053	0.62	0.51			
242.5	1.2753	1.10	0.86			
225.3	1.3593	1.63	1.20			
207.9	1.4618	2.16	1.47			
190.6	1.5856	2.62	1.65			
173.4	1.7371	2.99	1.72			
156.3	1.9258	3.27	1.70			
139.1	2.1694	3.46	1.59			
121.8	2.4909	3.56	1.43			
104.5	2.9251	3.59	1.23			
70.0	4.4848	3.51	0.78			
35.5	9.1807	3.34	0.36			
33.8	9.6666	3.33	0.34			

In the tables above the numbering refers to the following:

1. Relative Volume = V/Vsat i.e. volume at indicated pressure per volume at dew point pressure
2. Retrograde liquid volume as a percentage of the volume at dew point pressure.
3. Retrograde liquid volume as a percentage of the volume at indicated pressure.
4. Calculated using the method of Lee, Fonzales and Eakin, JPT, Aug 1966

B.2 Liquid Dropout curve plots from CCE data.

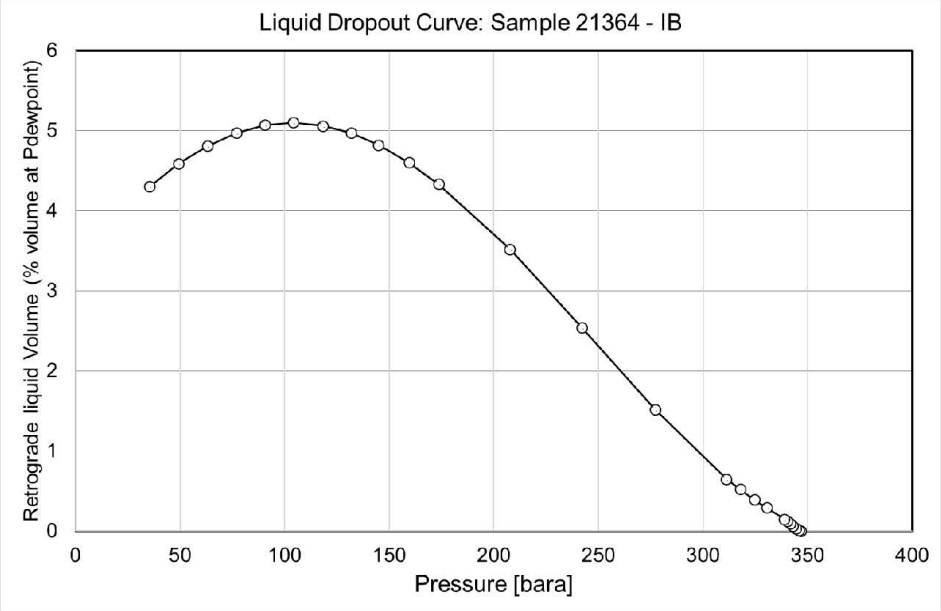

Figure B-1 Liquid dropout curve CCE experiment sample 21364-IB

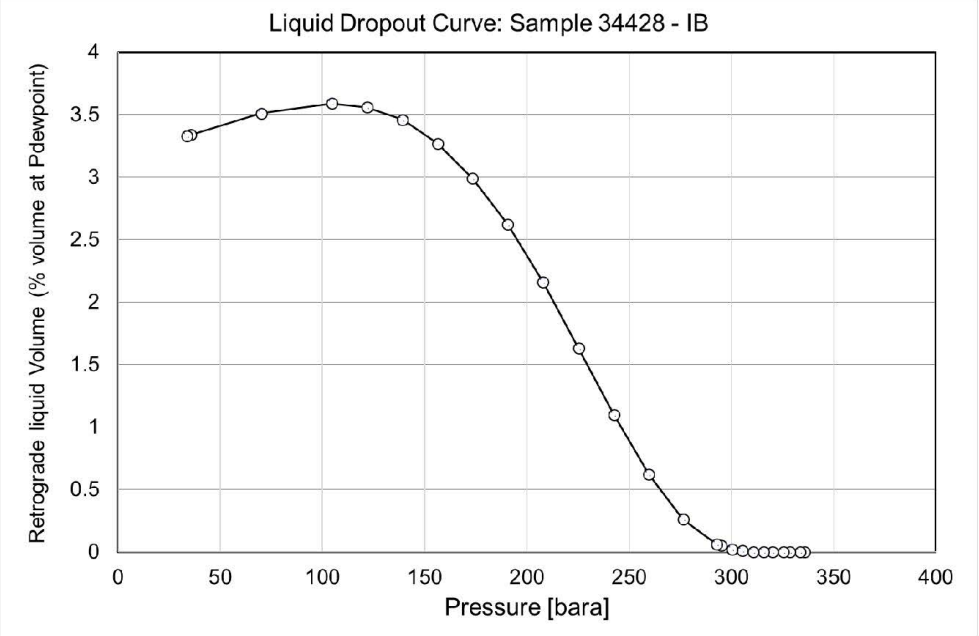

Figure B-2 Liquid dropout curve CCE experiment sample 34428-IB

Appendix C

C.1 Comparison of CoreLab reported composition and PhazeComp calculated composition - Contaminated Samples

Table C.1 Contaminated sample table

All components	Sample 21346-IB			Sample 34428-IB		
	CoreLab Appendix	CoreLab Reported	PhazeComp Calculated	CoreLab Appendix	CoreLab Reported	PhazeComp Calculated
	MW	mole %	mole %	MW	mole %	mole %
N2	28.013	0.5510	0.5514	28.013	0.4800	0.4800
CO2	44.010	1.8270	1.8268	44.010	2.2770	2.2770
C1	16.043	84.8490	84.8473	16.043	85.7180	85.7177
C2	30.07	4.5470	4.5474	30.07	4.9770	4.9772
C3	44.10	3.1090	3.1087	44.10	2.7930	2.7930
I-C4	58.12	0.5170	0.5167	58.12	0.4060	0.4064
N-C4	58.12	1.0570	1.0575	58.12	0.7590	0.7589
NEO-C5	72.15	0.0040	0.0044	72.15	0.0040	0.0036
ISO-C5	72.15	0.3050	0.3054	72.15	0.1870	0.1873
N-C5	72.15	0.3510	0.3509	72.15	0.2010	0.2014
C6	86.18	0.3570	0.3569	86.18	0.2080	0.2080
MC-C5	84.16	0.1320	0.1324	84.16	0.0860	0.0857
BENZENE	78.11	0.0220	0.0223	78.11	0.0140	0.0136
C-C6	84.16	0.1560	0.1555	84.16	0.0970	0.0967
C7*	100.2	0.2340	0.2335	100.2	0.1440	0.1439
MC-C6	98.19	0.2340	0.2339	98.19	0.1630	0.1634
TOLUENE	92.14	0.0850	0.0850	92.14	0.0560	0.0559
C8*	114.23	0.2370	0.2367	114.23	0.1660	0.1657
E-BENZENE	106.17	0.0220	0.0218	106.17	0.0160	0.0161
M-xylene	106.17	0.0640	0.0644	106.17	0.0550	0.0549
O-xylene	106.17	0.0240	0.0243	106.17	0.0180	0.0177
C9*	128.26	0.1460	0.1464	128.26	0.1090	0.1087
123TM-BEN	120.19	0.0190	0.0187	120.19	0.0180	0.0182
C10*	142.28	0.1370	0.1370	142.28	0.1040	0.1042
C11	147	0.1070	0.1071	147	0.0830	0.0831
C12	161	0.1710	0.1710	161	0.1840	0.1841
C13	175	0.3210	0.3207	175	0.4030	0.4029
C14	190	0.0820	0.0822	190	0.0740	0.0737
C15	206	0.0730	0.0727	206	0.0620	0.0620
C16	222	0.0450	0.0449	222	0.0320	0.0320
C17	237	0.0320	0.0323	237	0.0190	0.0195
C18	251	0.0330	0.0330	251	0.0200	0.0198
C19	263	0.0240	0.0245	263	0.0130	0.0129
C20	275	0.0200	0.0198	275	0.0090	0.0089

C21	291	0.0180	0.0176	291	0.0080	0.0079
C22	305	0.0160	0.0155	305	0.0060	0.0062
C23	318	0.0130	0.0135	318	0.0050	0.0050
C24	331	0.0120	0.0118	331	0.0040	0.0044
C25	345	0.0110	0.0107	345	0.0030	0.0034
C26	359	0.0080	0.0084	359	0.0030	0.0028
C27	374	0.0070	0.0074	374	0.0020	0.0025
C28	388	0.0060	0.0061	388	0.0020	0.0021
C29	402	0.0050	0.0048	402	0.0020	0.0018
C30	416	0.0030	0.0035	416	0.0010	0.0015
C31	430	0.0020	0.0024	430	0.0010	0.0012
C32	444	0.0020	0.0016	444	0.0010	0.0010
C33	458	0.0010	0.0011	458	0.0010	0.0008
C34	472	0.0010	0.0007	472	0.0010	0.0006
C35	486	0.0000	0.0005	486	0.0010	0.0006
C36+	529	0.0010	0.0012	565	0.0040	0.0039
sum		100.00	100.00		100.00	100.00

C.2 Comparison of CoreLab reported composition and PhazeComp calculated composition - Decontaminated Samples

Table C.2 Decontaminated sample table

All components	Sample 21346-IB			Sample 34428-IB		
	CoreLab Appendix	CoreLab Reported	PhazeComp Calculated	CoreLab Appendix	CoreLab Reported	PhazeComp Calculated
	MW	mole %	mole %	MW	mole %	mole %
N2	28.013	0.5540	0.5535	28.013	0.4830	0.4832
CO2	44.010	1.8340	1.8344	44.010	2.2910	2.2910
C1	16.043	85.2050	85.2028	16.043	86.2480	86.2474
C2	30.07	4.5660	4.5665	30.07	5.0080	5.0080
C3	44.10	3.1220	3.1219	44.10	2.8100	2.8105
I-C4	58.12	0.5190	0.5187	58.12	0.4090	0.4089
N-C4	58.12	1.0620	1.0621	58.12	0.7640	0.7637
NEO-C5	72.15	0.0040	0.0043	72.15	0.0040	0.0037
ISO-C5	72.15	0.3070	0.3066	72.15	0.1880	0.1885
N-C5	72.15	0.3520	0.3524	72.15	0.2030	0.2025
C6	86.18	0.3580	0.3583	86.18	0.2090	0.2093
MC-C5	84.16	0.1330	0.1330	84.16	0.0860	0.0862
BENZENE	78.11	0.0220	0.0225	78.11	0.0140	0.0138
C-C6	84.16	0.1560	0.1563	84.16	0.0970	0.0972
C7*	100.2	0.2340	0.2344	100.2	0.1450	0.1448
MC-C6	98.19	0.2350	0.2349	98.19	0.1640	0.1644
TOLUENE	92.14	0.0850	0.0854	92.14	0.0560	0.0563

C8*	114.23	0.2380	0.2378	114.23	0.1670	0.1666
E-BENZENE	106.17	0.0220	0.0217	106.17	0.0160	0.0162
M-xylene	106.17	0.0650	0.0646	106.17	0.0550	0.0553
O-xylene	106.17	0.0240	0.0244	106.17	0.0180	0.0179
C9*	128.26	0.1460	0.1463	128.26	0.1080	0.1081
123TM-BEN	120.19	0.0190	0.0187	120.19	0.0180	0.0182
C10*	142.28	0.1360	0.1360	142.28	0.1020	0.1025
C11	147	0.1040	0.1041	147	0.0780	0.0784
C12	161	0.0870	0.0869	161	0.0610	0.0607
C13	175	0.0720	0.0723	175	0.0390	0.0389
C14	190	0.0520	0.0524	190	0.0300	0.0299
C15	206	0.0480	0.0481	206	0.0260	0.0260
C16	222	0.0370	0.0372	222	0.0210	0.0208
C17	237	0.0290	0.0290	237	0.0150	0.0146
C18	251	0.0270	0.0275	251	0.0120	0.0116
C19	263	0.0230	0.0225	263	0.0100	0.0100
C20	275	0.0190	0.0192	275	0.0080	0.0080
C21	291	0.0170	0.0166	291	0.0060	0.0063
C22	305	0.0150	0.0149	305	0.0050	0.0053
C23	318	0.0130	0.0131	318	0.0040	0.0044
C24	331	0.0120	0.0115	331	0.0040	0.0039
C25	345	0.0110	0.0105	345	0.0030	0.0031
C26	359	0.0080	0.0083	359	0.0030	0.0026
C27	374	0.0070	0.0073	374	0.0020	0.0023
C28	388	0.0060	0.0060	388	0.0020	0.0019
C29	402	0.0050	0.0047	402	0.0020	0.0016
C30	416	0.0030	0.0034	416	0.0010	0.0014
C31	430	0.0020	0.0023	430	0.0010	0.0010
C32	444	0.0020	0.0016	444	0.0010	0.0009
C33	458	0.0010	0.0010	458	0.0010	0.0007
C34	472	0.0010	0.0006	472	0.0010	0.0005
C35	486	0.0000	0.0005	486	0.0000	0.0005
C36+	529	0.0010	0.0010	565	0.0010	0.0005
sum		100.00	100.00		100.00	100.00

Appendix D

D.1 22-Component composition comparison

Table D.1 Decontaminated compositions used by Consultant A and lumped in PhazeComp from Table D.2 22-component system

Component	21364-IB		34428-IB	
	Consultant A	PhazeComp	Consultant A	PhazeComp
	mole %	mole %	mole %	mole %
N2	0.5540	0.5535	0.483	0.483
CO2	1.8340	1.8344	2.291	2.291
C1	85.2050	85.2028	86.248	86.247
C2	4.5660	4.5665	5.008	5.008
C3	3.1220	3.1219	2.810	2.811
I-C4	0.5190	0.5187	0.409	0.409
N-C4	1.0620	1.0621	0.764	0.764
I-C5	0.3110	0.3109	0.192	0.192
N-C5	0.3520	0.3524	0.203	0.203
C6	0.3580	0.3583	0.209	0.209
C7	0.5450	0.5462	0.342	0.342
C8	0.5580	0.5581	0.387	0.387
C9	0.2570	0.2571	0.197	0.198
C10	0.1550	0.1547	0.120	0.121
C11-C12	0.1910	0.1910	0.139	0.139
C13	0.0720	0.0723	0.039	0.039
C14	0.0520	0.0524	0.030	0.030
C15	0.0480	0.0481	0.026	0.026
C16	0.0370	0.0372	0.021	0.021
C17-C18	0.0560	0.0566	0.027	0.026
C19-C23	0.0950	0.0864	0.036	0.034
C24-C80	0.0510	0.0586	0.019	0.021
Sum	100	100	100	100

55

Table D.2 Contaminated compositions used by Consultant A and lumped in PhazeComp from Table D.1 22-component system

Component	21364-IB		34428-IB	
	Consultant A mole %	PhazeComp mole %	Consultant A mole %	PhazeComp mole %
N2	0.5510	0.5514	0.4800	0.4800
CO2	1.8270	1.8268	2.2770	2.2770
C1	84.8540	84.8473	85.7250	85.7177
C2	4.5470	4.5474	4.9770	4.9772
C3	3.1090	3.1087	2.7930	2.7930
I-C4	0.5170	0.5167	0.4060	0.4064
N-C4	1.0570	1.0575	0.7590	0.7589
I-C5	0.3090	0.3098	0.1910	0.1909
N-C5	0.3510	0.3509	0.2010	0.2014
C6	0.3570	0.3569	0.2080	0.2080
C7	0.5440	0.5437	0.3410	0.3399
C8	0.5560	0.5556	0.3850	0.3850
C9	0.2560	0.2569	0.1980	0.1974
C10	0.1560	0.1557	0.1220	0.1224
C11-C12	0.2780	0.2781	0.2670	0.2672
C13	0.3210	0.3207	0.4030	0.4029
C14	0.0820	0.0822	0.0740	0.0737
C15	0.0730	0.0727	0.0620	0.0620
C16	0.0450	0.0449	0.0320	0.0320
C17-C18	0.0650	0.0653	0.0390	0.0393
C19-C23	0.0920	0.0908	0.0300	0.0409
C24-C80	0.0530	0.0601	0.0280	0.0267
Sum	100	100	100	100

56

D.2 10-component composition comparison

Table D.3 Decontaminated compositions used by Consultant A and lumped in PhazeComp from Table D.2 10-component system

Component	21364-IB		34428-IB	
	Consultant A mole %	PhazeComp mole %	Consultant A mole %	PhazeComp mole %
N2-C1	85.759	85.756	86.731	86.731
CO2-C2	6.400	6.401	7.299	7.299
C3-N-C4	4.703	4.703	3.983	3.983
I-C5-C6	1.021	1.022	0.604	0.604
C7	0.545	0.546	0.342	0.342
C8	0.558	0.558	0.387	0.387
C9	0.257	0.257	0.197	0.198
C10-C12	0.346	0.346	0.259	0.260
C13-C15	0.172	0.173	0.095	0.095
C16-C80	0.239	0.239	0.103	0.102
Sum	100	100	100	100

Table D.4 Contaminated compositions used by Consultant A and lumped in PhazeComp from Table D.1 10-component system

Component	21364-IB		34428-IB	
	Consultant A mole %	PhazeComp mole %	Consultant A mole %	PhazeComp mole %
N2-C1	85.413	85.399	86.205	86.198
CO2-C2	6.375	6.374	7.255	7.254
C3-N-C4	4.684	4.683	3.958	3.958
I-C5-C6	1.017	1.018	0.600	0.600
C7	0.544	0.544	0.341	0.340
C8	0.556	0.556	0.385	0.385
C9	0.256	0.257	0.198	0.197
C10-C12	0.434	0.434	0.389	0.390
C13-C15	0.476	0.476	0.539	0.539
C16-C80	0.245	0.261	0.129	0.139
Sum	100	100	100	100

Appendix E

E.1 Additional krg/kro plots reservoir zone 1

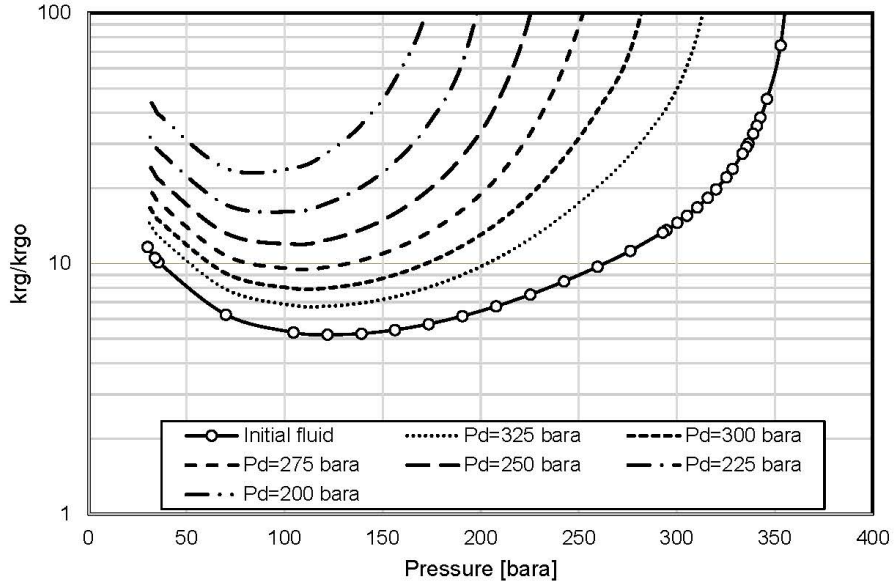

Figure E-2 krg/kro for sample 24583-IB from reservoir zone 1. T_R = 109.9 °C and P_{Ri} = 362.7 bara

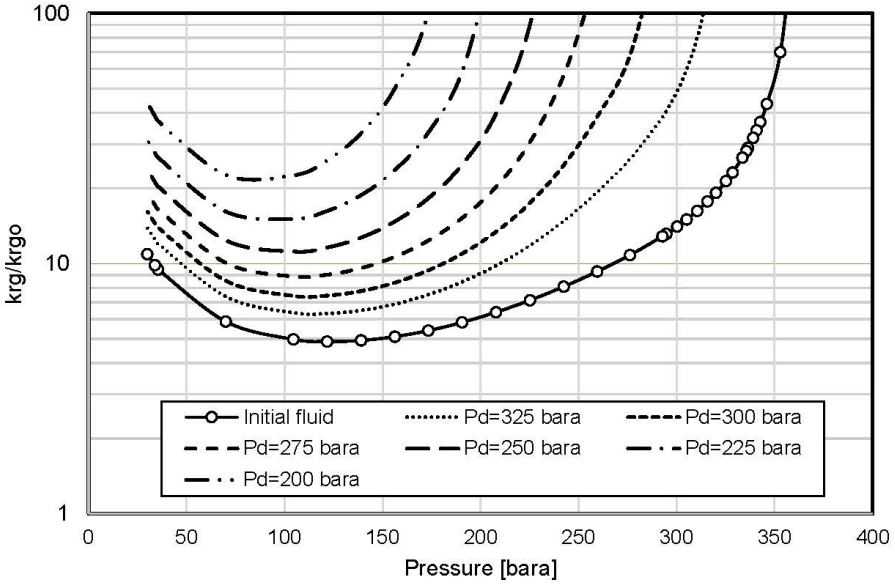

Figure E-1 krg/kro for sample 34434-IB from reservoir zone 1. T_R = 109.9 °C and P_{Ri} = 362.7 bara

E.2 Additional krg/kro plots reservoir zone 2

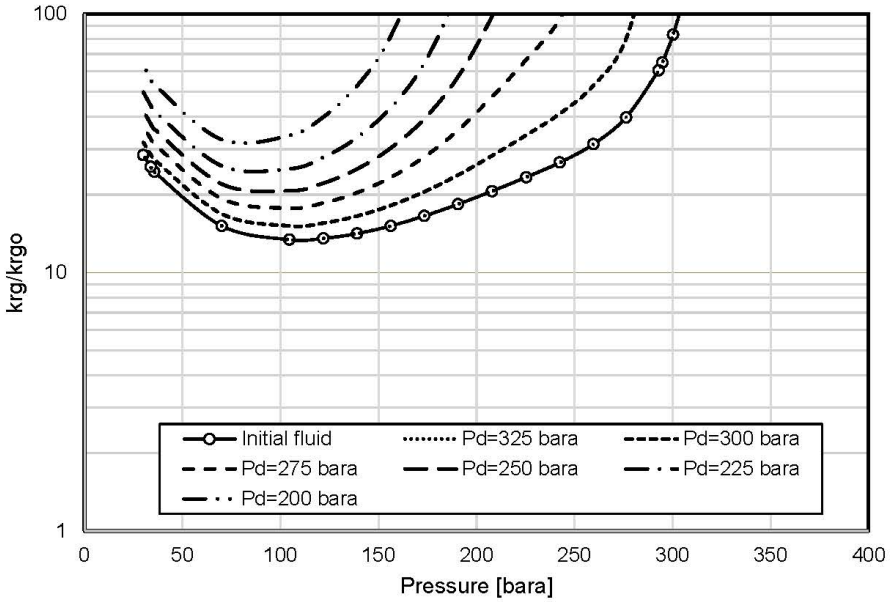

Figure E-3 krg/kro for sample 24582-IB from reservoir zone 2. T_R = 115.2 °C and P_{Ri} = 374.3 bara

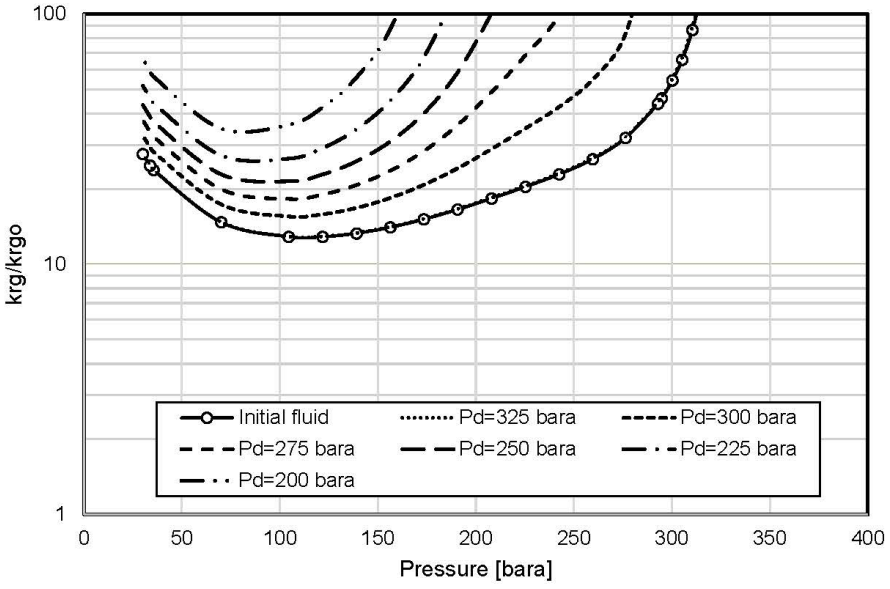

Figure E-4 krg/kro for sample 34430-IB from reservoir zone 2. T_R = 115.2 °C and P_{Ri} = 374.3 bara

E.3 Additional krg/kro plots reservoir zone 3

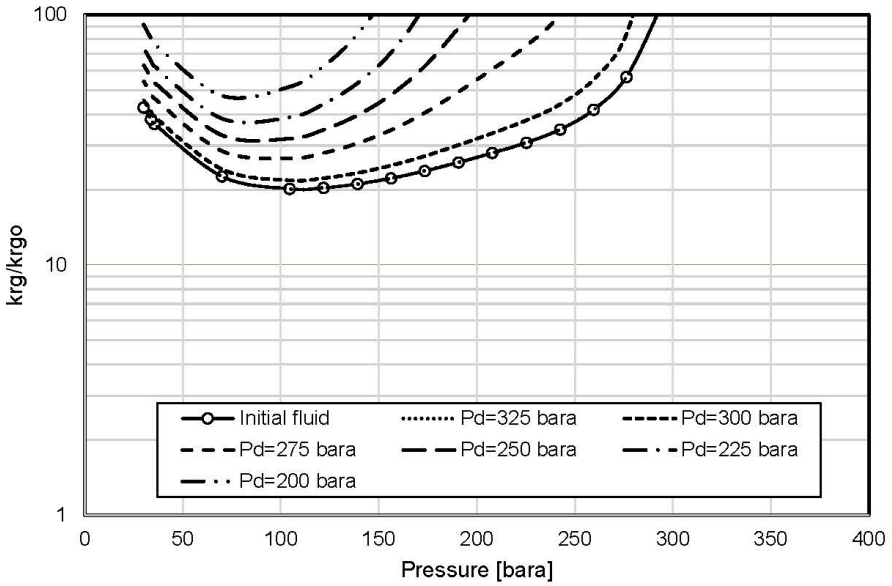

Figure E-5 krg/kro for sample 24592-IB from reservoir zone 3. T_R = 121.2 °C and P_{Ri} = 385.7 bara

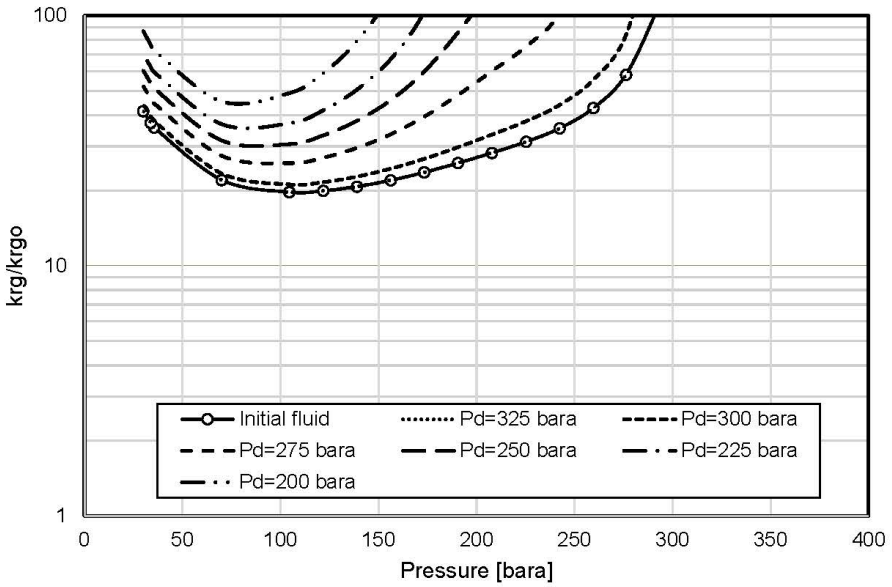

Figure E-6 krg/kro for sample 24577-IB from reservoir zone 3. T_R = 121.2 °C and P_{Ri} = 385.7 bara

60

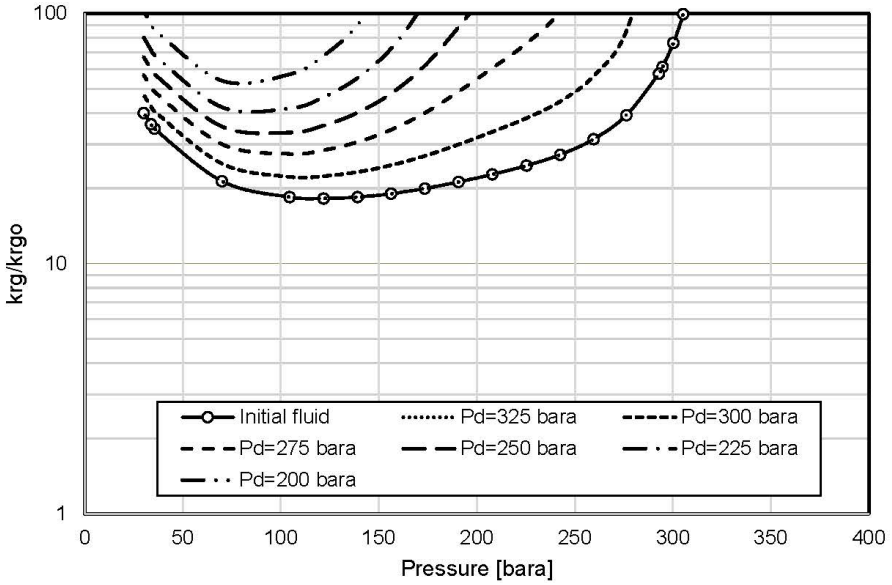

Figure E-7 krg/kro for sample 34434-IB from reservoir zone 3. T_R = 121.2 °C and P_{Ri} = 385.7 bara

Erlend Torheim

Condensate Blockage - A study from the Norwegian Continental shelf

NTNU
Norwegian University of
Science and Technology